Modulational Instability of Optical Solitary Waves

Dmitry Vladimirovich Skryabin

Thesis submitted for the degree of

Doctor of Philosophy

in the Department of Physics and Applied Physics

University of Strathclyde

January 12, 1999

Abstract

Modulational instability and instability induced dynamics of different kinds of spatially localised solutions of nonlinear equations describing propagation of optical waves are studied using numerical and analytical methods. The main problems considered in the thesis are modulational instability of one dimensional spatial solitons due to group velocity dispersion and azimuthal modulational instability of two-dimensional ring-like structures. These phenomena are studied in media with cubic, quadratic and saturable types of nonlinearity.

Acknowledgments

I want to express my special thanks to two people whose impact on my knowledge of nonlinear physics and on my work which ended up with this thesis was clearly dominating. These people are my Ph.D. supervisor Prof. William Firth and Dr. Andrey Vladimirov (St. Petersburg State University).

Thank you, Willie, for encouragement and support through out my two years in Glasgow, for numerous discussions and for giving to me an idea how to see physics behind equations.

Thank you, Andrey, for my first knowledge of what are bifurcations, normal forms and all other nonlinear stuff which I learned from you.

I also acknowledge financial support from the British Goverment via an Overseas Research Studentship and from University of Strathclyde John Anderson Studentship.

Contents

Chapter 1

What is this thesis about?

Nonlinear physics is one of the subfields of the classical physics which remains on the frontier of the modern science. It deals with such ubiquitous phenomena as pattern formation, chaos and solitary waves (solitons), which are possible only due to the nonlinear nature of the response of the medium to applied perturbations. This thesis is focused on the properties of the solitons arising in the context of nonlinear interaction between optical waves and matter.

One of the most fundamental models of nonlinear physics and nonlinear optics is the Nonlinear Schrödinger (NLS) equation which describes evolution of any quasi-monochromatic wave packet in a dispersive weakly nonlinear medium. The NLS equation describes for example propagation of optical beams in nonlinear media, optical pulses in waveguides, deep water waves, evolution of order-parameter in Bose condensate, Langmuir waves in plasma and so on. The name Schrödinger and possibility of the compensation of the dispersive spreading by the self-focusing action of the nonlinearity also call for analogy with de Broglie's idea to represent elementary particles as wave packets.

To introduce very basic ideas which will underline the material presented in thesis, we [1] will briefly show how NLS equation can be obtained from elementary

[1] Throughout this thesis $we = author + reader$

considerations. Let us take a complex wave field in the general form

$$E(t,z) = A(t,z)e^{i(kz-\omega t)} \tag{1.1}$$

and try to construct an equation describing propagation of the wave envelope A starting just from some general assumptions about dependence of wave number k on frequency ω and wave intensity $I = |A|^2$, i.e. we allow that $k = k(\omega, I)$. Then expansion in the vicinity of some carrier frequency ω_0 and for $I \ll 1$ gives

$$k = k_0 + \frac{\partial k}{\partial \omega}(\omega - \omega_0) + \frac{1}{2}\frac{\partial^2 k}{\partial \omega^2}(\omega - \omega_0)^2 + \frac{\partial k}{\partial I}I + \ldots, \tag{1.2}$$

where $k_0 = k(\omega_0, 0)$. To transform this equation into the coordinate space we use substitutions

$$(\omega - \omega_0) \to -i\frac{\partial}{\partial t}, \quad (k - k_0) \to i\frac{\partial}{\partial z}. \tag{1.3}$$

Now we can easily construct an equation obeying the dispersion law (1.2). It has the form

$$i\partial_z A = -i\frac{\partial k}{\partial \omega}\partial_t A - \frac{1}{2}\frac{\partial k^2}{\partial \omega^2}\partial_t^2 A + \frac{\partial k}{\partial I}|A|^2 A, \tag{1.4}$$

where $\partial_\omega k$ and $\partial_\omega^2 k$ are inversely proportional, respectively, to the group velocity and to the group velocity dispersion (GVD). Introducing retarted time $\tau = t - \partial_\omega k z$ and replacing $A(z,t)$ by $A(z,\tau)$, we can rewrite Eq. (1.4) in the form

$$i\partial_z A + \gamma\partial_\tau^2 A + \beta|A|^2 A = 0. \tag{1.5}$$

The γ and β are linked with $\partial_\omega^2 k$ and $\partial_I k$ and their absolute values can be scaled to any convenient constants via simple rescaling of τ and $|A|$. GVD is normal if $\gamma < 0$ and anomalous if $\gamma > 0$.

Eq. (1.5) has an important property: it is integrable equation, i.e. solutions of a certain class of the initial value problems formulated for Eq. (1.5) can be found analytically [1, 2]. This result puts NLS equation in line with other model nonlinear wave equations as for e.g. Korteveg-de-Vries (KdV) and Sine-Gordon (SG) equations which have the same integrability property, see e.g. [3]. Solitons are particular solutions of (1.5) which can be considered as nonlinear modes and building blocks for solving the initial value problem. Simplest of the solitary

solutions, and relevant in the context of the thesis, is the fundamental bright soliton. This solution exists if $\beta\gamma > 0$ and it is

$$A(\tau, z) = \sqrt{\frac{2\kappa}{\beta}} sech\left[\sqrt{\frac{\kappa}{\gamma}}(\tau - 2\gamma v z + \tau_0)\right] e^{i\kappa z + i\phi + iv\tau - i\gamma v^2 z}, \qquad (1.6)$$

here ϕ, τ_0, v, $|\kappa|$ are arbitrary constants and $sgn\kappa = sgn\gamma = sgn\beta$.

The integrability property implicitly contains information that solution (1.6) is stable with respect to small perturbations and that bright solitons survive collisions among themselves without any energy loss or exchange ('elastic' collisions) [3].

In spite of the great importance of integrable models, the property of integrability itself hardly can be identified as fundamental physical property, because it can be applied only to a certain very restricted set of models, and small deviations from these models generally destroy integrability and its consequences, as for example elasticity of interaction. However, presence of solitary solutions is not a feature of only integrable systems or even systems close to integrable. "Solitons" exist as solutions of a wide class of equations, which can be far from any integrable model. Thus *solitons themselves* can be considered as one of the fundamental manifestations of nonlinearity. We will use term "soliton" not only to describe solutions similar to (1.6), but also to describe more general exponentially localised states.

In this thesis we will consider stability properties and instability-induced dynamics of localised solutions of nonlinear partial differential equations of the parabolic type describing propagation of optical waves in media cubic, quadratic and saturable type of nonlinearities. These equations can be considered as generalisations of NLS equations to the cases of interaction of several waves in media with nonlinear and dispersion properties which are more complex then was assumed in Eq. (1.2).

General form of the model equations which we are going to consider below can

be written as

$$i\frac{\partial E_j}{\partial z} + \alpha_j \left(\frac{\partial^2 E_j}{\partial x^2} + \frac{\partial^2 E_j}{\partial y^2} \right) + \gamma_j \frac{\partial^2 E_j}{\partial t^2} + \mathcal{N}_j(E_1, E_1^*, \ldots, E_N, E_N^*) = 0, \quad (1.7)$$

where E_j $(j = 1, 2, \ldots N)$ are the complex functions describing multi-component field, $\mathcal{N}_j(E_1, E_1^*, \ldots, E_N, E_N^*)$ are linear and nonlinear terms arising due to interaction of the field components during propagation in the nonlinear medium, z is the propagation direction of the beams, x, y are the transverse coordinates, t is the time, α_j and γ_j are constants characterising, respectively, diffraction and group velocity dispersion.

All equations considered below are hamiltonian, i.e., one can construct a functional $H(E_j, E_j^*, \partial_x E_j, \partial_y E_j, \partial_t E_j, \partial_x E_j^*, \partial_y E_j^*, \partial_t E_j^*)$ such that

$$i\frac{\partial E_j}{\partial z} = \frac{\delta H}{\delta E_j^*}, \quad \frac{dH}{dz} = 0, \quad (1.8)$$

where $\delta H / \delta E_j^*$ is the variational derivative. Localisation of the solutions is assumed along one, several or all transverse coordinates. We will define the multi-component soliton $\vec{E}_s = (S_1, \ldots S_N)$ as stable if Eqs. (1.7) linearised near $\vec{E}_s$ do not have solutions growing in z. More precisely throughout this thesis only situations with exponential growth in z will be analysed, which excludes from the scope such special situations when exponentially growing modes are absent but power growth can exist, as it happens, e.g., for solitons in two-dimensional NLS equation [4].

We will consider three following classes of soliton instability:

- Instability of solitons with respect to perturbations, which are localised in the same dimensions as soliton itself and which in case of instability do not break the symmetry of the soliton (longitudinal or internal instability).
- Instability of one-dimensional spatial solitons with respect to temporal modulations arising due to group velocity dispersion (modulational instability of a soliton stripe).
- Instability of two-dimensional ring-like solitons with respect to perturbations along the rings (azimuthal modulational instability)

The author's main contribution to the knowledge about soliton stability is linked with the last two categories and this fact is reflected in the title of the thesis.

In talking about motivation for research in the field of optical solitons, the vast majority of authors refer to the potential applications for all-optical processing and transmission of information and I also share these hopes. However, up to now solitons remain fascinating physical phenomena, observed in numerous laboratories around the globe, studied in a huge number of theoretical papers and exciting minds of physicists and mathematicians of all ranks. My primary motivation for the research presented in this volume was a desire to develop my own understanding of the problem of the soliton stability and instability-induced dynamics.

After these short introductory comments the reader will find four Chapters, which constitute the main scientific content of the thesis, a summary of main results, list of references, list of the author's publications and several appendices. Each Chapter has its own introduction, which, together with references within the text itself, put the presented material in the context of the exesting knowledge.

Chapter 2

Modulational instability of bright solitary waves in incoherently coupled NLS equations

2.1 Introduction

The phenomenon of modulational instability (MI) can be defined as self-induced break up of an initially homogeneous wave during its evolution in a nonlinear medium. Study of this phenomenon has been initiated in the 1960's, when MI was predicted in plasma physics [5], nonlinear optics [6] and physics of fluids [7], and also observed experimentally in the form of filamentation of electromagnetic (e/m) waves in organic liquids [8]. Since that time MI has remained as one of the major topics of theoretical and experimental research in nonlinear physics and, in particularly, in nonlinear physics of conservative systems [9, 4, 10, 11, 12]. In this and following Chapters we will deal with several classic examples of such systems.

General formulation of the problem of nonlinear wave propagation via fundamental sets of equations, as for example, the Maxwell or Navier Stokes equations, is

a very demanding task even for modern computers. Therefore a number of simplified models have been introduced which approximately describe either propagation of the wave itself, e.g., KdV equation, or propagation of slowly varying wave envelope, e.g., the Nonlinear Schrödinger (NLS) equation [13].

The simplest solutions of the envelope equations are continuous wave (CW) solutions homogeneous in space and time. Development of MI of CWs in one-dimensional (1D) NLS equation leads to so-called Fermi-Pasta-Ulam (FPU) recurrence which consists of periodic alternation between homogeneous and filamentary profiles of wave envelope, see e.g. [11] and references therein. However, FPU recurrence is rather special, not a common property of nonlinear systems and perturbation of 1D NLS usually destroys it [14, 15]. Single NLS equation exhibits MI in cases when nonlinearity and group velocity dispersion (GVD) or diffraction act in opposite ways, i.e. when nonlinearity is positive GVD must be anomalous and if nonlinearity is negative GVD must be normal. This rule changes when one, accounting for the polarization, for the different directions of wave vectors, or for the different carrier frequencies of the interacting waves, replaces single NLS by the set of incoherently coupled NLS equations. Then, if nonlinear coupling is strong enough, MI becomes possible for any signs of nonlinearity and GVD [16-24].

Another important class of solutions of nonlinear equations are solitary solutions ('solitons'). These also exhibit MI when they are localized in some dimensions but extended in one or more others. MI of solitons was first considered by Zakharov in the context of single NLS equation [25] and later by Kadomtsev and Petviashvily for wave solitons in 2D generalization of KdV equation [26]. Later the problem was addressed in number of theoretical and experimental works. For reviews on MI of bright and dark solitary waves see, respectively, [9, 4, 10, 11] and [12].

From formal point of view the problem of the solitary wave MI can be considered as continuation of all discrete eigenvalues of the soliton spectrum at zero modulational frequency Ω into the region $\Omega \neq 0$. Important class of the discrete eigenmodes at $\Omega = 0$ are the zero eigenvalue (or neutral) modes, which can be

identified analytically considering small corrections to the solution appearing due to variations of the free parameters of the solution. Presence of these parameters can be associated with certain symmetry properties of the model equations.

On qualitative level similarities and differences between MI of solitons and CW solutions can be understood on the basis of the comparison between the corresponding neutral modes. E.g. 1D, bright spatial soliton of NLS equation is modulationally unstable in media with either anomalous or normal GVD. In the first case, neutral mode associated with the phase symmetry is excited ('neck' MI) and in latter situation translational mode associated with the shift along the direction perpendicular to the wave propagation becomes unstable ('snake' MI) [27]. Phase mode exists as well for CW solution and this leads to MI for anomalous GVD. However, translational mode of CW solution is null and therefore CWs are stable for normal GVD.

Increasing the number of the free parameters can lead to more complex scenarios of MI, because coexistence and competition between different types of the instabilities are likely to happen. In this Chapter we study MI of the bright solitary solutions in the incoherently coupled NLS equations. Incoherent nature of the coupling results in the presence of the two phase symmetries. These are responsible for appearance of the two free phases and parameterization of the solitons with two parameters characterising nonlinear corrections to the wavenumbers. This extra phase symmetry makes the main difference in MI of solitons in coupled NLS equations compare to single NLS. On the other hand major differences with previously mentioned case of CWs should be expected, due to presence of the translational neutral mode of the soliton spectrum.

The rest of this Chapter is organized as follows. In Section 2.2 we derive coupled NLS equations in the context of nonlinear optics. In Section 2.3 problem of MI of the solitary waves is formulated in general terms. MI of different kinds of the solitary solutions and physical interpretation in terms of the polarization dynamics are detailed in Sections 2.4 and 2.5. Discussion and summary of main results are given in Sections 2.6 and 2.7.

2.2 Incoherently coupled NLS equations in optics

2.2.1 Maxwell equations

Nonlinear dynamics of optical waves is the main subject of this work. Natural starting point to describe this dynamics is the fundamental set of Maxwell equations, which we consider for a particular case of a dielectric and nonmagnetic medium

$$\vec{\nabla} \times \vec{E} = -\mu_0 \partial_t \vec{H}, \tag{2.1}$$

$$\vec{\nabla} \times \vec{H} = \varepsilon_0 \partial_t \vec{E} + \partial_t \vec{P}. \tag{2.2}$$

Here $\vec{\nabla} = \vec{i}_x \partial_x + \vec{i}_y \partial_y + \vec{i}_z \partial_z$, vectors $\vec{i}_x, \vec{i}_y, \vec{i}_z$ constitute a Cartesian basis, $\vec{E}$ is the electric field, $\vec{H}$ is the magnetic field, $\vec{P}$ is the polarisation of the medium, ε_0 and μ_0 are, respectively, the electric and magnetic permittivities of the free space. Using standard manipulation and introducing velocity of light in free space $c = (\varepsilon_0 \mu_0)^{-1/2}$, Maxwell equations reduce to the equation linking the vectors of the electric field and of the polarisation

$$-\vec{\nabla}^2 \vec{E} + \vec{\nabla}(\vec{\nabla} \cdot \vec{E}) + \frac{1}{c^2} \partial_t^2 \vec{E} = -\frac{1}{\varepsilon_0 c^2} \partial_t^2 \vec{P}. \tag{2.3}$$

Now we are going to pass through a series of transformations, which reduce Maxwell equations to a set of simplified equations for slowly varying wave envelopes. Procedure which we apply is far from mathematically rigorous in the sense of the counting of all terms with the same order of magnitudes. It rather relies on physical intuition and is found to be in good agreement with many experiments.

Assuming that the electric field $|\vec{E}|$ is sufficiently weak compare to internal atomic fields, the polarisation can be presented as the power series of the components of $\vec{E}$

$$\vec{P} = \vec{P}^{(1)} + \vec{P}^{(2)} + \vec{P}^{(3)} + \ldots, \tag{2.4}$$

here $|\vec{P}^{(n)}| \sim |\vec{E}|^n$. Writing Eq. (2.4) we assumed absence of any static polarisation in the medium. Considering a medium with local response, and invoking the time-invariance principle and causality condition, the general form of terms in Eq. (2.4) appears to be [28]

$$P_i^{(1)}(\vec{r},t) = \varepsilon_0 \int_{-\infty}^{+\infty} d\tau R_{ij}^{(1)}(t-\tau) E_j(\vec{r},\tau), \tag{2.5}$$

$$P_i^{(2)}(\vec{r},t) = \varepsilon_0 \int_{-\infty}^{+\infty}\int_{-\infty}^{+\infty} d\tau_1 d\tau_2 R_{ijk}^{(2)}(t-\tau_1, t-\tau_2) E_j(\vec{r},\tau_1) E_k(\vec{r},\tau_2), \tag{2.6}$$

$$P_i^{(3)}(\vec{r},t) = \tag{2.7}$$

$$\varepsilon_0 \int_{-\infty}^{+\infty}\int_{-\infty}^{+\infty}\int_{-\infty}^{+\infty} d\tau_1 d\tau_2 d\tau_3 R_{ijkl}^{(3)}(t-\tau_1, t-\tau_2, t-\tau_3) E_j(\vec{r},\tau_1) E_k(\vec{r},\tau_2) E_l(\vec{r},\tau_3).$$

Here $R^{(n)}$ is the $n+1$ order tensor, indices i,j,k,l can be x,y or z, $\vec{r} = (x,y,z)$ and summation of the repeated indices is assumed. Because of causality condition $R^{(n)}(\xi_1, \ldots \xi_n) = 0$ if any $\xi_i < 0$. We will use below complex representation for field and polarisations, decomposing the real functions E_i and P_i into sum of two complex components

$$E_i = \tilde{E}_i + \tilde{E}_i^*, \tag{2.8}$$

In its turn $\tilde{E}_i$ is thought as superposition of quasimonochromatic waves:

$$\tilde{E}_i = \sum_\omega \tilde{E}_{\omega i} = \sum_\omega A_{\omega i}(x,y,z,t) e^{i\vec{k}_\omega \vec{r} - i\omega t}. \tag{2.9}$$

$A_{\omega i}$ are complex functions which vary slowly compare to the fast oscillations in space and in time described by the exponential multipliers. To consider polarisation of the nonlinear medium which drives the field, we introduce complex polarization $\tilde{P}_i$ in the following maner

$$P_i = \tilde{P}_i + \tilde{P}_i^*, \ \tilde{P}_i = \sum_\omega \tilde{P}_{\omega i}, \tag{2.10}$$

where $\tilde{P}_{\omega i}$ is the polarization at frequency ω.

2.2.2 Linear terms

First we simplify the linear part of Eqs. (2.3). Assuming that $R^{(1)}(t-\tau)$ is significantly different from zero only for small values of $t-\tau$, i.e. that linear

response of the medium is almost, but not exactly, instantaneous, we get

$$\tilde{P}_i^{(1)} \simeq \varepsilon_0 \sum_\omega e^{i\vec{k}_\omega \vec{r} - i\omega t} \int_{-\infty}^{+\infty} d\xi R_{ij}^{(1)}(\xi) e^{i\omega\xi} \left(1 - \xi\partial_t + \frac{1}{2}\xi^2\partial_t^2 + \ldots\right) A_{j\omega}(x,y,z,t) = \tag{2.11}$$

$$\varepsilon_0 \sum_\omega e^{i\vec{k}_\omega \vec{r} - i\omega t} \left(\chi_{ij}^{(1)}(\omega) + i\frac{\partial \chi_{ij}^{(1)}}{\partial\omega}\partial_t - \frac{1}{2}\frac{\partial^2 \chi_{ij}^{(1)}}{\partial\omega^2}\partial_t^2 + \ldots\right),$$

here

$$\chi_{ij}^{(1)}(\omega) = \int_{-\infty}^{+\infty} d\xi R_{ij}^{(1)}(\xi) e^{i\omega\xi}.$$

Considering spatial derivatives one has to remember that the Maxwell equations should be supplemented by the Gauss law, which in our case takes the form $\vec{\nabla} \cdot (\varepsilon_0 \vec{E} + \vec{P}) = 0$. Nonlinearity is assumed to be weak and fast, therefore, applying the Gauss law, we neglect the contribution of the terms $\vec{\nabla} \cdot \vec{P}^{(n)}$ with $n > 1$ and the corrections due to the non-instantaneous response of the medium. Results of further derivations depend on the specific properties of the medium, which we will keep as simple as possible. Simplest example is, of course, an isotropic medium ($\chi_{xx}^{(1)} = \chi_{yy}^{(1)} = \chi_{zz}^{(1)}$). In this case

$$0 = \vec{\nabla} \cdot (\varepsilon_0 \vec{E} + \vec{P}) \simeq \varepsilon_0 \varepsilon_x \vec{\nabla} \cdot \vec{E},$$

here $\varepsilon_i = (1 + \chi_{ii}^{(1)})$ and an implicit assumption was made that a coordinate system oriented along optical axis of the medium is used. Thus Eq. (2.3) becomes

$$-\vec{\nabla}^2 \vec{E} + \frac{1}{c^2}\partial_t^2 \vec{E} = -\frac{1}{\varepsilon_0 c^2}\partial_t^2 \vec{P}. \tag{2.12}$$

To use an approximation of slowly varying amplitudes it is convenient to move from the crystal basis (x, y, z) into the coordinate system (x', y', z') related to the beam propagating along z' axis. To make further simplifications of the linear operator acting on the electric field we assume that $|\partial_t \vec{A}_\omega| \ll \omega |\vec{A}_\omega|$ and $|\partial_{z'} \vec{A}_\omega| \ll k_\omega |\vec{A}_\omega|$, where z' is the propagation direction. Obviously without restriction of generality for the linearly isotropic medium we can choose $(x', y', z') = (x, y, z)$. Then linear parts of the equations for $A_{\omega i}$ take the form

$$-(i2k_\omega \partial_z + \partial_x^2 + \partial_y^2) A_{\omega i} = \frac{\omega^2}{c^2}(i\partial_\omega \chi^{(1)} \partial_t - \frac{1}{2}\partial_\omega^2 \chi^{(1)} \partial_t^2) A_{\omega i} + holnt. \tag{2.13}$$

Here k_ω obeys

$$k_\omega^2 = \frac{\omega^2}{c^2}(1 + \chi^{(1)}(\omega)), \tag{2.14}$$

and *'holnt'* stands for 'higher order linear and nonlinear terms'. In the paraxial approximation $A_{z\omega} = 0$, therefore $i = x, y$. In the leading order, derivatives of the first order susceptibility can be approximated as

$$\partial_\omega \chi^{(1)} \simeq \frac{2k_\omega c^2}{\omega^2}\partial_\omega k_\omega, \quad \partial_\omega^2 \chi^{(1)} \simeq \frac{2k_\omega c^2}{\omega^2}\partial_\omega^2 k_\omega,$$

for more see e.g. [11]. In its finally simplified, but not yet renormalised, form the linear parts of the equations are

$$-(i2k_\omega \partial_z + \partial_x^2 + \partial_y^2)A_{\omega x,y} = 2k_\omega(i\partial_\omega k_\omega \partial_t - \frac{1}{2}\partial_\omega^2 k_\omega \partial_t^2)A_{\omega x,y} + holnt. \tag{2.15}$$

2.2.3 Nonlinear terms

For an isotropic medium replacing of $\vec{E}$ with $-\vec{E}$ should not lead to modification of governing equations therefore $R^{(2)} = 0$ and lowest order nonlinearity is the cubic one. Remembering that nonlinearity is small and fast, we neglect all effects related with delay of the nonlinear response. Thus general form of the nonlinear response at frequency $\omega_4 = \omega_1 + \omega_2 + \omega_3$ is [29]

$$\tilde{P}^{(3)}_{\omega_4 i} = \varepsilon_0 \sum_\omega \chi^{(3)}_{ijkl}(\omega_1, \omega_2, \omega_3)\tilde{E}_{j\omega_1}\tilde{E}_{k\omega_2}\tilde{E}_{l\omega_3}, \tag{2.16}$$

where

$$\chi^{(3)}_{ijkl}(\omega_1, \omega_2, \omega_3) = \int_{-\infty}^{+\infty} d\xi_1 \int_{-\infty}^{+\infty} d\xi_2 \int_{-\infty}^{+\infty} d\xi_3 R^{(3)}_{ijkl}(\xi_1, \xi_2, \xi_3)e^{i\omega_1\xi_1 + i\omega_2\xi_2 + i\omega_3\xi_3}$$

Summation in (2.16) is assumed over all sets of $(\omega_1, \omega_2, \omega_3)$ which satisfy $(\omega_1 + \omega_2 + \omega_3 = \omega_4)$. In this Chapter we will consider the case when field propagating in the nonlinear medium has only one frequency component ω. Thereby we neglect the third and other harmonics, which generally appear during propagation in nonlinear media. Terms responsible for harmonic generation are negligible providing that $|(Nk(\omega) - k(N\omega))A_\omega| \gg |\partial_z A_\omega|$, $N = 2, 3, \ldots$. Resulting expressions for the nonlinear polarisation components are [28]

$$\tilde{P}^{(3)}_{x,y} = \varepsilon_0(6\chi_{xxyy}\tilde{E}_{x,y}(|\tilde{E}_x|^2 + |\tilde{E}_y|^2) + 3\chi_{xyyx}\tilde{E}^*_{x,y}(\tilde{E}_x^2 + \tilde{E}_y^2)), \tag{2.17}$$

where index ω was omitted. Thus equations describing propagation of single frequency electromagnetic field in isotropic media are in fact coupled nonlinear Schrödinger equations

$$(i2k_\omega\partial_z + \partial_x^2 + \partial_y^2 - k_\omega(\partial_\omega^2 k_\omega)\partial_\tau^2)A_x + \tag{2.18}$$

$$\frac{\omega^2}{c^2}(6\chi_{xxyy}A_x(|A_x|^2 + |A_y|^2) + 3\chi_{xyyx}A_x^*(A_x^2 + A_y^2)) = 0,$$

$$(i2k_\omega\partial_z + \partial_x^2 + \partial_y^2 - k_\omega(\partial_\omega^2 k_\omega)\partial_\tau^2)A_y + \tag{2.19}$$

$$\frac{\omega^2}{c^2}(6\chi_{xxyy}A_y(|A_x|^2 + |A_y|^2) + 3\chi_{xyyx}A_y^*(A_x^2 + A_y^2)) = 0,$$

where $\tau = t - (\partial_\omega k_\omega)z$. Below we consider the case of self-focusing nonlinearity, i.e. $\chi^{(3)}_{ijkl} > 0$.

Now we introduce dimensionless independent and dependent variables

$$\xi = \frac{x}{w},\ \eta = \frac{y}{w},\ \tau' = \frac{\tau}{T},\ \zeta = \frac{z}{k_\omega w^2},\ A'_{x,y} = \frac{\omega w}{c}\sqrt{3\chi_{xxyy}}A_{x,y},$$

where w is the characteristical transverse size of the pulse, T is the pulse duration, $k_\omega w^2$ is the diffraction length. In new variables Eqs. (2.18),(2.19) become

$$(i2\partial_\zeta + \partial_\xi^2 + \partial_\eta^2 - \frac{w^2 k_\omega \partial_\omega^2 k_\omega}{T^2}\partial_\tau^2)A_{x,y} + \tag{2.20}$$

$$(2A_{x,y}(|A_x|^2 + |A_y|^2) + \frac{\chi_{xyyx}}{\chi_{xxyy}}A_{x,y}^*(A_x^2 + A_y^2)) = 0,$$

where we dropped all primes. Obviously, τ can be rescaled again in such a way to make the absolute value of the coefficient in front of ∂_τ^2 by any convenient constant. However it is useful to first note that the closer our pulse is to a monochromatic wave ($T \to \infty$) the less important the GVD term is. On the other hand, the closer the transverse profile of the pulse to infinitely extended plane wave ($w \to \infty$) the less important the diffraction term compared to the GVD one.

Introducing circularly polarised basis

$$E_{1,2} = \frac{1}{\sqrt{2}}(A_x \pm iA_y)$$

and rescaling τ, we find that $A_{1,2}$ obey

$$i\partial_z E_{1,2}+\frac{1}{2}\left(\partial_x^2+\partial_y^2-sgn(\partial_\omega^2 k)\partial_t^2\right)E_{1,2}+\left(|E_{1,2}|^2+\left[1+\frac{\chi_{xyyx}}{\chi_{xxyy}}\right]|E_{2,1}|^2\right)E_{1,2}=0, \tag{2.21}$$

where for the sake of clarity we informally reintroduced x, y, z and t variables. Putting $\gamma = -sgn(\partial_\omega^2 k)/2$ and $\beta = 1 + \chi_{xyyx}/\chi_{xxyy}$ we obtain coupled NLS equations in the final form we are going to work with

$$\begin{aligned} i\partial_z E_1 + \frac{1}{2}\vec{\nabla}_\perp^2 E_1 + \gamma\partial_t^2 E_1 + (|E_1|^2 + \beta|E_2|^2)E_1 = 0, \\ i\partial_z E_2 + \frac{1}{2}\vec{\nabla}_\perp^2 E_2 + \gamma\partial_t^2 E_2 + (|E_2|^2 + \beta|E_1|^2)E_2 = 0, \end{aligned} \tag{2.22}$$

here $\vec{\nabla}_\perp = \vec{i}\partial_x + \vec{j}\partial_y$. Longitudinal z and transverse x, y coordinates are respectively measured in units of a suitable diffraction length $l_{dif} = kw^2$ and of a transverse pulse size w. Temporal coordinate t is the retarded time scaled to the parameter $T\sqrt{l_{dif}/l_{dis}}$, where $l_{dis} = T^2/|\partial_\omega^2 k|$ is the characteristic GVD length. Examples of practically relevant choices of β are: $\beta = 2$ for the nonresonant electronic nonlinearity and $\beta = 7$ for the nonlinearity due to molecular orientation [28].

Counterpropagation of scalar waves in nonlinear media also obeys Eqs. (2.22) with β describing the wavelength-scale refractive index gratings written by the interference pattern [21, 22]. Value of β in this situation is directly linked with diffusion which washes out the grating making $1 \leq \beta \leq 2$ ($\beta = 2$ for zero diffusion). Envelopes of incoherent copropagating waves in Kerr media also obey Eqs. (1) with $\beta = 2$ [19]. In these two situations the group velocity difference of the wave envelopes can be removed by a suitable phase shift [11].

2.3 Modulational instability of solitons. General formulation of the problem

The primary target of this Chapter is understanding of the instabilities of the ground-state, i.e. nodeless, spatially localised solutions of Eqs. (2.22) under

the action of the t-dependent perturbations. Here, we restrict ourselves to the situation when the solitary waves are stable for $\partial_t = 0$. Therefore we assume that $\vec{\nabla}_\perp = \vec{i}\partial_x$, to avoid collapse [4, 10, 30]. General properties of these solitons for $\gamma = 0$ are known, see, e.g. [31, 32, 33, 34, 35] and refs. therein.

It is important for the following to summarize relevant symmetry properties of Eqs. (1) with suppressed time derivatives ($\partial_t = 0$). Invariance with respect to the two-parameter gauge transformation

$$(E_1, E_2) \to (E_1 e^{i\phi_1}, E_2 e^{i\phi_2}), \tag{2.23}$$

leads to conservation of the energies $Q_{1,2} = \int dx |E_{1,2}|^2$ or their equivalent combinations. There are also invariances with respect to transverse translations and Galilean transformation,

$$E_{1,2}(x) \to E_{1,2}(x + x_0), \tag{2.24}$$

$$E_{1,2}(x) \to E_{1,2}(x - vz) e^{iv(x - vz/2)}. \tag{2.25}$$

ϕ_1, ϕ_2, x_0 and v are free parameters.

Symmetry property (2.23) indicates that the solitary solutions can be presented in the form

$$E_{1,2}(x, z) = A_{1,2}(x) e^{i\kappa_{1,2} z}. \tag{2.26}$$

$A_{1,2}(x)$ are real functions obeying the system of ordinary differential equations

$$\frac{1}{2}\partial_x^2 A_{1,2} = \kappa_{1,2} A_{1,2} - (A_{1,2}^2 + \beta A_{2,1}^2) A_{1,2}. \tag{2.27}$$

Exponential localization of the solitons requires $\kappa_{1,2} > 0$. Actually one of these parameters can always be scaled away, which means that fixing one of them and varying the other in the whole region of the solitary wave existence one will capture all possible situations. However, for convenience of analytical calculations it is better to keep them both.

To study MI we seek solutions of Eq. (2.22) in the form of spatial solitons weakly modulated in time at frequency $\Omega \geq 0$

$$E_{1,2}(x, z) = (A_{1,2}(x) +$$
$$(U_{1,2}(x, z) + iW_{1,2}(x, z)) \cos \Omega t) e^{i\kappa_{1,2} z + i\phi_{1,2}}. \tag{2.28}$$

Presenting solution of the linearized real system for the small perturbations U_m, W_m in the form $U_m \sim u_m(x)e^{\lambda z}$ and $W_m \sim w_m(x)e^{\lambda z}$ we obtain following eigenvalue problem (EVP)

$$(\hat{\mathcal{L}}_1 + \gamma\Omega^2\hat{I})\vec{u} = -\lambda\vec{w}, \qquad (2.29)$$
$$(\hat{\mathcal{L}}_0 + \gamma\Omega^2\hat{I})\vec{w} = \lambda\vec{u},$$

where $\vec{u} = (u_1, u_2)^T$, $\vec{w} = (w_1, w_2)^T$ and $\hat{I}$ is the unit operator. $\hat{\mathcal{L}}_0$ and $\hat{\mathcal{L}}_1$ are:

$$\hat{\mathcal{L}}_0 = \begin{pmatrix} -\frac{1}{2}\partial_x^2 + \kappa_1 - A_1^2 - \beta A_2^2 & 0 \\ 0 & -\frac{1}{2}\partial_x^2 + \kappa_2 - A_2^2 - \beta A_1^2 \end{pmatrix}, \qquad (2.30)$$

$$\hat{\mathcal{L}}_1 = \begin{pmatrix} -\frac{1}{2}\partial_x^2 + \kappa_1 - 3A_1^2 - \beta A_2^2 & -2\beta A_1 A_2 \\ -2\beta A_1 A_2 & -\frac{1}{2}\partial_x^2 + \kappa_2 - 3A_2^2 - \beta A_1^2 \end{pmatrix}. \qquad (2.31)$$

By means of simple transformation one can reduce EVP (2.29) to the two following EVPs for real and imaginary parts of the perturbations:

$$(\hat{\mathcal{L}}_0 + \gamma\Omega^2\hat{I})(\hat{\mathcal{L}}_1 + \gamma\Omega^2\hat{I})\vec{u} = -\lambda^2\vec{u}, \qquad (2.32)$$
$$(\hat{\mathcal{L}}_1 + \gamma\Omega^2\hat{I})(\hat{\mathcal{L}}_0 + \gamma\Omega^2\hat{I})\vec{w} = -\lambda^2\vec{w}. \qquad (2.33)$$

EVPs (2.32), (2.33) are adjoint to each other. Therefore they have identical spectra and in case of instability the imaginary and real parts of perturbations grow with the same rates. To answer stability question it is thus enough to study only one of the EVPs, and we concentrate below on the EVP (2.33).

Let suppose that $(\kappa_{1,2} + \gamma\Omega^2) \geq 0$. Then, generally, $\lambda^2 \in (-\infty, -\lambda_g^2)$ is a continuous part of the spectrum with unbounded eigenfunctions, where $\lambda_g = \min(\xi_1, \xi_2)$ and $\xi_{1,2} = \kappa_{1,2} + \gamma\Omega^2$. For particular cases when $\hat{\mathcal{L}}_1$ becomes a diagonal operator the continuum splits into two independent bands, $(-\infty, -\xi_{1,2}^2)$, corresponding to unboundness of $w_1(x)$ and $w_2(x)$, respectively. Eigenvalues which do not belong to the continuum constitute the discrete part of the spectrum with bounded eigenfunctions. Stable eigenmodes of the discrete spectrum ('gap' modes) can have eigenvalues only inside the gap of the negative part of the real axis in the $(Re\lambda^2, Im\lambda^2)$-plane from the edge of continuum up to $\lambda^2 = 0$. Presence of any

other mode of the discrete spectrum indicates instability of solitons. If $\xi_1 < 0$ and/or $\xi_2 < 0$, the gap is closed, $\lambda_g = 0$.

Procedure which we mainly follow to study stability of different types of solitary solutions consists of three basic steps. First, using analytical and numerical analysis we identify the discrete spectrum of the EVP (2.33) for $\Omega = 0$. Second, we develop perturbation theory for the neutral eigenmodes in the low-frequency limit, $\Omega \ll 1$. Third, we numerically build continuations of all discrete eigenvalues into the region of positive Ω. We also allow for possible splitting of discrete eigenvalues from the edge of the continuum, but this was never actually observed.

2.4 Instabilities of circularly polarized and Manakov solitons

The single wave solitons of Eqs. (2.27) corresponding to the right and left circular polarized e/m waves are

$$A_1(x) = \sqrt{2\kappa_1}sech\sqrt{2\kappa_1}x, \quad A_2 = 0, \tag{2.34}$$

$$A_1 = 0, \quad A_2(x) = \sqrt{2\kappa_2}sech\sqrt{2\kappa_2}x. \tag{2.35}$$

For these solutions, EVP (2.33), separates in two independent scalar problems. Considering for example stability of solution with $A_1 \neq 0$ we get:

$$(\hat{\mathcal{N}}_1 + \gamma\Omega^2)(\hat{\mathcal{N}}_0 + \gamma\Omega^2)w_1 = -\lambda^2 w_1, \tag{2.36}$$

$$\left(-\frac{1}{2}\partial_x^2 + \kappa_2 + \gamma\Omega^2 - \beta A_1^2\right)^2 w_2 = -\lambda^2 w_2, \tag{2.37}$$

where $\hat{\mathcal{N}}_0 = -\frac{1}{2}\partial_x^2 + \kappa_1 - A_1^2$, $\hat{\mathcal{N}}_1 = -\frac{1}{2}\partial_x^2 + \kappa_1 - 3A_1^2$.

Operator on the left hand side of (2.37) has nonnegative spectrum therefore corresponding values of λ_n^2 ($n = 0, 1, 2, 3\ldots$) must be nonpositive, which means absence of unstable eigenmodes. In fact eigenvalue problem (2.37) can be solved analytically, see, e.g. [36]. The eigenvalues are

$$\lambda_n^2 = -\left(\kappa_2 + \gamma\Omega^2 - \frac{\kappa_1}{4}\left[\sqrt{8\beta + 1} - 2n - 1\right]^2\right)^2. \tag{2.38}$$

For $\Omega = 0$ points $\lambda_n = 0$ specify surfaces in the parameter space where single wave solitary solution (2.34) branches giving onset to the ground state ($n = 0$) and higher order ($n \geq 1$) coupled ($A_{1,2} \neq 0$) solitary solutions. Let us note, that soliton dynamics caused by an excitation of the gap modes within framework of the time independent Eqs. (1) is fascinating subject on its own [33].

Eq. (2.36) is exactly an EVP arising in theory of MI of solitons in single NLS equation [9, 10]. The discrete spectrum of operator $\hat{\mathcal{N}}_1\hat{\mathcal{N}}_0$ consists of two neutral ($\lambda = 0$) eigenmodes which can be readily identified by applying infinitesimal phase and Galilean transforms to solitary wave solution. These modes are $w_{1\phi_1} = A_1$ and $w_{1v} = xA_1$. Infinitesimal translations and variations of κ_1 generate two neutrally stable modes of the adjoint operator $\hat{\mathcal{N}}_0\hat{\mathcal{N}}_1$ which are $u_{1x} = \partial_x A_1$ and $u_{1\kappa_1} = \partial_{\kappa_1} A_1$. These modes obey the following identities: $\hat{\mathcal{N}}_0 w_{1\phi_1} = 0$, $\hat{\mathcal{N}}_0 w_{1v} = -u_{1x}$, $\hat{\mathcal{N}}_1 u_{1\kappa_1} = -w_{1\phi_1}$, $\hat{\mathcal{N}}_1 u_{1x} = 0$.

Following [27] we assume $\Omega^2 \ll 1$ and substitute the asymptotic expansions

$$w_1 = (w_1^{(0)} + \Omega^2 w_1^{(1)} + \ldots), \tag{2.39}$$

and

$$\lambda^2 = \Omega^2(\lambda^{(1)^2} + \Omega^2\lambda^{(2)^2} + \ldots) \tag{2.40}$$

into Eq. (2.36). In the first two orders we have $\hat{\mathcal{N}}_1\hat{\mathcal{N}}_0 w^{(0)} = 0$ and $\hat{\mathcal{N}}_1\hat{\mathcal{N}}_0 w^{(1)} = -\lambda^{(1)^2} w^{(0)} - \gamma(\hat{\mathcal{N}}_0 + \hat{\mathcal{N}}_1) w^{(0)}$. Solution in leading order is $w_1^{(0)} = C_{\phi_1} w_{1\phi_1} + C_v w_{1v}$, where C_{ϕ_1}, C_v are constants. Orthogonality properties $\langle w_{1\phi_1}, u_{1x}\rangle = \langle w_{1v}, u_{1\kappa_1}\rangle = 0$ (here and below $\langle \vec{f}, \vec{g}\rangle = \sum_m \int dx f_m g_m$) result in the independence of the branches produced by the phase and Galilean neutral modes. Therefore C_{ϕ_1} and C_v are in fact independent constants. Solvability condition of the 1st order problem in the class of the spatially localised functions gives

$$\lambda_{\phi_1}^{(1)^2} = 2\gamma \frac{Q_1}{\partial_{\kappa_1} Q_1} = 4\gamma\kappa_1, \tag{2.41}$$

$$\lambda_v^{(1)^2} = -2\gamma \frac{\langle u_{1x}, u_{1x}\rangle}{Q_1} = -\frac{4}{3}\gamma\kappa_1. \tag{2.42}$$

Eqs. (2.41), (2.42) indicate onset of instability for either sign of γ. However, the character of the instability depends on the sign of γ. For anomalous GVD

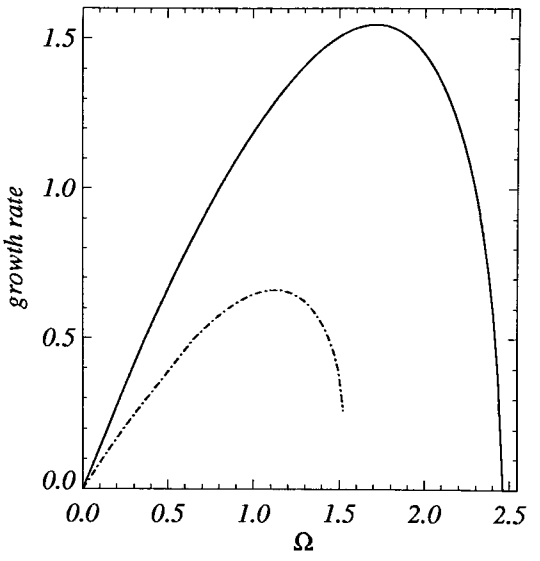

Figure 2.1: Instability growth rates of the circularly polarized soliton vs Ω, $\kappa_1 = 1$. *Full (dot-dashed) line is for neck (snake) MI,* $\gamma = 0.5$ ($\gamma = -0.5$).

($\gamma > 0$) the spatially symmetric eigenmode gets unstable leading to clustering of the soliton stripe into filaments which collapse during propagation (neck MI). For normal GVD ($\gamma < 0$) an excitation of the antisymmetric eigenmode leads to the spatial symmetry breaking and bending of the solitary stripe along the temporal coordinate (snake MI). Period of the modulations is approximately equal to $2\pi/\Omega_{max}$, where Ω_{max} can be defined by the condition $\partial\lambda/\partial\Omega = 0$.

Typical dependencies of the MI growth rates vs Ω are presented at Fig. 2.1. Neck instability disappears at $\Omega_{\phi_1} = \sqrt{3\kappa_1/\gamma}$ having $w_1 = 0$ and $u_1 = sech^2\sqrt{2\kappa_1}x$. For $\Omega > \Omega_{\phi_1}$ corresponding eigenmode becomes the gap one. Note, that for $\gamma > 0$ the gap becomes wider with increasing of Ω. Scenario of the snake instability disappearance is very difficult to track numerically because corresponding eigenmode develops oscillating tails and becomes weakly localized therefore a larger number of the grid points is required. However, our numerical analysis clearly indicates that the branch of the snake MI does not disappear stepwise at the point where the gap is closed, $\Omega_g = \sqrt{-\kappa_1/\gamma}$, as was suggested in Ref. [9], but continues beyond this point and probably approaches $\lambda^2 = 0$ with further increasing of Ω.

Nonlinear stage of MI is also perfectly analogous to MI in single NLS. Most

intense among the filaments, formed as the result of the neck MI development, collapse to singularity during further propagation [4, 10]. The snake MI leads to soliton spreading due to unbalanced action of the self-focusing nonlinearity and normal GVD [10]. The second field E_2 is not affected by the discussed instabilities. Obviously, this is the consequence of the incoherent nature of the coupling between E_1 and E_2.

In special case $\beta = 1$ Eqs.(1),(2) are invariant under the arbitrary rotations in (E_1, E_2) plane, $E_{1,2} \to \cos\vartheta E_{1,2} \pm \sin\vartheta E_{2,1}$, it leads to a new parameterization of the ground state solitons. These usually called Manakov solitons [37] and they are given by the solutions of Eqs. (2.27) with $\kappa_{1,2} = \kappa$:

$$A_1 = \cos\theta A(x), \quad A_2 = \sin\theta A(x), \tag{2.43}$$

here the angle θ is a new free parameter characterizing the polarization angle and $A(x) = \sqrt{2\kappa} sech \sqrt{2\kappa} x$.

Because of the rotational invariance, Manakov solitons with different polarizations are equivalent and analysis of their MI always leads to the same results, independent of polarization angle. Therefore one can always fix $\theta = 0$, then the corresponding EVP coincides with Eqs. (2.36), (2.37). Stress, that this equivalence holds only if Eqs. (1) with $\partial_t = 0$ and with $\partial_t \neq 0$ are both invariant on the above mentioned rotations, which is the case for $\alpha_1 = \alpha_2$, $\gamma_1 = \gamma_2$.

2.5 Instabilities of linearly and elliptically polarized solitons

2.5.1 Soliton family and associated neutral modes

To study solitons of an arbitrarily polarization for $\beta \neq 1$, i.e. $A_1 \neq 0$ and $A_2 \neq 0$, it is more convenient to introduce total, $\varphi = \frac{1}{2}(\phi_1 + \phi_2)$, and relative, $\psi = \frac{1}{2}(\phi_1 - \phi_2)$, phases. Then corresponding integrals of motion are the total

energy $Q = Q_1 + Q_2$ and energy unbalance $Q_u = Q_1 - Q_2$. Associated soliton parameters are $\kappa = \frac{1}{2}(\kappa_1 + \kappa_2)$ and $\delta = \frac{1}{2}(\kappa_1 - \kappa_2)$.

Obviously for $\delta = 0$ there is an analytical solution of Eqs. (2.27)

$$A_{1,2}(x) = A(x) = \sqrt{\frac{2\kappa}{1+\beta}} sech\sqrt{2\kappa}x, \tag{2.44}$$

corresponding to the linearly polarized soliton. It is important for the following study of MI to understand the question about continuation of this solution into the region of finite δ, i.e. its link with the family of the elliptically polarized solitons. Expanding $A_{1,2}$ in a Taylor series around $\delta = 0$, $A_{1,2}(x) = A \pm \partial_\delta A_1 \delta + O(\delta^2)$, and substituting into Eqs. (2.27) we get the equation for the unknown value of $\partial_\delta A_1$ at $\delta = 0$:

$$\left(\frac{1}{2}\partial_x^2 - \kappa + (3-\beta)A^2\right)\partial_\delta A_1 = A. \tag{2.45}$$

Using numerical solution of either Eq. (2.45) or Eq. (2.27) one can verify that for $\beta \neq 1$ the exact solution (2.44) belongs to the family of the solitary solutions parameterized by κ and δ. For $\beta = 1$ the homogeneous problem associated with Eq. (2.45) has solution $\sqrt{2}A$, which is obviously not orthogonal to the right-hand side of Eq. (2.45). Thus spatially bounded solution of Eq. (2.45) does not exist and therefore different parameterization of the solitons must be considered, see Eqs. (2.43).

Using Eq. (2.38) for $n = 0$ and its analog for the solution (2.35) we conclude that for the fixed values of κ and β, a family of the ground state coupled solitary solutions of Eqs. (3) exists for $\delta \in (-\delta_c, \delta_c)$, where

$$\delta_c = \kappa \left| \frac{1 - 4\beta + \sqrt{1+8\beta}}{3 + 4\beta - \sqrt{1+8\beta}} \right|. \tag{2.46}$$

$\delta_c = 0$ for $\beta = 1$ and the coupled solitons parameterized by κ and δ values do not exist in accord with the asymptotical analysis for small $|\delta|$. Obviously Eq. (2.46) can be equally reformulated to find critical values of either κ or β for other two parameters fixed. Expression under the modulus in eq. (2.46) changes its sign from plus to minus once β changes from $\beta < 1$ to $\beta > 1$. It follows that for $\beta < 1$ the family of elliptically polarized solitons splits from the family $A_2 = 0$ ($A_1 = 0$)

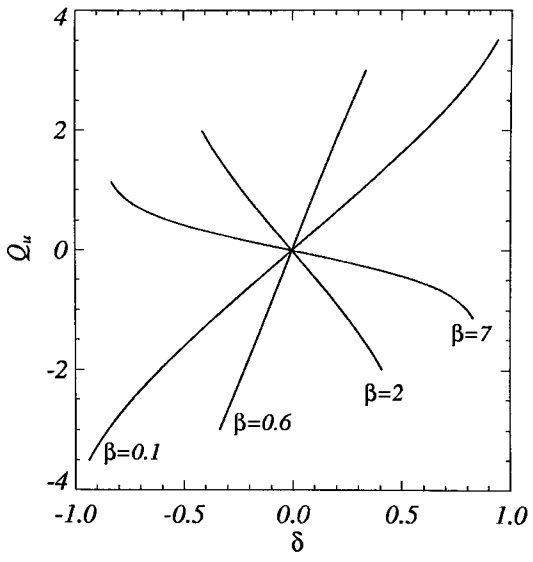

Figure 2.2: Energy unbalancing Q_u vs δ, $\kappa = 1$.

of the circularly polarized ones at $\delta = \delta_c$ ($\delta = -\delta_c$) and this is *vice versa* for $\beta > 1$. Continuous variation of δ from $-\delta_c$ to δ_c for fixed κ and $\beta < 1$ ($\beta > 1$) results in monotonic decay of Q_2 (Q_1) from its maximal value Q_+ (Q_-) down to zero and in growth of Q_1 (Q_2) from zero up to Q_+ (Q_-), where $Q_\pm = 2\sqrt{2(\kappa \pm \delta_c)}$. Therefore, we can make another conclusion important for us, that for $\beta < 1$ $\partial_\delta Q_u > 0$ and for $\beta > 1$ $\partial_\delta Q_u < 0$. Numerically build dependencies of Q_u vs δ for different values of β are presented in Fig. 2.2.

Consider now main spectral properties of this soliton family for $\Omega = 0$ and $\beta \neq 0$. Phase and Galilean symmetries generate three neutral eigenmodes of the EVP (2.33), they are $\vec{w}_\varphi = (A_1, A_2)^T$, $\vec{w}_\psi = (A_1, -A_2)^T$, and $\vec{w}_v = x(A_1, A_2)^T$. Infinitesimal variations of κ and δ, and translational symmetry generate neutral modes of the adjoint problem (2.32): $\vec{u}_\kappa = \partial_\kappa(A_1, A_2)^T$, $\vec{u}_\delta = \partial_\delta(A_1, A_2)^T$, and $\vec{u}_x = \partial_x(A_1, A_2)^T$. These six modes obey the following identities $\hat{\mathcal{L}}_0\vec{w}_\varphi = 0$, $\hat{\mathcal{L}}_0\vec{w}_\psi = 0$, $\hat{\mathcal{L}}_0\vec{w}_v = -\vec{u}_x$, $\hat{\mathcal{L}}_1\vec{u}_\kappa = -\vec{w}_\varphi$, $\hat{\mathcal{L}}_1\vec{u}_\delta = -\vec{w}_\psi$, $\hat{\mathcal{L}}_1\vec{u}_x = 0$.

For $\beta = 0$ our problem separates in two independent NLS equations. The independence of the two fields results in additional translational and Galilean symmetries characterizing freedom of the relative transverse translation and motion

of the two waves. Therefore EVPs (2.32) and (2.33) have additional neutral modes $\vec{u}_{\delta x} = \partial_x(A_1, -A_2)^T$, $\vec{w}_{\delta v} = x(A_1, -A_2)^T$. As shows numerical solution for $0 < \beta < 1$ the corresponding eigenvalue produces stable branch of the discrete spectrum. For $|\beta| \ll 1$ approximate expression for this eigenvalue can be readily found [33], $\lambda^2_{\delta v} = -64\beta/15$. Excitation of the corresponding eigenmode results in the anti-phase snaking of the soliton upon its propagation along z direction [33]. When $\beta \to 1$ this eigenmode disappears into the continuum [33].

Numerical investigation shows that, for the coupled solitons discussed here, EVP (2.33) for $\Omega = 0$ has only the four above mentioned eigenmodes in its discrete spectrum.

2.5.2 Asymptotical stability analysis

Now assuming that $\beta \gg \Omega^2$ we can use the asymptotic techniques described in the previous section to continue zero-eigenvalue modes into the region of $\Omega^2 \ll 1$. Making substitutions

$$\vec{w} = (\vec{w}^{(0)} + \Omega^2 \vec{w}^{(1)} + \ldots) \tag{2.47}$$

and of Eq. (2.40) into (2.33) we get in the first two orders: $\hat{\mathcal{L}}_1 \hat{\mathcal{L}}_0 \vec{w}^{(0)} = 0$ and

$\hat{\mathcal{L}}_1 \hat{\mathcal{L}}_0 \vec{w}^{(1)} = -{\lambda^{(1)}}^2 \vec{w}^{(0)} - \gamma(\hat{\mathcal{L}}_0 + \hat{\mathcal{L}}_1)\vec{w}^{(0)}$. Solution in the leading order is $\vec{w}^{(0)} = C_\varphi \vec{w}_\varphi + C_\delta \vec{w}_\delta + C_v \vec{w}_v$. In analogy with previous subsection one can show that the branches produced by the two phase modes on the one hand and by the Galilean mode on the other are independent. The solvability condition of the first order problem for the Galilean mode gives

$$\lambda_v^{(1)^2} = -2\gamma \frac{\langle \vec{u}_x, \vec{u}_x \rangle}{Q}, \tag{2.48}$$

which implies snake instability for $\gamma < 0$. When $\delta = 0$, $\lambda_v^{(1)^2} = -4\gamma\kappa/3$, cf. Eq. (2.42).

For the two phase modes solvability condition results in a quadratic equation for

$\lambda^{(1)^2}$

$$a\lambda^{(1)^4} + b\lambda^{(1)^2} + c = 0, \tag{2.49}$$

where

$$4a = \partial_\kappa Q_u \partial_\delta Q - \partial_\kappa Q \partial_\delta Q_u,$$

$$2b = \gamma Q(\partial_\kappa Q + \partial_\delta Q_u) - \gamma Q_u(\partial_\kappa Q_u + \partial_\delta Q),$$

$$c = -4\gamma^2 Q_1 Q_2.$$

Corresponding values of C_φ and C_ψ are linked through the equality

$$\frac{C_\varphi}{C_\psi} = \frac{2\gamma Q - \lambda^{(1)^2}\partial_\delta Q_u}{\lambda^{(1)^2}\partial_\delta Q - 2\gamma Q_u},$$

where $\lambda^{(1)^2}$ is the corresponding root of Eq. (2.49). In the general case expressions for the roots of Eq. (2.49) can not be analyzed analytically, but it is already clear that four symmetric neck type eigenmodes exist and two of them can be potentially responsible for instability.

If $\delta = 0$ then $\langle \vec{w}_\varphi, \vec{u}_\delta \rangle = \langle \vec{w}_\psi, \vec{u}_\kappa \rangle = 0$ and therefore $\vec{w}_\varphi$ and $\vec{w}_\psi$ eigenmodes produce independent branches of the discrete spectrum. It results in the independence between C_φ and C_ψ and simplifies formulas for the associated eigenvalues:

$$\lambda_\varphi^{(1)^2} = 2\gamma \frac{Q}{\partial_\kappa Q} = 4\gamma\kappa, \tag{2.50}$$

$$\lambda_\psi^{(1)^2} = 2\gamma \frac{Q}{\partial_\delta Q_u} = 2\gamma\kappa f(\beta). \tag{2.51}$$

Here $f(\beta) = (\int sechx\ g(x,\beta)\ dx)^{-1}$ and function g obeys $(\partial_x^2 - 1 + 2\frac{3-\beta}{1+\beta} sech^2 x)g = sechx$, cf. Eq. (2.45). $f(\beta)$ changes its sign from plus to minus when β passes through unity, see Fig. 2.3. Alternatively, Eq. (2.51) can be rewritten as $\lambda_\psi^{(1)^2} = 2\gamma Q_1 / \partial_\delta Q_1$.

$\lambda_\varphi^{(1)^2}$ eigenvalue and associated neutral mode $\vec{w}_\varphi$ are linked to the symmetry in the total phase φ and have their analogies in the spectral problem for the single wave solitons described in the previous section, see Eq. (2.41). The $\lambda_\psi^{(1)^2}$ eigenvalue and the neutral mode $\vec{w}_\psi$ are novel. They can be directly attributed to the symmetry in the differential phase ψ. This branch of the discrete spectrum generates instability for normal GVD ($\gamma < 0$) if $\beta > 1$ and for anomalous GVD

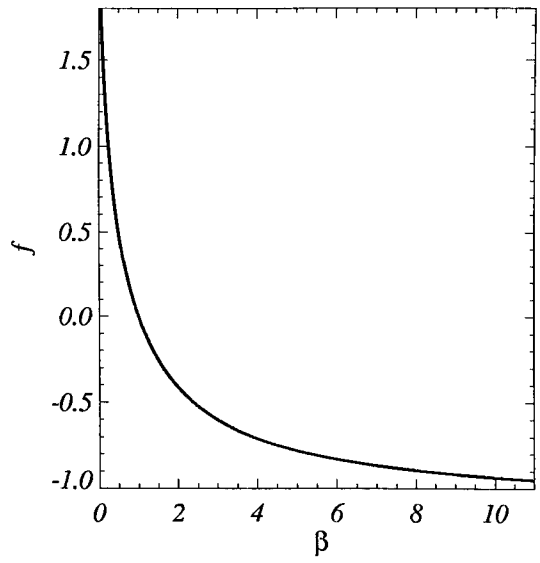

Figure 2.3: Function $f(\beta)$, see Eq. (2.51).

if $\beta < 1$, see Figs. 2.2, 2.3. Thus, the asymptotical analysis indicates that for $\beta > 1$, $\gamma < 0$ neck and snake instabilities coexist, and for $\beta < 1$, $\gamma > 0$ two different types of neck instability coexist. Numerical evaluation of the roots of Eq. (2.49) shows that the same conclusions hold also for $\delta \neq 0$, throughout the whole existence region of the family of elliptically polarized solitons. Solving the EVP (2.33) numerically, we find that in the low-frequency limit the instability growth rates match those predicted by our perturbation theory within a few percent up to $\Omega \simeq 0.5$. Numerical investigation, for more details see below, also shows that apart from the three instabilities discussed in previous subsection, a fourth MI associated with continuation of $\vec{w}_{\delta v}$ into the region of $\beta \neq 0$, $\Omega \neq 0$ also exists. Analytical treatment of this instability is also possible, but it belongs to the rather wide class of problems involving development of the second order perturbation theory and it will not be persued here.

Let us first, discuss in general terms physical meaning of all the different types of the instabilities in simple situation with zero imbalancing ($\delta = 0$), and only then we will proceed with the details of numerical analysis.

2.5.3 Instability induced polarization dynamics

All eigenmodes of the EVPs (2.32), (2.33) are two component vectors, where first and second components are responsible for the spatial form of modulations of the fields E_1 and E_2, respectively. The eigenmodes $\vec{w}_\varphi$ and $\vec{w}_v$ corresponding to the variations of the absolute phase φ and of the absolute velocity v of the coupled solitons have first and second components which are in phase for any value of x. This property holds in fact through out the whole region of the existence of the associated branches of the discrete spectrum. Therefore an excitation of these eigenmodes is not accompanied by the breaking of the polarization of the initial state. In contrast, the eigenmodes linked with $\vec{w}_\psi$ and $\vec{w}_{\delta v}$ neutral modes, or in other words with variations of the relative phase ψ and of the relative velocity δv, have anti-phased first and second components. Therefore their excitation does lead to polarization symmetry breaking. In particular, one should expect that destabilization of the eigenmode associated with the relative phase ψ will result in breaking of the linearly polarized soliton stripe into a chain of circularly polarized clusters, where neighboring clusters have opposite (left and right, if $\delta = 0$) polarizations.

Note here, that by the direct substitution of the linearly polarized solution Eq. (2.44) into the EVPs (2.32), (2.33) one can easily show independence from β of the eigenvalues of the eigenmodes with in-phase first and second components.

2.5.4 Numerical results for normal GVD

We start description of our numerical results from the discussion of the normal GVD case. We found two snake instabilities for $\beta < 1$. One of them corresponds to the in-phase snaking of both fields, see Fig. 4(c), and its growth rate in the low frequency limit is given by the Eq. (2.48). The other one corresponds to the anti-phase snaking, see Figs. 4(d). Examples of the growth rate dependencies vs Ω and details of the anti-phase snaking appearance are presented in Fig. 4(a) and Fig. 5, respectively. Dependencies of the maximal instability growth rate vs

β are presented in Fig. 2.4(b). We found that the in-phase snaking dominates the anti-phase one for any values of δ. A typical example is shown in Fig. 4(b). Dominating role of the in-phase snake instability means that breaking of the polarization state imposed by the initial conditions is unlikely to happen upon propagation. Introducing nonzero imbalancing for a fixed total energy also leads to the growth of the in-phase snake MI and to the suppression of the anti-phase one, see Fig. 4(a). Thus, when $\beta < 1$, the linearly polarized solitons are more stable compare to any other state of polarization.

For $\beta = 1$ the anti-phase snake mode disappears inside the continuum and does not appear again for $\beta > 1$. However, the anti-phase neck MI associated with the relative phase ψ appears for $\beta > 1$, see Eq. (2.51) and Figs. 6(b). The in-phase snake instability obviously also exists, see Eq. (2.48) and Figs. 6(c),(d). The in-phase snake MI dominates the anti-phase neck for $1 < \beta < \beta_{sn}$ and vice versa for $\beta > \beta_{sn}$, see Fig. 7. This fact can also be seen from the comparison of the perturbative results for $\delta = 0$. Accordingly to the Eqs. (2.50), (2.51) and Fig. (2.7) the neck instability dominates the snake in the low frequency limit starting from $\beta \simeq 3.55$. Numerical stability analysis gives that $\beta_{sn} \simeq 3.47$ at $\Omega = \Omega_{max}$ for $\delta = 0$. Introducing imbalancing always leads to the suppression of the both instabilities, see Figs. 6(a),(c) and Fig. 7. Therefore the circular polarized soliton is most stable for a given energy.

In analogy with MI of circularly polarized solitons for normal GVD, the neck and snake unstable eigenmodes become weakly confined and develop oscillating tails as Ω increases beyond the point where the gap is closed, $\lambda_g = 0$.

To test our linear stability analysis and study the nonlinear evolution we performed a series of computer simulations of the Eqs. (1) with initial conditions in the form of a soliton stripe perturbed by spatio-temporal white noise of order of few percent. Typical simulation results are presented in Figs. 2.8,2.9,2.10. For $\beta < \beta_{sn}$ we observed in-phase snaking of the stripe along the temporal dimension, see Fig. 2.8. For $\beta > \beta_{sn}$ the soliton stripe breaks in such a way as to form the interleaved intensity peaks of E_1 and E_2, 2.9($a_{1,2}$),($b_{1,2}$), as expected when the

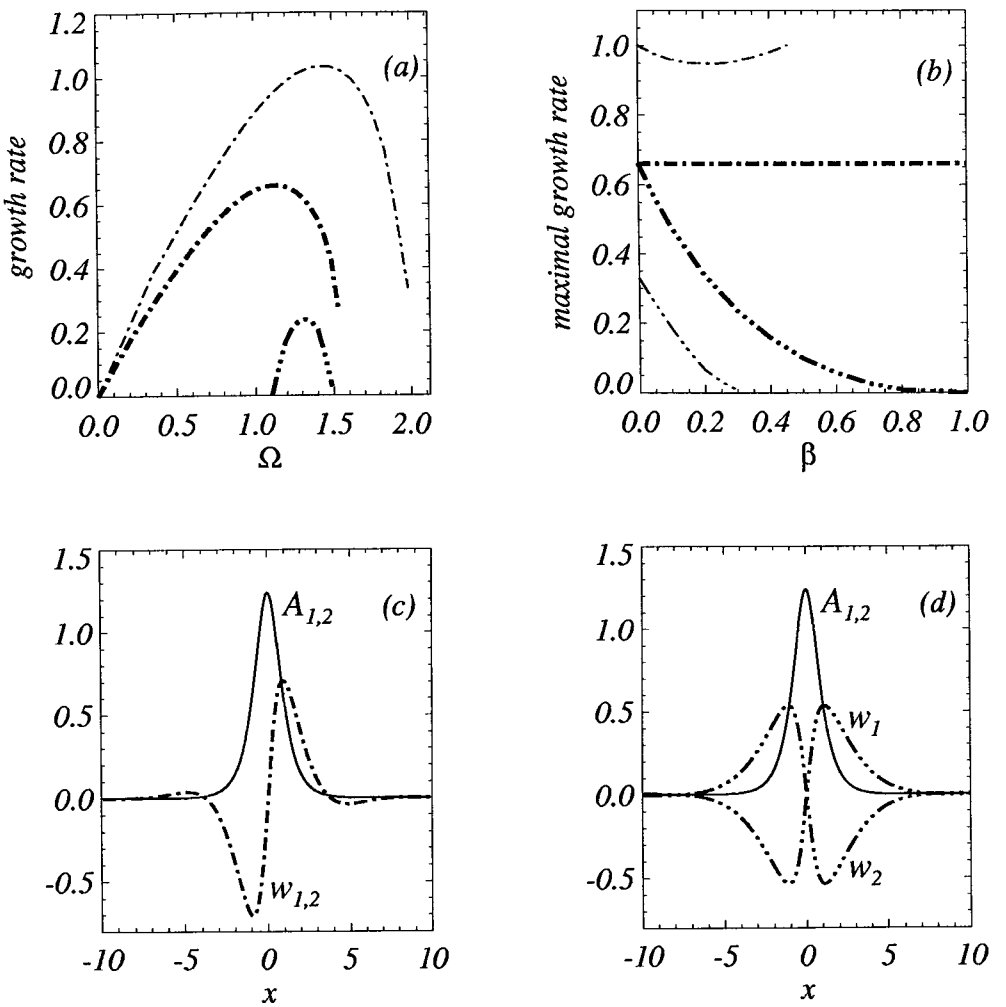

Figure 2.4: Instability growth rates, spatial profiles of the solitary solutions and of the unstable eigenmodes for $\beta < 1$, $\gamma = -0.5$. Dash-dot (dash-dot-dot-dot) lines correspond to the in-phase (anti-phase) snake MI. (a) Growth rates vs Ω, $\beta = 0.3$. Thin (thick) lines correspond to $\kappa = 1$, $\delta = 0$, $Q \simeq 4.04$, $Q_u = 0$ ($\kappa = 1.155$, $\delta = 0.5$, $Q \simeq 4.04$, $Q_u \simeq 2.18$). (b) Maximal growth rate vs β. Thin (thick) lines correspond to $\delta = 0$ ($\delta = 0.5$). (c) Components of the eigenmode corresponding to the in-phase snake MI, $\beta = 0.3$, $\delta = 0$, $\Omega = 1$. (d) Componets of the eigenmode corresponding to the anti-phase snake MI, $\beta = 0.3$, $\delta = 0$, $\Omega = 0.92$.

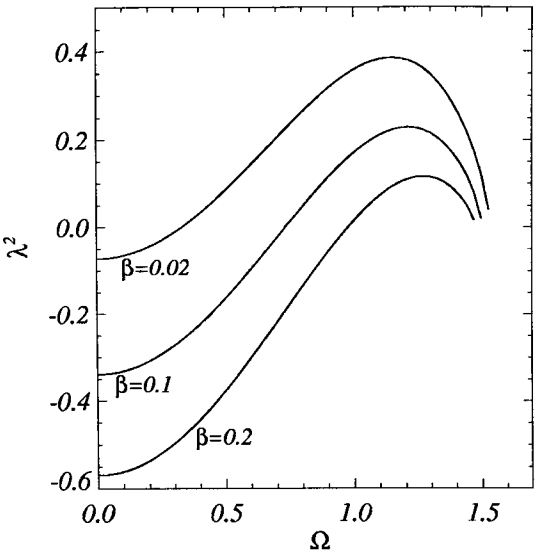

Figure 2.5: Eigenvalues corresponding to the anti-phase snake MI vs Ω for several choices of β: $\kappa = 1$, $\delta = 0$, $\gamma = -0.5$.

out of phase neck MI is dominant. The spatio-temporal patterns formed at the initial stage of MI finally spread because of the unbalanced action of the normal GVD and self-focusing nonlinearity. For $\beta \simeq \beta_{sn}$ we observed competition between the neck and snake MIs, see Fig. 2.10. Looking at Figs. 2.10 (b_1), (b_2) one can clearly see that at the intermediate stage of MI the typical in-phase snake pattern is superimposed on the anti-phase neck pattern.

Thus, we conclude, that in the media with normal GVD spatial soliton stripes develop snake MI without polarization symmetry breaking if $\beta \in (0, \beta_{sn})$ and neck MI with polarization symmetry breaking if $\beta \in (\beta_{sn}, +\infty)$.

2.5.5 Numerical results for anomalous GVD

There are two neck MIs in this case for $\beta < 1$, see Fig. 2.11. One of them is associated with the total phase φ and corresponds to the in-phase neck MI. The other one is associated with the relative phase ψ and corresponds to the anti-phase neck MI. The in-phase MI dominates the anti-phase one for any value of δ and β, which means conservation of the polarization state imposed by the initial

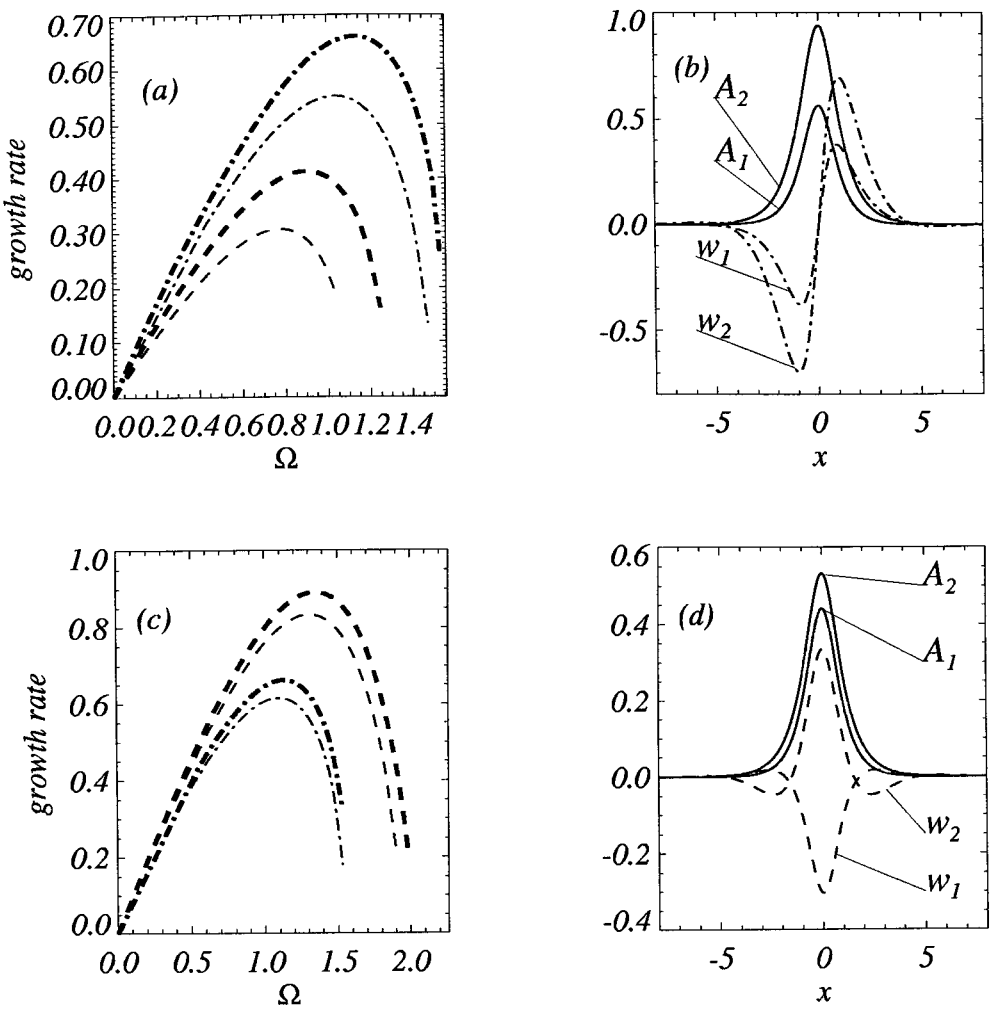

Figure 2.6: Instability growth rates, spatial profiles of the solitary solutions and of the unstable eigenfunctions for $\beta > 1$, $\gamma = -0.5$. Dash-dot (dash) lines correspond to in-phase snake (anti-phase neck) MIs. (a) Growth rates vs Ω, $\beta = 2$. Thin (thick) lines correspond to $\kappa = 1$, $\delta = 0$, $Q = 1.75$, $Q_u = 0$ ($\kappa = 0.93$, $\delta = 0.2$, $Q = 1.75$, $Q_u = -0.91$). (b) Components of the eigenmode corresponding to in-phase snake MI, $\beta = 2$, $\delta = 0.2$, $\Omega = 0.8$. (c) Growth rates vs Ω, $\beta = 7$. Thin (thick) lines correspond to $\kappa = 1$, $\delta = 0$, $Q \simeq 0.68$, $Q_u = 0$ ($\kappa = 0.97$, $\delta = 0.2$, $Q \simeq 0.68$, $Q_u \simeq -0.16$). (d) Componets of the eigenmode corresponding to anti-phase neck MI, $\beta = 7$, $\delta = 0.2$, $\Omega = 1$.

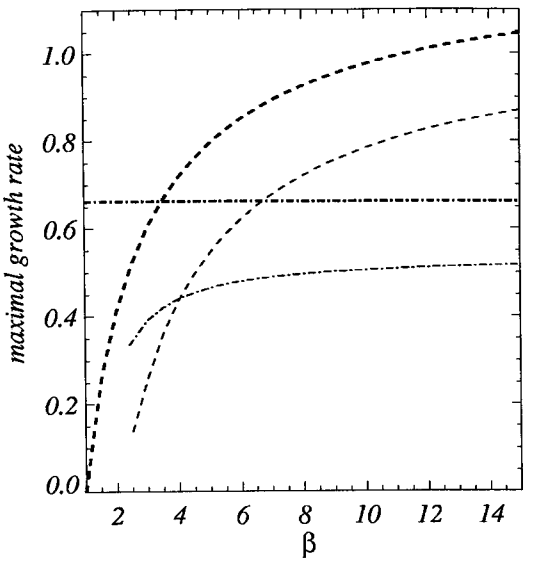

Figure 2.7: Maximal growth rates of the in-phase snake (dash-dot line) and the anti-phase neck (dash line) MIs vs β for $\beta > 1$, $\gamma = -0.5$. Thin (thick) lines correspond to $\delta = 0$ ($\delta = 0.5$). $\beta_{sn} \simeq 3.47$ for $\delta = 0$ and $\beta_{sn} \simeq 4.04$ for $\delta = 0.5$.

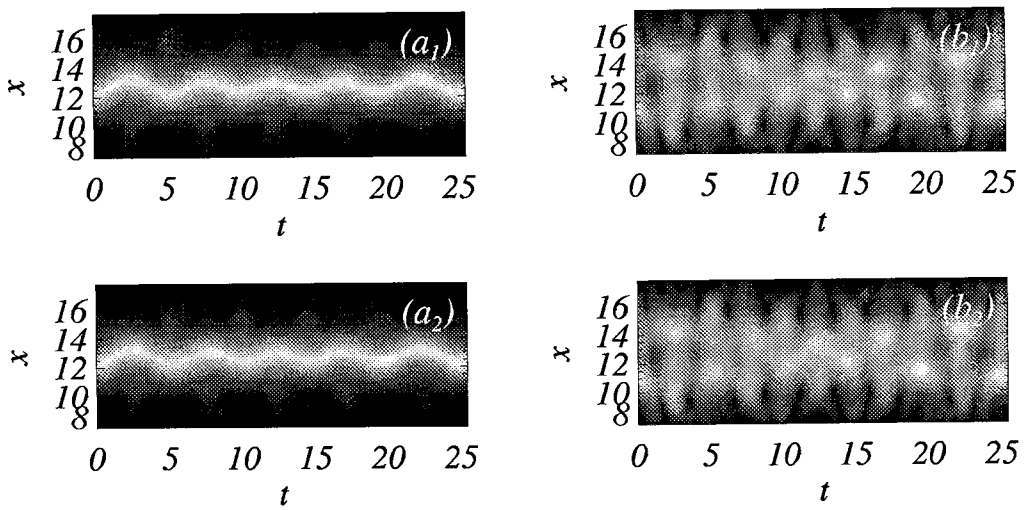

Figure 2.8: Development of the in-phase snake MI for $\beta = 2$, $\kappa = 1$, $\delta = 0$, $\gamma = -0.5$. $(a_{1,2})$ $|E_{1,2}|$ for $z = 12$; $(b_{1,2})$ $|E_{1,2}|$ for $z = 14.7$.

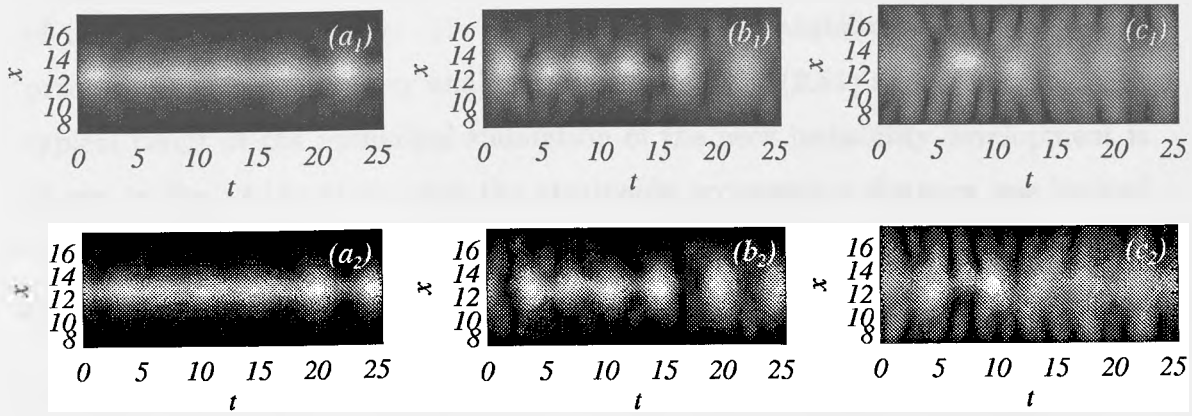

Figure 2.9: Development of the anti-phase neck MI for $\beta = 7$, $\kappa = 1$, $\delta = 0$, $\gamma = -0.5$. $(a_{1,2})$ $|E_{1,2}|$ for $z = 8.4$; $(b_{1,2})$ $|E_{1,2}|$ for $z = 10.2$; $(c_{1,2})$ $|E_{1,2}|$ for $z = 12.6$.

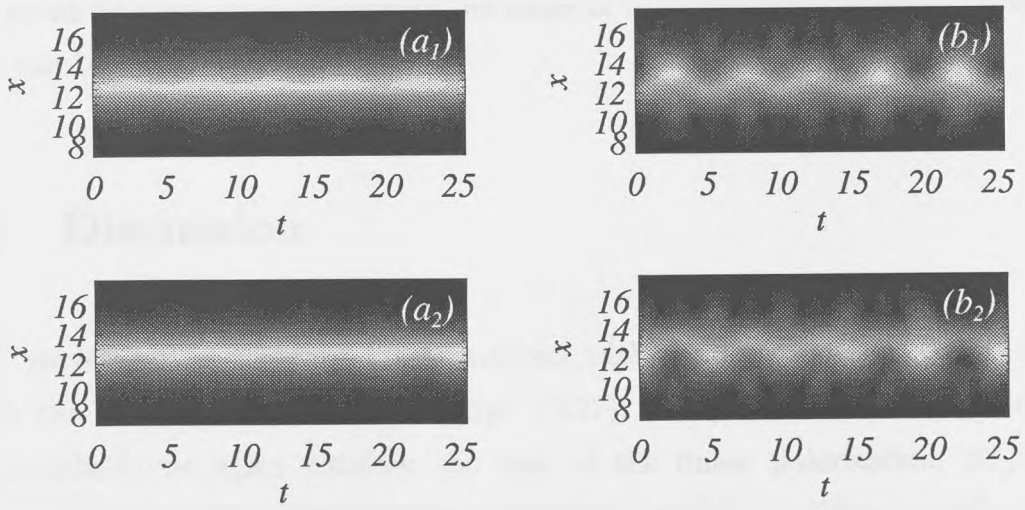

Figure 2.10: Competition between the in-phase snake and anti-phase neck MIs: $\beta = 3.47$, $\kappa = 1$, $\delta = 0$, $\gamma = -0.5$. $(a_{1,2})$ $|E_{1,2}|$ for $z = 9$; $(b_{1,2})$ $|E_{1,2}|$ for $z = 12$

conditions. Nonzero imbalancing for fixed total energy leads to the growth of the in-phase MI and to the suppression of the anti-phase one, see Fig. 10(a). For $\beta > 1$ only in-phase instability exists, but now imbalancing leads to the suppression of the instability, see Fig. 11. Presence of these instabilities agrees with the predictions of low-frequency analysis, see Eqs. (2.50), (2.51) and Figs. 2.2,2.3. A typical result of the numerical simulation of the neck instability development is shown in Fig. 2.13. Note, that the attainable propagation distance was limited by the distance at which the most intense of the filaments formed at the initial stage of MI collapse to singularities.

Cut-off frequencies, where the neck MIs disappear can be found analytically for $\delta = 0$. Growth rate of the in-phase MI becomes zero at $\Omega = \sqrt{3\kappa/\gamma}$ in full analogy with single NLS equation, see section IV. The anti-phase MI disappears at $\Omega^2 = \kappa(D-B)/(2\gamma)$ having $\vec{w} = 0$ and $u_{1,2} = (sech\sqrt{2\kappa}x)^{(B-1)/2}$, here $D = (11-5\beta)/(1+\beta)$, $B = \sqrt{(25-7\beta)/(1+\beta)}$.

Thus, in the media with anomalous GVD spatial soliton stripe always develops neck MI without polarization symmetry breaking and filamentary structure formed during this process collapses upon propagation. Detailed study of collapse in coupled NLS equations is outwith the scope of this thesis. Some details on this issue can be found in [30].

2.6 Discussion

It is interesting to compare MI of solitons with results on MI of CWs [16], which can be easily recovered from Eqs. (2.27), (2.32), (2.33) putting $\partial_x^2 = 0$. For simplicity we again consider the case of the linear polarization, $E_{1,2} = \sqrt{\kappa/(1+\beta)}e^{i\kappa z}$. Then corresponding eigenvalues are $\lambda_\varphi^2 = \gamma\Omega^2(2\kappa - \gamma\Omega^2)$ and $\lambda_\psi^2 = \gamma\Omega^2(2\kappa(1-\beta)/(1+\beta) - \gamma\Omega^2)$. For normal GVD, λ_ψ^2 can be positive only for $\beta > 1$. For anomalous GVD, λ_φ^2 generates instability for any β and λ_ψ^2 only for $\beta < 1$. Thus, as one could expect neck instabilities of solitons related to the phase

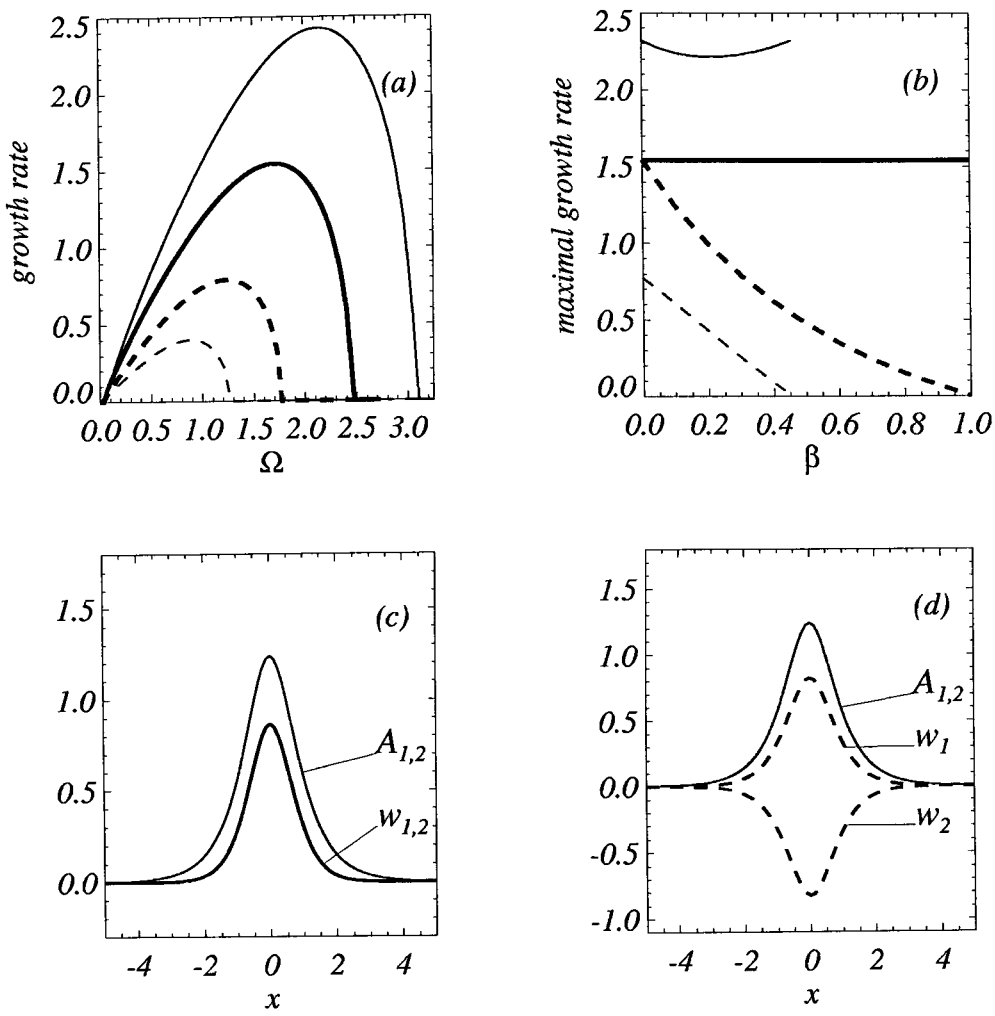

Figure 2.11: Instability growth rates, spatial profiles of the solitary solutions and of the unstable eigenfunctions for $\beta < 1$, $\gamma = 0.5$. Full (dash) lines correspond to in-phase (anti-phase) neck MIs. (a) Growth rates vs Ω, $\beta = 0.3$. Thin (thick) lines correspond to $\kappa = 1$, $\delta = 0$, $Q \simeq 4.04$, $Q_u = 0$ ($\kappa = 1.155$, $\delta = 0.5$, $Q \simeq 4.04$, $Q_u \simeq 2.18$). (b) Maximal growth rate vs β. Thin (thick) lines correspond to $\delta = 0$ ($\delta = 0.5$). (c) Components of the eigenmode corresponding to in-phase snake MI, $\beta = 0.3$, $\delta = 0$, $\Omega = 1.5$. (d) Componets of the eigenmode corresponding to anti-phase snake MI, $\beta = 0.3$, $\delta = 0$, $\Omega = 0.9$.

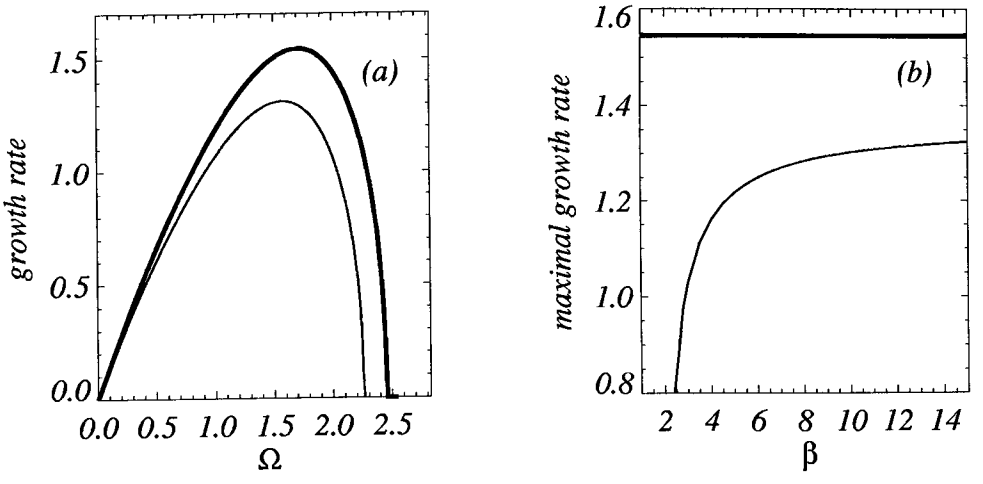

Figure 2.12: In-phase MI growth rates for $\beta > 1$, $\gamma = 0.5$. (a) Growth rates vs Ω, $\beta = 2$. Thin (thick) lines correspond to $\kappa = 1$, $\delta = 0$, $Q \simeq 4.04$, $Q_u = 0$ ($\kappa = 1.155$, $\delta = 0.5$, $Q \simeq 4.04$, $Q_u \simeq 2.18$). (b) Maximal growth rate vs β. Thin (thick) lines correspond to $\delta = 0$ ($\delta = 0.5$).

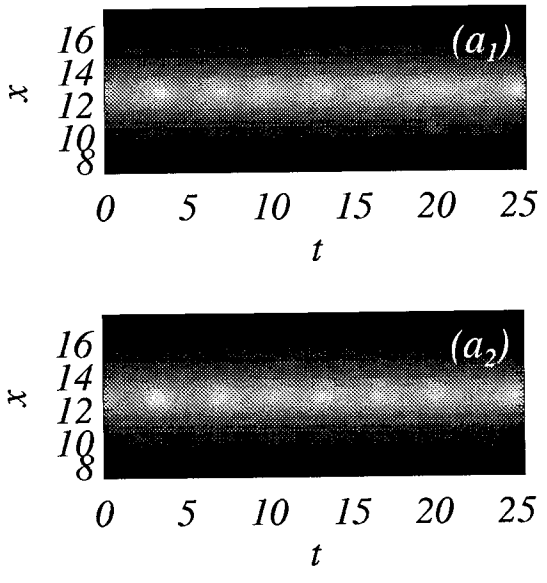

Figure 2.13: Development of the in-phase neck MI for $\beta = 2$, $\kappa = 1$, $\delta = 0$, $\gamma = 0.5$. $(a_{1,2})$ $|E_{1,2}|$ for $z = 4.6$. With further increasing of z most intense filaments develop collapse.

symmetries have their analogies for CWs. Snake instabilities are obviously absent for CWs, which is the main difference between the dynamics of spatially confined solitons and infinitely extended CWs. Namely, in the case of normal GVD, CWs are modulationally stable for $\beta < 1$ and unstable for $\beta > 1$ demonstrating polarization symmetry breaking. Solitons are snake unstable in this situation for any β and this instability does not involve changes in the polarization state. However, starting from a critical value of $\beta = \beta_{sn}$ the snake instability becomes suppressed by the neck one, which is analogous to instability of CW. This instability does lead to polarization symmetry breaking. In particularly, linearly polarized soliton breaks, due to this instability, into the chain of circularly polarized clusters. Because, snake instability leads to spatial symmetry breaking and neck MI does not, the change in MI of solitons at $\beta = \beta_{sn}$ can be interpreted as a transition from spatial symmetry breaking to polarization symmetry breaking.

In limiting situation $\beta \gg 1$ self-phase effects are negligible compare to cross-phase ones and development of the in-phase and anti-phase neck MIs can be qualitatively explained using Fermat's principle. Due to MI development the effective refractive index for E_1 and E_2 fields gets modulated through the XPM mechanism with period $2\pi/\Omega_{max}$. It results in temporal cross-defocusing of filaments in media with normal GVD and in cross-focusing for anomalous GVD. Thus, in the case of normal GVD, interleaved pattern of the intensity peaks of E_1 and E_2 fields should be preferable because it enables each field to see a refractive index that increases to its peak, i.e. one that is in accord with Fermat's principle. This is clearly verified in Fig.9. The same arguments lead to the conclusion that a pattern with all intensity peaks coincident is preferable for anomalous GVD.

Phenomena and theoretical approaches presented above can be developed and generalized in number of ways which can be subjects of future investigation. One of them, for example, can be the study of MI in the more realistic situation with two spatial dimensions and with inclusion of saturation effects which are often relevant in experiments. Applications of coupled NLS equations to describe propagation of spatio-temporal envelopes in planar waveguides is another example. However, here effects of the breaking of the symmetry in differential phase,

due to linear and/or nonlinear anisotropy, will come into play.

Considering possibility of experimental observations of predicted phenomena, we have to say that diffraction induced MI of soliton-like stripe, which is formally equivalent to the case of anomalous GVD, is probably easiest to observe. However, it is less interesting at the same time because it is perfectly analogous to MI of CWs and it is not accompanied by any polarization effects. More interesting dynamics is expected in media with normal GVD. In fact, experimental observation of temporal splitting induced by normal GVD of spatially confined pulses in a self-focusing medium was recently reported in [38, 39]. However, transverse and polarization effects, which, accordingly to our results, should play an important role, were not studied during this experiment. Numerical studies [38, 39] presented to support the experimental results were restricted by scalar approximation and radial geometry.

Rescaled instability growth rate λ as function of the modulational frequency Ω can be recalculated back into physical units using formulae:

$$\lambda_{ph} = \frac{\lambda}{4kw^2\kappa}, \ \Omega_{ph}^2 = \frac{\gamma\Omega^2}{2kk''w^2\kappa}.$$

Here λ_{ph} and Ω_{ph} are the instability growth rate and modulational frequency in physical units, k is the wave vector, w is the beam width, $k'' = \partial_\omega^2 k$. κ and γ are the same parameters which have been used throughout the text. For example for radiation at $1\mu m$ propagating in AlGaAs planar waveguide $k'' \simeq -10^{-23}s^2/m$ [40] and for typical soliton transverse size $w \simeq 50\mu m$ [41] we get $\lambda_{ph} \simeq \lambda/(\kappa \cdot 5cm)$ and $\Omega_{ph}^2 \simeq \Omega^2/(\kappa \cdot 10^{-25}s^2)$.

2.7 Summary

We have analysed and described dispersive MI of families of nodeless spatial solitons in the system of the two incoherently coupled NLS equations. Considering coupled soliton states, we have established the existence of the four branches of instabilities, which are linked to the symmetries in the total and relative phases

and in the absolute and relative motions of solitons. We gave a physical interpretation of our results in terms of the applications of the coupled NLS equations to the interaction of the circularly polarized waves. In particularly, we found that in media with normal GVD the MI induced spatial symmetry breaking changes to the polarization symmetry breaking when the relative strength of the cross-phase modulation exceeds certain threshold value. In media with anomalous GVD, MI results in breaking of spatial solitons into spatio-temporal clusters which collapse upon further propagation. This is not followed by either spatial or polarization symmetry breaking.

Chapter 3

Bright solitary waves due to three-wave mixing

3.1 Introduction

Phenomenon of soliton formation due to the balance between diffraction and/or group velocity dispersion (GVD) from one side and nonlinearity from the other is not restricted to the frames of the centrosymmetric media where the lowest order nonlinearity is the cubic one. It is also possible in noncentrosymmetric media where quadratic nonlinearity is dominant. Of course the case of an isotropic medium considered in the previous Chapter is a particular case of centrosymmetric media. The pioneering papers on soliton formation due to quadratic nonlinearity [42, 43] appeared ten years after the well known work of Chiao, Garmire, and Townes [44] on solitary waves in cubic medium. Solitons due to cubic nonlinearity has been a subject of intense experimental and theoretical research since 60s. In contrast, the problem of self-trapping in quadratic media had remained practically forgotten till the beginning of 90s, when it suddenly exploded. Starting from 1993-94 [45, 46, 47, 48] and especially after experimental work [49], quadratic solitons have been an issue of large amount of theoretical and experimental publications.

The interest to quadratic solitons can be easily understood because this phenomenon is in fact a new conception of light self-trapping. Conventional solitons are formed due to the selfaction of the optical beam propagating in nonlinear material. Quadratic solitons are intrinsically multicomponent. In simplest case they require two fields with frequencies ω and 2ω. Interaction between both harmonics leads to the **mutual** trapping and to formation of 'two-colour' solitary wave.

There are generally infinite number of possible wave processes in quadratically nonlinear media leading to generation not only second but also all higher harmonics and it is very likely that each of these processes can support solitary waves in both spatial and temporal domains. Most important from practical point of view and simplest for theoretical consideration are degenerate and non-degenerate three-wave mixings. Degenerate three-wave mixing is a process of resonant interaction between two waves at frequencies ω and 2ω and non-degenerate three-wave mixing is a mixing of three physically distinct waves with frequencies obeying $\omega_1 + \omega_2 = \omega_3$. In the context of second-harmonic generation (SHG) degenerate case is referred as type I SHG and non-degenerate case as type II SHG. In the last case $\omega_1 = \omega_2$ but corresponding waves are orthogonally polarised. Formation of spatial quadratic solitons was observed due to type I and type II SHG in both bulk media [49, 50, 51] and planar waveguides [52, 53]. More recently temporal localisation due to type I SHG was also observed [54].

Theoretical understanding of the quadratic solitons goes back to already mentioned papers by Karamzin and Sukhorukov. In these papers first numerical evidence of spatial trapping due to quadratic nonlinearity has been presented and simplest analytical solution of the problem has been found. Theoretical development of last years was started from understanding of the fact that the analytical solution of Karamzin and Sukhorukov belongs to the whole soliton family, which was approximated variationally and numerically [48, 55, 56, 57, 58, 59]. Stability issue was probably most intriguing issue of the quadratic soliton theory [60, 57, 61, 62, 63, 64]. However, now, when understanding of this problem is nearly finished, it is clear that the stability properties are mainly underlined not

by the particular choice of nonlinearity, but by the symmetry properties of the model equations.

In this Chapter we start consideration of several theoretical problems related to quadratic solitons. First we derive model equations describing propagation of electromagnetic beams in noncentrosymmetric media. Then we review results on numerical and analytical studies of existence and stability of ground state solitary solutions in one-, two-, and three-dimensional geometries. In the last section existence and stability of two-dimensional higher order solitary solutions is studied.

3.2 Equations for wave propagation in noncentrosymmetric media

3.2.1 Linear terms

For the linearly isotropic media or in the case when all frequency components propagate along any of the optical axes of the crystal, the linear parts of the equations for wave envelopes are obviously the same as were derived in previous Chapter, see Eqs. (2.15). An important example of the linearly isotropic, i.e. *non-birefringent*, and, at the same time, noncentrosymmetric medium is GaAs crystal, which belong to the wide class of the cubic crystals ($\chi^{(1)}_{xx} = \chi^{(1)}_{yy} = \chi^{(1)}_{zz}$) with nonzero second-order susceptibility tensor. The simplest example of linearly anisotropic, i.e. *birefringent*, medium is the uniaxial crystal ($\chi^{(1)}_{xx} = \chi^{(1)}_{yy} \neq \chi^{(1)}_{zz}$). Using Gauss law for uniaxial crystal one can show [65] that in the crystal basis

$$0 = \frac{1}{\varepsilon_0}\vec{\nabla}\cdot(\varepsilon_0\vec{E} + \vec{P}) \simeq \varepsilon_x\vec{\nabla}\cdot\vec{E} + (\varepsilon_z - \varepsilon_x)\partial_z E_z.$$

Therefore spatial part of the linear operator acting on the electric field, see Eq. (2.3), becomes

$$-\vec{\nabla}^2\vec{E} + (1 - \frac{\varepsilon_z}{\varepsilon_x})\vec{\nabla}\partial_z E_z.$$

Now transformation to the basis related with direction of the beam propagation is not trivial and it gives so-called spatial walk-off terms. Suppose that crystal and beam systems are related through the transformation

$$\begin{bmatrix} x' \\ y' \\ z' \end{bmatrix} = \begin{bmatrix} -\cos\phi & \sin\phi & 0 \\ -\cos\theta\sin\phi & -\cos\theta\cos\phi & \sin\theta \\ \sin\theta\sin\phi & \sin\theta\cos\phi & \cos\theta \end{bmatrix} \begin{bmatrix} x \\ y \\ z \end{bmatrix}.$$

Taking into account that in paraxial approximation $E_{z'} \simeq 0$, after some calculations one finds following spatial parts of the operators acting on the components of the field envelope [65]

$$\left(2ik_{\omega ex}\frac{n^2_{\omega e}}{n^2_{\omega ex}}\partial_{z'} + \partial^2_{x'} + [\cos^2\theta + \frac{n^2_{\omega e}}{n^2_{\omega o}}\sin^2\theta]\partial^2_{y'}\right) A_{\omega y} \tag{3.1}$$

$$-ik_{\omega ex}(1 - \frac{n^2_{\omega e}}{n^2_{\omega o}})\sin 2\theta\partial_{y'}A_{\omega y'} + olnt = 0,$$

$$\left(2ik_{\omega o}\frac{n^2_{\omega e}}{n^2_{\omega ex}}\partial_{z'} + \partial^2_{x'} + \partial^2_{y'}\right) A_{\omega x'} + olnt = 0, \tag{3.2}$$

where *'olnt'* means 'other linear and nonlinear terms'. The temporal derivatives are analogous to what was obtained in the previous Chapter, see (2.15). Writing Eq. (3.1),(3.2) we introduced following constants

$$n_{\omega ex} = \left[\frac{\cos^2\theta}{n^2_{\omega o}} + \frac{\sin^2\theta}{n^2_{\omega e}}\right]^{-1/2},$$

$$k^2_{\omega ex} = \frac{\omega^2 n_{\omega ex}}{c^2},\ k^2_{\omega o} = \frac{\omega^2 n^2_{\omega o}}{c^2},\ k^2_{\omega e} = \frac{\omega^2 n^2_{\omega e}}{c^2}$$

$$n^2_{\omega o} = 1 + \chi_{xx}(\omega),\ n^2_{\omega e} = 1 + \chi_{zz}(\omega).$$

The extraordinary beam polarised along y' axis (i.e. the polarization vector lies in the zz' plane) experiences spatial walk-off and it sees refractive index $n_{\omega ex}$ depending from the direction of propagation. The ordinary beam is x' polarised and obeys the same equation as beam propagating in the linearly isotropic medium with refractive index n_o.

3.2.2 Nonlinear terms

Generally in noncentrosymmetric media lowest order nonzero susceptibility is the second order one, therefore in leading approximation nonlinear polarisation at frequency $\omega_3 = \omega_1 + \omega_2$ is

$$\tilde{P}^{(2)}_{\omega 3 i} = \varepsilon_0 \sum_{\omega} \chi^{(2)}_{ijk}(\omega_1, \omega_2) \tilde{E}_{j\omega_1} \tilde{E}_{k\omega_2}, \tag{3.3}$$

where

$$\chi^{(2)}_{ijk}(\omega_1, \omega_2) = \int_{+\infty}^{+\infty} d\xi_1 \int_{-\infty}^{+\infty} d\xi_2 R^{(2)}_{ijk}(\xi_1, \xi_2) e^{i\omega_1 \xi_1 + i\omega_2 \xi_2},$$

summation is assumed over all sets of (ω_1, ω_2) which satisfy $\omega_1 + \omega_2 = \omega_3$ and $E_{j\omega} = A_{j\omega} e^{i\vec{k}_\omega \vec{r} - i\omega t}$. Throughout this and next two Chapters we will consider degenerate and nondegenerate three wave mixing. In degenerate case two waves at frequencies $\omega_1 = \omega_2$ are identical. In the nondegenerate case either $\omega_1 \neq \omega_2$ or $\omega_1 = \omega_2$ but corresponding waves are orthogonally polarised.

Taking into account Kleinman symmetry which holds for nonresonant nonlinearities [29] the 27 elements of $\chi^{(2)}_{ijk}$ can be reduced to 18 and polarisation at frequency ω_3 can be written as

$$\begin{bmatrix} \tilde{P}_{x\omega_3} \\ \tilde{P}_{y\omega_3} \\ \tilde{P}_{z\omega_3} \end{bmatrix} = 2\varepsilon_0 \begin{bmatrix} d_{11} & \dots & d_{16} \\ d_{21} & \dots & d_{26} \\ d_{31} & \dots & d_{36} \end{bmatrix} \begin{bmatrix} \tilde{E}_{x\omega_1} \tilde{E}_{x\omega_2} \\ \tilde{E}_{y\omega_1} \tilde{E}_{y\omega_2} \\ \tilde{E}_{z\omega_1} \tilde{E}_{z\omega_2} \\ \tilde{E}_{y\omega_1} \tilde{E}_{z\omega_2} + \tilde{E}_{y\omega_2} \tilde{E}_{z\omega_1} \\ \tilde{E}_{x\omega_1} \tilde{E}_{z\omega_2} + \tilde{E}_{x\omega_2} \tilde{E}_{z\omega_1} \\ \tilde{E}_{x\omega_1} \tilde{E}_{y\omega_2} + \tilde{E}_{x\omega_2} \tilde{E}_{y\omega_1} \end{bmatrix}. \tag{3.4}$$

For particular crystal classes the number of nonzero elements can be very small. For example, for such practically important crystals as KDP and GaAs only nonzero elements are

$$d_{14} = d_{25} = d_{36} = d, \tag{3.5}$$

for more details see [29]. Polarization response at frequencies $\omega_{1,2}$ can be recovered from Eq. (3.4) taking into account that $\tilde{E}_{i-\omega} = \tilde{E}^*_{i\omega}$.

For the sake of simplification of the derivation procedure I will consider situation when $\omega_{1,2} = \omega$, $\omega_3 = 2\omega$. However, final equations will be presented for the

general case when all three frequencies are different. Waves with frequencies ω_1 and ω_2 are assumed to be, respectively, extraordinary and ordinary waves. Due to quadratic nonlinearity these two waves are coupled with ordinary and extraordinary waves at frequencies $N\omega$, where $N = 0, 2, 3, 4 \ldots$. But we will keep only terms which describe their coupling with one extraordinary wave at frequency 2ω. This will allow us to get general form of equations which are relevant to describe both type I and type II SHGs. We neglect all other resonant contributions into nonlinear polarisation assuming that corresponding conditions of the matching of the wave vector are not satisfied. More general equations describing coupling of two ordinary and two extraordinary waves have been derived in Ref. [66]. Note, that frequency resonances is something that is imposed by the nature of the $\chi^{(2)}$ nonlinearity. In contrast wave vector resonances between ordinary and extraordinary waves can be controlled in birefringent media by choosing direction of propagation. Other methods of the controlling of the wave vector resonances will be briefly discussed below. After a series of calculations for the simplest birefringent crystal, see Eq. (3.5), one can get the following set of equations

$$-\left(2ik_{\omega ex}\frac{n_{\omega e}^2}{n_{\omega ex}^2}\partial_z + \partial_x^2 + \left[\cos^2\theta + \frac{n_{\omega e}^2}{n_{\omega o}^2}\sin^2\theta\right]\partial_y^2\right)A_{\omega y} \tag{3.6}$$

$$-ik_{\omega ex}\left(1 - \frac{n_{\omega e}^2}{n_{\omega o}^2}\right)\sin 2\theta\partial_y A_{\omega y} =$$

$$2k_{\omega e}\left(i\partial_\omega k_{\omega e}\partial_t - \frac{1}{2}\partial_\omega^2 k_{\omega e}\partial_t^2\right)A_{\omega y} + \frac{\omega^2\chi_{2,eff}^{(2)}}{c^2}A_{\omega x}^* A_{2\omega y}e^{-i\tilde{\beta}_2 z};$$

$$-\left(2ik_{\omega o}\partial_z + \partial_x^2 + \partial_y^2\right)A_{\omega x} = 2k_{\omega o}\left(i\partial_\omega k_{\omega o}\partial_t - \frac{1}{2}\partial_\omega^2 k_{\omega o}\partial_t^2\right)A_{\omega x} \tag{3.7}$$

$$+\frac{\omega^2\chi_{2,eff}^{(2)}}{c^2}A_{\omega y}^* A_{2\omega y}e^{-i\tilde{\beta}_2 z} + \frac{\omega^2\chi_{1,eff}^{(2)}}{c^2}A_{\omega x}^* A_{2\omega y}e^{-i\tilde{\beta}_1 z};$$

$$-\left(2ik_{2\omega ex}\frac{n_{2\omega e}^2}{n_{2\omega ex}^2}\partial_z + \partial_x^2 + \left[\cos^2\theta + \frac{n_{2\omega e}^2}{n_{2\omega o}^2}\sin^2\theta\right]\partial_y^2\right)A_{2\omega y} \tag{3.8}$$

$$-ik_{2\omega ex}\left(1 - \frac{n_{2\omega e}^2}{n_{2\omega o}^2}\right)\sin 2\theta\partial_y A_{2\omega y} = 2k_{2\omega e}\left(i\partial_{2\omega}k_{2\omega e}\partial_t - \frac{1}{2}\partial_{2\omega}^2 k_{2\omega e}\partial_t^2\right)A_{2\omega y}$$

$$+\frac{4\omega^2\chi^{(2)}_{2,eff}}{c^2}A_{\omega x}A_{\omega y}e^{i\tilde{\beta}_2 z}+\frac{2\omega^2\chi^{(2)}_{1,eff}}{c^2}A^2_{\omega x}e^{i\tilde{\beta}_1 z},$$

here

$$\tilde{\beta}_1 = 2k_{\omega o} - k_{2\omega ex},\ \tilde{\beta}_2 = k_{\omega ex} + k_{\omega o} - k_{2\omega ex},$$

$$\chi^{(2)}_{1,eff} = 2d\sin\theta\sin 2\phi,\ \chi^{(2)}_{2,eff} = -2d\sin 2\theta\cos 2\phi.$$

$A_{\omega x}, A_{\omega y}, A_{2\omega y}$ are the slowly varying wave envelopes, see (3.63). If $|\tilde{\beta}_2| \gg |\tilde{\beta}_1|$ one can neglect terms proportional to $e^{-i\tilde{\beta}_2 z}$ and this is the case of Type I SHG. Similarly, if $|\tilde{\beta}_1| \gg |\tilde{\beta}_2|$ we can neglect terms proportional to $e^{-i\tilde{\beta}_1 z}$ and this is the case of Type II SHG.

In linearly isotropic media, as cubic crystal, angular dependence of $\chi^{(2)}_{1,eff}$ and $\chi^{(2)}_{2,eff}$ can be omitted. In the following we actually never study influence of birefringence, assuming either nonbirefringent medium ($n_{\omega o} = n_{\omega e}$) or noncritical matching of wave vectors, $\theta \ll 1$. Note also, that the problem of the influence of the non-zero walk-off on formation and internal stability of solitary waves have been addressed in several papers [67, 63, 64, 68]. The question of its influence on modulational instability of solitons still remain to be analysed and will not be considered in this thesis.

Taking into account all the just mentioned simplifying assumptions one can adopt Eqs. (3.6),(3.7),(3.8) for the cases of degenerate and non-degenerate three-wave mixing in general situation, when specific details of chosen geometry are irrelevant.

Degenerate three-wave mixing:

$$-\left(2ik_1\partial_z + \partial_x^2 + \partial_y^2\right)A_1 = 2k_1\left(ik_1'\partial_t - \frac{1}{2}k_1''\partial_t^2\right)A_1 + \frac{\omega^2\chi^{(2)}_{1,eff}}{c^2}A_1^* A_2 e^{-i\beta_1 z}, \quad (3.9)$$

$$-\left(2ik_2\partial_z + \partial_x^2 + \partial_y^2\right)A_2 = 2k_2\left(ik_2'\partial_t - \frac{1}{2}k_2''\partial_t^2\right)A_2 + \frac{2\omega^2\chi^{(2)}_{1,eff}}{c^2}A_1^2 e^{i\beta_1 z}, \quad (3.10)$$

where k_1 and k_2 are the wave vectors of the fields with frequencies ω and 2ω, $k_1' = \partial k_1/\partial\omega$, $k_2' = \partial k_2/\partial(2\omega)$, $k_1'' = \partial^2 k_1/\partial\omega^2$, $k_2'' = \partial^2 k_2/\partial(2\omega)^2$, and $\beta_1 = 2k_1 - k_2$. A_1 and A_2 are the amplitudes, respectively, of the first and second harmonics.

Nondegenerate three-wave mixing:

$$-\left(2ik_1\partial_z+\partial_x^2+\partial_y^2\right)A_1=2k_1\left(ik_1'\partial_t-\frac{1}{2}k_1''\partial_t^2\right)A_1+\frac{\omega_1^2\chi_{2,eff}^{(2)}}{c^2}A_1^*A_3e^{-i\beta_2 z}, \quad (3.11)$$

$$-\left(2ik_2\partial_z+\partial_x^2+\partial_y^2\right)A_2=2k_2\left(ik_2'\partial_t-\frac{1}{2}k_2''\partial_t^2\right)A_2+\frac{\omega_2^2\chi_{2,eff}^{(2)}}{c^2}A_2^*A_3e^{-i\beta_2 z}, \quad (3.12)$$

$$-\left(2ik_3\partial_z+\partial_x^2+\partial_y^2\right)A_3=2k_3\left(ik_3'\partial_t-\frac{1}{2}k_3''\partial_t^2\right)A_3+\frac{\omega_3^2\chi_{2,eff}^{(2)}}{c^2}A_1A_2e^{i\beta_2 z}, \quad (3.13)$$

where k_n $(n=1,2,3)$ are the wave vectors of the fields with frequencies ω_n, $k_n'=\partial k_n/\partial\omega_n$, $k_n''=\partial^2 k_n/\partial\omega_n^2$, and $\beta_2=k_1+k_2-k_3$. A_n are the amplitudes of the fields with frequencies ω_n.

Introducing dimensionless parameters and variables we obtain normalised model equations for degenerate and nondegenerate three-wave mixings.

Degenerate case:

$$i\partial_\zeta E_1+i\delta_1\partial_\tau E_1+\alpha_1\vec{\nabla}_\perp^2E_1+\gamma_1\partial_\tau^2E_1+E_1^*E_2=0, \quad (3.14)$$

$$i\partial_\zeta E_2+i\delta_2\partial_\tau E_2+\alpha_2\vec{\nabla}_\perp^2E_2+\gamma_2\partial_\tau^2E_2+\frac{1}{2}E_1^2=\beta E_2, \quad (3.15)$$

where

$$\zeta=\frac{z}{l_{dif}},\ \xi=\frac{x}{w},\ \eta=\frac{y}{w},\ \tau=\frac{t-k'z}{T}$$

$$\beta=(2k_1-k_2)l_{dif},\ \vec{\nabla}_\perp^2=\partial_\xi^2+\partial_\eta^2,$$

$$l_{dif}=w^2k,\ l_{dis}=\frac{T^2}{k''},\ k=\frac{k_1+k_2}{2},$$

$$k'=\frac{k_1'+k_2'}{2},\ \ k''=\frac{|k_1''|+|k_2''|}{2}$$

$$\alpha_n=\frac{k}{2k_n},\ \gamma_n=\frac{l_{dif}}{2l_{dis}}\frac{k_n}{k}\frac{k_n''}{k''},\ \delta_n=\frac{l_{dif}}{T}(k_n'-k')$$

$$E_1=A_1\frac{\omega^2w^2k\chi_{1,eff}^{(2)}}{c^2\sqrt{2k_1k_2}},\ E_2=A_2\frac{\omega^2w^2k\chi_{1,eff}^{(2)}}{2c^2k_1}e^{i\beta\zeta},$$

$n=1,2$; T is a characteristic pulse duration, w is a characteristic beam size.

Nondegenerate case:

$$i\partial_z E_1+i\delta_1\partial_\tau E_1+\alpha_1\vec{\nabla}_\perp^2E_1+\gamma_1\partial_\tau^2E_1+E_2^*E_3=0, \quad (3.16)$$

$$i\partial_z E_2+i\delta_2\partial_\tau E_2+\alpha_2\vec{\nabla}_\perp^2E_2+\gamma_2\partial_\tau^2E_2+E_1^*E_3=0, \quad (3.17)$$

$$i\partial_z E_3+i\delta_3\partial_\tau E_3+\alpha_3\vec{\nabla}_\perp^2E_3+\gamma_3\partial_\tau^2E_3+E_1E_2=\beta E_3, \quad (3.18)$$

where

$$\beta = (k_1 + k_2 - k_3)l_{dif},\ k = \frac{k_1 + k_2 + k_3}{3},$$

$$k' = \frac{k_1' + k_2' + k_3'}{3},\ k'' = \frac{|k_1''| + |k_2''| + |k_3''|}{3}$$

$$\alpha_n = \frac{k}{2k_n},\ \gamma_n = \frac{l_{dif}}{2l_{dis}}\frac{k_n}{k}\frac{k_n''}{k''},\ \delta_n = \frac{l_{dif}}{T}(k_n' - k')$$

$$E_1 = A_1\frac{\omega_2\omega_3 w^2 k\chi^{(2)}_{2,eff}}{2c^2\sqrt{k_2k_3}},\ E_2 = A_2\frac{\omega_1\omega_3 w^2 k\chi^{(2)}_{2,eff}}{2c^2\sqrt{k_1k_3}},$$

$$E_3 = A_3\frac{\omega_1\omega_2 w^2 k\chi^{(2)}_{2,eff}}{2c^2\sqrt{k_1k_2}}e^{i\beta\zeta},$$

$n = 1, 2, 3.$

All temporal derivatives in Eqs. (3.14),(3.15),(3.16),(3.17),(3.18) can be ignored if one is interested only in spatial effects, i.e. duration of the pulse tends to infinity, $T \to \infty$. Generally, the group velocity mismatches δ_n are all different and play very important role in the process of pulse propagation in quadratic media. However, below, studying temporal effects, I will consider only simplified model situation with

$$\delta_n = 0. \tag{3.19}$$

The primary reason for this simplification comes from the fact that size of the matrices which are needed for numerical stability analysis presented in the next Chapter would be doubled in case of $\delta_n \neq 0$. That basically made impossible numerical work on the computers which were available for me at the time when this work was done. A couple of more scientific reasons for this simplification also can be presented. First, group velocity difference can be compensated by some special techniques [54]. Second, considering degenerate three-wave mixing in doubly periodic Bragg grating embedded in the quadratically nonlinear medium He and Drummond [69], and Conti with coworkers [70] showed that for frequencies close to the center of the forbidden gap the model equations governing propagation dynamics can be reduced to a form which formally coincides with Eqs. (3.14),(3.15) when $\delta_n = 0$. The only difference is that temporal and longitudinal coordinates should be interchanged as well as the wave numbers (k) and frequencies (ω). The reason for this is that in the Bragg gratings dominating dispersive

effects originate from the delayed spatial, not temporal, response of the medium. One can expect that the same analogy can be valid in nondegenerate case.

3.2.3 Phase matching

Most important practical application of quadratically nonlinear materials is the frequency conversion. The mismatch of the wave vectors, which is often called phase mismatch, is a crucial parameter to control efficiency of the frequency conversion. Details on this issue can be found in any text book on nonlinear optics, see e.g. [29, 28]. Obviously with increasing phase mismatch nonlinear terms becomes less and less significant and this generally results in a decreasing of the conversion efficiency. Maximal conversion is normally achieved for zero phase mismatch. The classical way to tune phase mismatch is by the adjusting of the propagation direction in birefringent crystal in such a way that refractive indices for ordinary and extraordinary waves at different frequencies become equal.

Another way to achieve phase matching is so-called quasi-phase matching (QPM). The idea of QPM was proposed in 60s in one of the pioneering works on frequency conversion [71], but it has begun to be widely used for fabrication of practical devices only during the last decade [72]. The idea consists in making second-order susceptibility a periodic function of propagation direction, i.e. $\chi^{(2)}_{eff}(z) = \chi^{(2)}_{eff}(z+Z)$. Any periodic function can be of course represented as a Fourier series: $\chi^{(2)}_{eff}(z) = \sum_{n=-\infty}^{+\infty} d_n e^{inZz}$. If, for some $n = n_q$, $n_q Z$ is equal or approximately equal to phase mismatch than effective quadratic nonlinearity will be proportional to d_{n_q} and influence of other nonlinear terms can be neglected because they are far from the phase matching condition. It is straightforward to show that in the leading order equations (3.14),(3.15),(3.16), (3.17),(3.18) are also valid for QPM structures, see [72, 73, 74]. Only difference is that phase mismatch parameters have to be replaced by $\beta - n_q Z$. QPM techniques has some advantages and disadvantages, which of course depend from experimental configuration. One of the advantages, for example, is that QPM can be used in nonbirefringent media. On the other hand, in birefringent crystal, QPM gives flexibility to choose the

propagation direction with maximal $\chi^{(2)}$ without suffering from spatial walk-off. One of the disadvantages is scattering losses on inhomogeneities appearing due to the writing of the grating.

Another techniques, which remained practically unknown until recently [75], is Van der Ziel method [76]. This method allows the creation of artificial birefringence in linearly isotropic materials as, for example, GaAs, by growing thin layers of other material along proposed direction of propagation. These layers destroy linear isotropy and create possibility for phase matching. We stress that here modification of the crystal occurs *along* the planes parallel to the propagation direction, not perpendicular to it as in QPM structures, therefore one can expect fewer energy losses.

3.3 Ground-state two-wave solitons

3.3.1 Stationary problem.

Throughout this section the problems of existence and stability of ground-state, i.e. nodeless, solitary solutions of Eqs. (3.14),(3.15) will be considered. Taking into account Eq. (3.19), model system is

$$i\partial_z E_1 + \frac{1}{2}(\partial_x^2 + \partial_y^2)E_1 + \gamma_1 \partial_\tau^2 E_1 + E_1^* E_2 = 0, \tag{3.20}$$

$$i\partial_z E_2 + \frac{1}{4}(\partial_x^2 + \partial_y^2)E_2 + \gamma_2 \partial_\tau^2 E_2 + \frac{1}{2}E_1^2 = \beta E_2, \tag{3.21}$$

here practically relevant choice $k_2/k_1 = 2$ was made and spatial variables were rescaled in an obvious way. Possibility of the existence of the solitary solution of Eqs. (3.20),(3.21) become clear from the consideration of the limit $\beta \gg 1$ (*cascading limit*). In a very rough approximation derivatives of the second field can be neglected, i.e. $E_2 \simeq \frac{1}{2\beta}E_1^2$ and the system (3.20),(3.21) can be approximated by the NLS equation for fundamental harmonic

$$i\partial_z E_1 + \frac{1}{2}(\partial_x^2 + \partial_y^2)E_1 + \gamma_1 \partial_\tau^2 E_1 + \frac{1}{2\beta}|E_1|^2 E_1 = 0.$$

This equation has well known bright solitary solutions in one, two and three dimensions. The last is true, providing that $\gamma_1 > 0$. More accurate derivation of approximate equation in cascading limit can be found in Refs. [77, 78]. The solitons of NLS equations are stable only in one dimensional geometry and develop collapse in higher dimensions [9, 4, 10]. However, as it is already well known [10, 59, 60, 57, 61, 62, 63, 64] and will be shown in some details below, quadratic nonlinearity can support stable solitons in all physically relevant dimensions.

Eqs. (3.20),(3.21) can be reduced to a set of stationary equations for the soliton profile using substitution

$$E_1 = A_1(x, y, \tau)e^{i\kappa z}, \; E_2 = A_2(x, y, \tau)e^{i2\kappa z}, \tag{3.22}$$

where κ is the soliton parameter characterising correction to the wave number, and $A_{1,2}$ are real functions obeying

$$\begin{aligned} (\partial_x^2 + \partial_y^2)A_1 + \gamma_1\partial_\tau^2 A_1 &= 2\kappa A_1 - 2A_1A_2, \\ (\partial_x^2 + \partial_y^2)A_2 + 2\gamma_2\partial_\tau^2 A_2 &= 4(2\kappa + \beta)A_2 - 2A_1^2. \end{aligned} \tag{3.23}$$

Existence of bright solitary solutions with tails decaying in both space and time require $\kappa > max(0, -\beta/2)$ and $\gamma_{1,2} > 0$. Eqs. (3.23) are still partial differential equations which are difficult to solve numerically. Therefore we will suppose that $\gamma_1 = 2\gamma_2$ and rescale time, $\tau = \sqrt{\gamma_1}t$, then for spherically symmetric solutions (*optical bullets*) Eqs. (3.23) become

$$\begin{aligned} \frac{d^2A_1}{d\rho^2} + \frac{D-1}{\rho}\frac{dA_1}{d\rho} &= 2\kappa A_1 - 2A_1A_2, \\ \frac{d^2A_2}{d\rho^2} + \frac{D-1}{\rho}\frac{dA_2}{d\rho} &= 4(2\kappa + \beta)A_2 - 2A_1^2. \end{aligned} \tag{3.24}$$

Here D is the dimension of the problem: for $D = 3$ (optical bullet) $\rho = \sqrt{x^2 + y^2 + t^2}$, while $D = 2$, with $\rho = \sqrt{x^2 + y^2}$, corresponds to the spatial soliton in bulk media or to the spatio-temporal soliton propagating in planar waveguide, $D = 1$. $\rho = x$ corresponds to one dimensional soliton. For given D and β Eqs. (3.25) have a family of solitons with different energies, each with different κ. In fact one of the parameters β or κ can be scaled away. However, it is more convenient to keep them both. β is not very natural for scaling because it can be zero or negative.

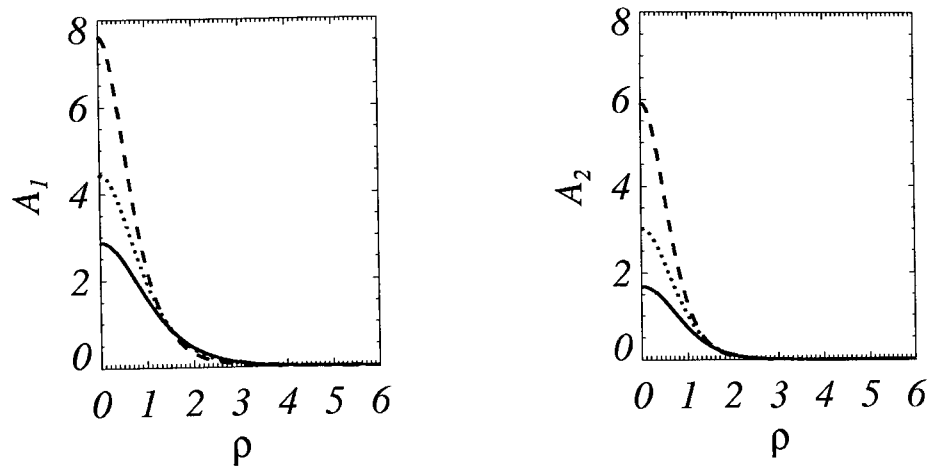

Figure 3.1: Profiles of the one-, two- and three- dimensional solitons are marked, respectively, by the full, dotted and dashed lines: $\beta = 0$, $\kappa = 1$.

Although κ is always positive, it is natural parameter for stability analysis and scaling κ away would seriously complicate derivation of stability criteria and adiabatic theory described below. Typical examples of such useless complications can be found in [60, 79].

Exact analytical solution of Eqs. (3.25) can be found in special case $D = 1$ and $\beta = -\frac{3}{2}\kappa$, when Eqs. (3.25) reduce to

$$\frac{d^2 f}{dx^2} = 2(\kappa - f)f.$$

This equation has following localised solution

$$f(x) = \frac{3\kappa}{2} sech^2 \sqrt{\frac{\kappa}{2}} x = A_{1,2}(x) \tag{3.25}$$

Eqs. (3.25) can be easily solved numerically using shooting or relaxation techniques [80]. Fig. 3.1 shows numerically built transverse profiles of the solitons in all three physically relevant dimensions. There is also possibility of approximating transverse profiles analytically by using variational approach and it was done by many authors [55, 61, 58, 59], see also Appendix A for details.

3.3.2 Internal stability.

In this Section we will discuss the stability problem of the ground-state quadratic solitons with respect to perturbations which are localised in the same dimensions where soliton itself is localised (internal stability). We start from the general problem of stability of two-dimensional stationary solution of Eqs. (3.23) ($\gamma_{1,2} = 0$), $A_{1,2} = A_{1,2}(r = \sqrt{x^2+y^2})$. Consider small complex perturbations of the stationary solution $A_{1,2}(r)$,

$$E_n = (A_n + (U_n(z,x,y) + iW_n(z,x,y))e^{in\kappa z},\ n = 1,2. \tag{3.26}$$

Linearization of Eqs. (3.20),(3.21) and substitutions $U_n \sim u_n(x,y)e^{\lambda z}$ and $W_n \sim w_n(x,y)e^{\lambda z}$ result in the following eigenvalue problem (EVP)

$$\begin{aligned} \hat{\mathcal{L}}_1\vec{u} &= -\lambda\vec{w}, \\ \hat{\mathcal{L}}_0\vec{w} &= \lambda\vec{u}, \end{aligned} \tag{3.27}$$

where $\vec{u} = (u_1, u_2)^T$, $\vec{w} = (w_1, w_2)^T$. $\hat{\mathcal{L}}_0$ and $\hat{\mathcal{L}}_1$ are:

$$\hat{\mathcal{L}}_0 = \begin{pmatrix} -\frac{1}{2}\vec{\nabla}_\perp^2 + \kappa + A_2 & -A_1 \\ -A_1 & -\frac{1}{4}\vec{\nabla}_\perp^2 + 2\kappa + \beta \end{pmatrix}, \tag{3.28}$$

$$\hat{\mathcal{L}}_1 = \begin{pmatrix} -\frac{1}{2}\vec{\nabla}_\perp^2 + \kappa - A_2 & -A_1 \\ -A_1 & -\frac{1}{4}\vec{\nabla}_\perp^2 + 2\kappa + \beta \end{pmatrix}. \tag{3.29}$$

The EVP (3.27) can be solved only numerically. However, some general conclusions can be made without numerics. Eigenvalues of the continuous part of the spectrum with stable and spatially unbounded eigenfunctions belong to the rays $(i\Omega_c, i\infty)$ and $(-i\Omega_c, -i\infty)$, where $\Omega_c = min(\kappa, 2\kappa + \beta)$. Unstable spatially localised eigenmodes of the discrete part of the spectrum have eigenvalues with $Re\lambda > 0$. They must always have a counterpart with $Re\lambda < 0$ because of the hamiltonian nature of our problem.

Phase

$$(E_1, E_2) \to (E_1 e^{i\phi}, E_2 e^{i2\phi}), \tag{3.30}$$

and translational symmetries, $(x, y) \to (x+x_0, y+y_0)$, of model equations generate three neutrally stable ($\lambda = 0$) eigenmodes which are

$$\vec{u}_\phi = 0,\ \vec{w}_\phi = \begin{pmatrix} A_1 \\ 2A_2 \end{pmatrix}; \tag{3.31}$$

$$\vec{u}_x = \partial_x \begin{pmatrix} A_1 \\ A_2 \end{pmatrix}, \vec{w}_x = 0; \tag{3.32}$$

$$\vec{u}_y = \partial_y \begin{pmatrix} A_1 \\ A_2 \end{pmatrix}, \vec{w}_y = 0. \tag{3.33}$$

EVP (3.27) can be reduced to the two EVPs, $\hat{\mathcal{L}}_0\hat{\mathcal{L}}_1\vec{v} = -\lambda^2\vec{v}$ and $\hat{\mathcal{L}}_1\hat{\mathcal{L}}_0\vec{w} = -\lambda^2\vec{w}$, which have identical spectra and these spectra are equivalent to the spectrum of the original EVP. Now it is clear that every zero eigenvalue corresponding to the eigenmodes (3.31),(3.32),(3.33) is doubly degenerate. Degeneracy of translational modes is attributed to presence of two-dimensional Galilean invariance

$$(E_1, E_2, \vec{r}) \to (E_1 e^{i\Phi}, E_2 e^{2i\Phi}, \vec{\xi}), \tag{3.34}$$

where

$$\Phi = \frac{\vec{v}}{2}(\vec{r} - \frac{1}{2}\vec{v}z),\ \vec{\xi} = \vec{r} - \vec{v}z,\ \vec{v} = \vec{i}v_x + \vec{j}v_y.$$

Degeneracy of the phase mode is attributed to infinitesimal variations of κ. Thus zero eigenvalue has sixfold degeneracy. So called *associated* eigenmodes can be assigned to these three additional zeros. These modes are

$$\vec{u}_\kappa = \partial_\kappa \begin{pmatrix} A_1 \\ A_2 \end{pmatrix},\ \vec{w}_\kappa = 0; \tag{3.35}$$

$$\vec{u}_{v_x} = 0, \vec{w}_{v_x} = x \begin{pmatrix} A_1 \\ 2A_2 \end{pmatrix}; \tag{3.36}$$

$$\vec{u}_{v_y} = 0, \vec{w}_{v_y} = y \begin{pmatrix} A_1 \\ 2A_2 \end{pmatrix} \tag{3.37}$$

Eigenmodes (3.31),(3.32),(3.33),(3.35),(3.36),(3.37) obey the following identities:

$$\hat{\mathcal{L}}_0\vec{w}_\phi = 0,\ \ \hat{\mathcal{L}}_0\vec{w}_{v_x} = -\vec{u}_x,\ \ \hat{\mathcal{L}}_0\vec{w}_{v_y} = -\vec{u}_y \tag{3.38}$$

$$\hat{\mathcal{L}}_1\vec{u}_x = 0, \quad \hat{\mathcal{L}}_1\vec{u}_y = 0, \quad \hat{\mathcal{L}}_1\vec{u}_\kappa = -\vec{w}_\phi \tag{3.39}$$

In the polar basis

$$\vec{\nabla}_\perp^2 = \frac{d^2}{dr^2} + \frac{1}{r}\frac{d}{dr} + \frac{1}{r^2}\frac{d^2}{d\theta^2},$$

and translational and Galilean modes take the form $\vec{u}_r = \partial_r(A_1, A_2)^T e^{\pm i\theta}$, $\vec{w}_v = r(A_1, 2A_2)^T e^{\pm i\theta}$.

It is clear that without restriction of generality solution of EVP (3.27) can be presented as superposition of azimuthal Fourier modes $\cos J\theta$ and $\sin J\theta$ ($J = 0, 1, 2, \ldots$) with complex coefficients depending on r and z:

$$\vec{u}(r,\theta) = \sum_J (\vec{u}_{cJ}(r)\cos J\theta + \vec{u}_{sJ}(r)\sin J\theta), \tag{3.40}$$

$$\vec{v}(r,\theta) = \sum_J (\vec{v}_{cJ}(r)\cos J\theta + \vec{v}_{sJ}(r)\sin J\theta). \tag{3.41}$$

Providing that original solution is azimuthally symmetric, $A_{1,2}(x,y) = A_{1,2}(r)$, it is straightforward to show that cosine and sine perturbations obey identical EVPs. Throughout this Chapter we deal only with stability of θ independent solutions, therefore subscripts 'c' and 's' will be omitted below. More general case, when cosine and sine perturbations are coupled will be considered in Chapter 5.

Resulting EVP for perturbations with azimuthal index J has the form of EVP 3.27 with following replacement

$$\vec{\nabla}_\perp^2 \to \frac{d^2}{dr^2} + \frac{1}{r}\frac{d}{dr} - \frac{J^2}{r^2}, \tag{3.42}$$

Considering perturbations with $J = 0$ it can be shown that famous Vakhitov-Kolokolov criterion [81]

$$2\langle \vec{u}_\kappa, \vec{w}_\phi \rangle = \partial_\kappa Q = 0, \tag{3.43}$$

where Q is the energy invariant of the Eqs. (3.20),(3.21),

$$Q = \int dV(|E_1|^2 + 2|E_2|^2) \tag{3.44}$$

gives stability threshold for quadratic solitons, see Sections 3.3.3 and 4.2 for more details. This condition generally holds for any nontopological envelope soliton

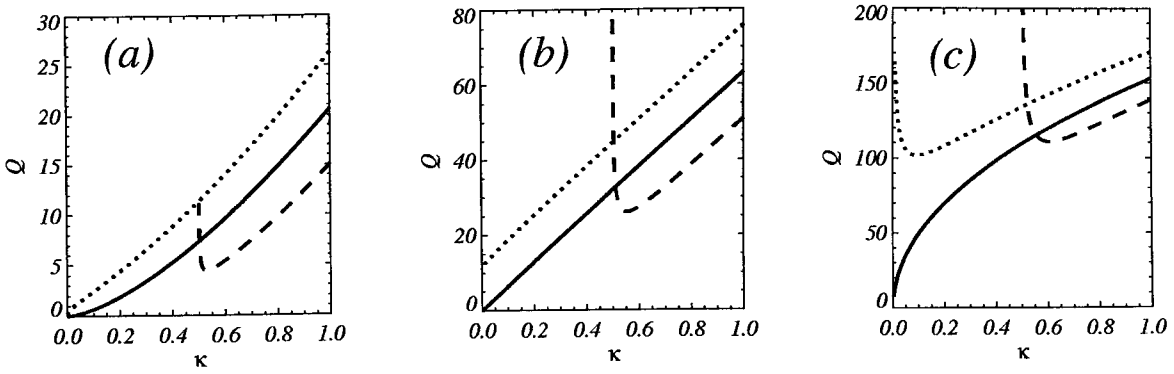

Figure 3.2: Q vs κ for one, two, and three dimensional solitons, respectively, presented at figures (a),(b),(c). $\beta = 0$ (full line), $\beta = 1$ (dotted line), $\beta = -1$ (dashed line)

originating as a solution of model equations possesing single phase symmetry [82]. Numerical and analytical [60, 83, 59], [Sec. 3.3.3], [Sec. 4.2] calculations show that, similarly to the generalised NLS equation [81], ground-state quadratic soliton is unstable providing that

$$\partial_\kappa Q < 0. \tag{3.45}$$

Dependencies of Q vs κ for different signs of β and different dimensions are presented in Fig. 3.2. One can see that one and two dimensional solitons can be unstable only for negative β and that optical bullets can be unstable for either sign of β. It is important to stress that Vakhitov-Kolokolov criterion generally gives only one instability threshold and possible presence of others always has to be checked numerically.

3.3.3 Soliton dynamics near instability threshold

Let us assume that all free soliton parameters vary adiabatically with propagation distance. E.g., in one-dimensional type I case soliton has four such parameters. They are ϕ, κ, x_0, and v. Knowing that we are seeking instability threshold given by (3.43), it is naturally to assume that only

$$\kappa = \kappa(\varepsilon z) = \kappa(\zeta),$$

where $\varepsilon \ll 1$. It can be shown that translational and Galilean modes are not responsible for instabilities of **bright** solitons in models with translational and Galilean symmetries. However, one must always be careful, because in models with broken Galilean symmetry, e.g. for quadratic solitons with walk-off or if $k_2/k_1 \neq 2$, translational and Galilean modes are very important ones [64].

To show how the adiabatic approach works we will use an example of 1D solitons. As one will see derivations for 2D and 3D geometries are perfectly analogous. Keeping in mind all previous comments, we expand solution of Eqs. (3.20),(3.21) near 'unknown' instability threshold, which happens at some $\kappa = \kappa_c$, in the asymptotical series

$$E_1 = e^{i\kappa_0 z}\left(A_1(x,\kappa) + i\varepsilon\phi_1(x,\kappa,\zeta) + \varepsilon^2\phi_2(x,\kappa,\zeta) + i\varepsilon^3\phi_3(x,\kappa,\zeta) + \ldots\right) \quad (3.46)$$

$$E_2 = e^{i2\kappa_0 z}\left(A_2(x,\kappa) + i\varepsilon\psi_1(x,\kappa,\zeta) + \varepsilon^2\psi_2(x,\kappa,\zeta) + i\varepsilon^3\psi_3(x,\kappa,\zeta) + \ldots\right) \quad (3.47)$$

Obviously κ_0 has to be close enough to κ_c, but how close will be clear from subsequent calculations. In main order ε^0 the Eqs. (3.25) are readily recovered. In first (ε^1), second (ε^2), and third (ε^3) orders, respectively, the following problems need to be solved

$$\hat{\mathcal{L}}_0\begin{pmatrix}\phi_1\\ \psi_1\end{pmatrix} = \dot{\kappa}\partial_\kappa\begin{pmatrix}A_1\\ A_2\end{pmatrix} \quad (3.48)$$

$$\hat{\mathcal{L}}_1\begin{pmatrix}\phi_2\\ \psi_2\end{pmatrix} = -\frac{d}{d\zeta}\begin{pmatrix}\phi_1\\ \psi_1\end{pmatrix} + \begin{pmatrix}\phi_1\psi_1\\ -\phi_1^2/2\end{pmatrix} \quad (3.49)$$

$$\hat{\mathcal{L}}_0\begin{pmatrix}\phi_3\\ \psi_3\end{pmatrix} = \frac{d}{d\zeta}\begin{pmatrix}\phi_2\\ \psi_2\end{pmatrix} + \begin{pmatrix}\phi_2\psi_1 - \phi_1\psi_2\\ \phi_1\phi_2\end{pmatrix}, \quad (3.50)$$

where

$$\dot{\kappa} = \frac{\partial\kappa}{\partial\zeta},\ \frac{d}{d\zeta} = \frac{\partial}{\partial\zeta} + \dot{\kappa}\frac{\partial}{\partial\kappa}.$$

All effects related to the energy radiation from the soliton will be neglected, although they can be treated within framework of the asymptotic series (3.46),(3.47). Consideration of the radiation requires application of an approach which involves spatially unbounded modes of the continuous spectrum, see e.g. [84].

We will focus on the dynamics of solitons due to excitation of the spatially localised mode of the EVP (3.27), which is close to neutrally stable eigenmode (3.31). Solvability condition of Eq. (3.48) in the class of spatially localised functions requires

$$\frac{\partial Q}{\partial \kappa} = 0, \tag{3.51}$$

that is in fact specifies value of $\kappa = \kappa_c$ suspicious for the change of stability. In the language of eigenmodes of the EVP (3.27) it means that some mode of the discrete spectrum coincides with neutral mode $(A_1, 2A_2)^T$ at the point where condition (3.51) is satisfied. Because Eq. (3.51) must be satisfied in first order, it means that we can consider values of κ_0 such that

$$\frac{\partial Q}{\partial \kappa}(\kappa = \kappa_0) \sim \varepsilon^2. \tag{3.52}$$

The solvability condition of second order problem is satisfied automatically. The solvability condition of third order problem will give some ordinary differential equation for κ. Thus the problem of soliton stability can be reduced to a study of the simple problem of stability of the fixed points of some ordinary differential equation. The only problem is to calculate coefficients in this equation. It requires that one knows the solutions of the Eqs. (3.48), (3.49). These solutions can be build in implicit form using Wronskian based techniques [85]. The resulting answers will be far from nice, simple expressions. They will be some cumbersome integrals of $A_{1,2}$ and their κ derivatives, which are difficult to simplify. Therefore we will apply the method based on the energy conservation [86]. This method does not require solving of Eq. (3.49), but generally speaking Eq. (3.48) still needs to be solved.

Solution of Eq. (3.48) can be presented in the form

$$\begin{pmatrix} \phi_1 \\ \psi_1 \end{pmatrix} = \dot{\kappa} \begin{pmatrix} x_{11} \\ x_{12} \end{pmatrix} = \dot{\kappa}\vec{x}_1, \tag{3.53}$$

than Eq. (3.49) can be rewritten as

$$\hat{\mathcal{L}}_1 \vec{x}_2 = -\ddot{\kappa}\vec{x}_1 - \dot{\kappa}^2 \partial_\kappa \vec{x}_1 + \dot{\kappa}^2 \vec{n} \tag{3.54}$$

where $\vec{n} = (x_{11}x_{12}, -\frac{1}{2}x_{11}^2)^T$. Now energy invariant at $\kappa = \kappa_0$ can be written in the form

$$Q(\kappa_0) = Q(\kappa) + 2\varepsilon^2 \left(\dot{\kappa}^2\langle\vec{x}_1, \vec{z}\rangle + 2\langle\vec{w}_\phi, \vec{x}_2\rangle\right) + O(\dot{\kappa})O(\varepsilon^4) = \tag{3.55}$$

$$Q(\kappa) + 2\varepsilon^2 \left(\dot{\kappa}^2\langle\vec{x}_1, \vec{z}\rangle - 2\langle\hat{\mathcal{L}}_1\partial_\kappa\vec{a}, \vec{x}_2\rangle\right) + O(\dot{\kappa})O(\varepsilon^4) =$$

$$Q(\kappa) + 2\varepsilon^2 \left(\langle\partial_\kappa\vec{a}, \vec{x}_1\rangle\ddot{\kappa} + \partial_\kappa(\langle\partial_\kappa\vec{a}, \vec{x}_1\rangle)\dot{\kappa}^2\right)$$

$$+\varepsilon^2\dot{\kappa}^2 \left(\langle\vec{x}_1, \vec{z}\rangle - 2\langle\partial_\kappa\vec{a}, \vec{n}\rangle - 2\langle\partial_\kappa^2\vec{a}, \vec{x}_1\rangle\right) + O(\dot{\kappa})O(\varepsilon^4),$$

where $\vec{a} = (A_1, A_2)^T$ and $\vec{z} = (x_{11}, 2x_{12})^T$. Performing cumbersome transformations and using Eqs. (3.38),(3.39) and identity $\hat{\mathcal{L}}_0\vec{x}_1 = \partial_\kappa\vec{a}$ one can show that Eq. (3.55) can be reduced to

$$Q(\kappa_0) - Q(\kappa) = \varepsilon^2 \left(2M\ddot{\kappa} + \frac{\partial M}{\partial\kappa}\dot{\kappa}^2\right) + O(\dot{\kappa})O(\varepsilon^4), \tag{3.56}$$

where

$$M = \langle\hat{\mathcal{L}}_0\vec{x}_1, \vec{x}_1\rangle = \langle\hat{\mathcal{L}}_0^{-1}\vec{u}_\kappa, \vec{u}_\kappa\rangle.$$

Assuming that deviations of κ from κ_0 are order of ε^2, $\kappa - \kappa_0 = \delta \sim \varepsilon^2$, and taking into account (3.52) one can easily show that Eq. (3.56) becomes

$$2\varepsilon^2 M\ddot{\delta} + Q'\delta + \frac{1}{2}Q''\delta^2 = 0, \tag{3.57}$$

where the prime stands for ∂_κ and Q' and Q'' are calculated at $\kappa = \kappa_0$. Previously mentioned cumbersome calculations leading to Eq. (3.56) can actually be ignored. Knowing that $Q' \sim \varepsilon^2$ and assuming that $Q'' \sim O(1)$, and that $Q'\delta$ and $Q''\delta^2$ have the same order of magnitude, than, it *follows* that $\delta \sim \varepsilon^2$. Thus all terms proportional to $\varepsilon^2\dot{\delta}^2$ have order of ε^6 and can be ignored already in Eq. (3.54), providing that substitution $\kappa - \kappa_0 = \delta$ had been made. This arguments immediately lead from Eq. (3.55) to Eq. (3.57). Now returning to the original variable z we transfrom Eq. (3.57) into

$$2M\frac{\partial^2\delta}{\partial z^2} + Q'\delta + \frac{1}{2}Q''\delta^2 = 0, \tag{3.58}$$

Eq. (3.58) has two fixed points $\delta = 0$ and $\delta = \delta_1 = -2Q'/Q''$. $\delta = 0$ corresponds to the solitary solution under consideration, $\kappa = \kappa_0$, and $\delta = \delta_1$ corresponds

to the solution with $\kappa = \kappa_0 + \delta_1$. Because $\hat{\mathcal{L}}_0$ is nonnegative operator, see e.g. [79], and $\vec{x}_1 \neq (A_1, 2A_2)^T$, it is clear that $M > 0$. Q has a minimum at $\kappa = \kappa_c$ therefore $Q'' > 0$. Knowing these facts one can analyse stability of the fixed points. Eigenvalues corresponding to the solution $\delta = 0$ are

$$\lambda = \pm\sqrt{-\frac{Q'}{2M}}, \tag{3.59}$$

and the other fixed point has eigenvalues

$$\lambda = \pm\sqrt{\frac{Q'}{2M}}. \tag{3.60}$$

Therefore when one of the fixed points is stable (center) the other one is unstable (saddle). This shows that Vakhitov-Kolokolov criteria is necessary condition for stability of the soliton under consideration ($\kappa = \kappa_0$), i.e. that for $\partial_\kappa Q < 0$ close to the point $\partial_\kappa Q = 0$ there is an unstable eigenvalue. This, of course, does not forbid presence of other unstable eigenvalues of the EVP (3.27). However, as we discussed earlier, numerical investigation shows that the instability threshold (3.51) is only one for ground-state solitons.

The phase portrait of the Eq. (3.58) in the plane $(\delta, \dot{\delta})$ is very simple [86]. It consists from the two already mentioned fixed points, the homoclinic trajectory starting and ending at the saddle point and surrounding the center. Once fixed point is centre, so any small deviation from it always leads to oscillations. Deviations from the saddle directed inside the homoclinic loop will lead to oscillations and ones directed outside the loop will lead to soliton spreading [86]. For three-dimensional solitons all possible scenarios of the soliton dynamics are shown in Fig. 3.3.

On the language of eigenmodes, oscillations of the soliton originate from the fact that discrete eigenmode with purely imaginary eigenvalue from the gap in the continuous spectrum is excited by perturbations. Close to the point $\partial_\kappa Q = 0$ approximate value of this eigenvalue is given by Eqs. (3.59). Nonlinearity of course leads to generation of frequencies which are multiple of the just mentioned eigenvalue. Generation of these harmonics means that part of the energy of the soliton transfers to the eigenmodes which belong to the continuum, that

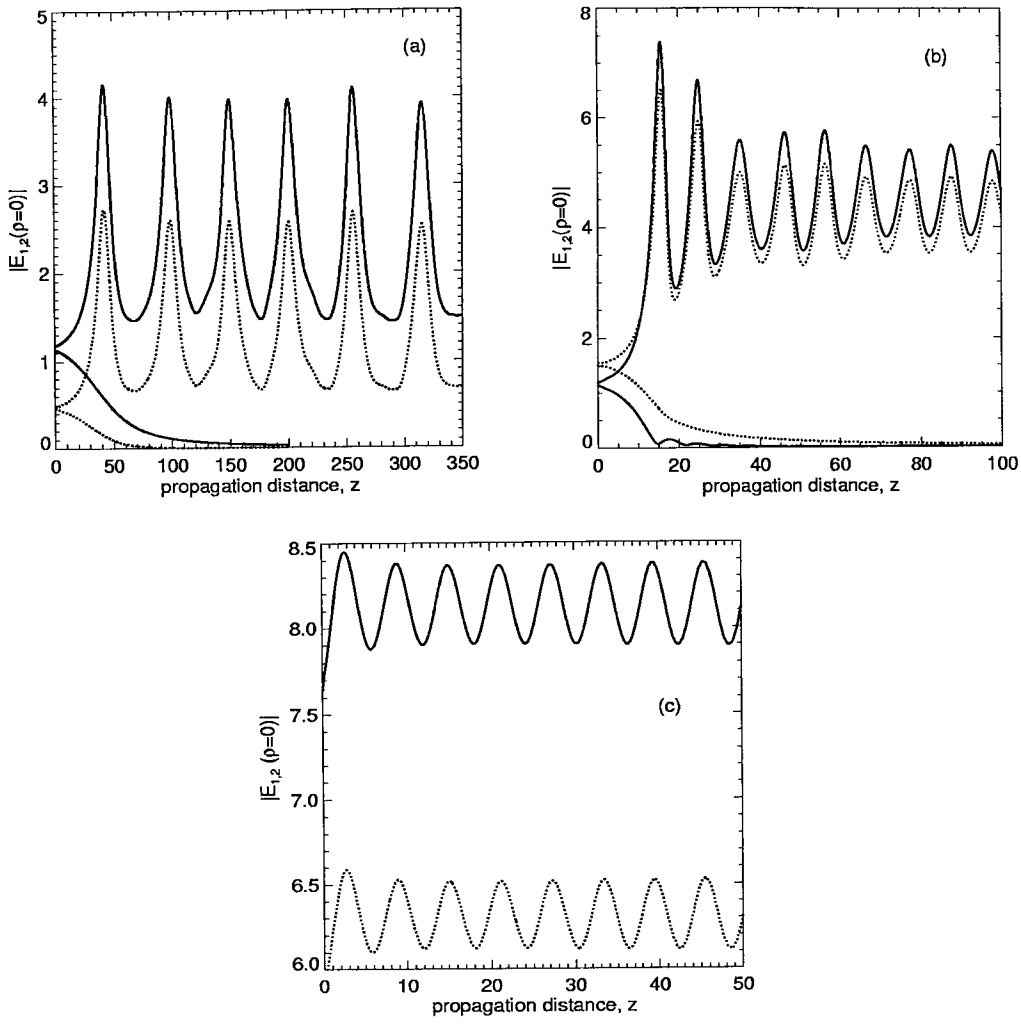

Figure 3.3: (a) Optical bullet instability scenarios for $\beta = 1$, $\kappa = 0.04$. (b) The same but for $\beta = -1$, $\kappa = 0.52$. (c) Long-lived pulsation, $\beta = 0$, $\kappa = 1$. Solid (dotted) lines correspond to fundamental (second) harmonic. Deviations from stationary transverse profiles are 2% for (a)-(c).

ultimately means radiation of the energy. However, this radiation is very weak and the oscillations persists very long time, see Fig. 3.3, for more details, see [84, 87].

3.4 Three-wave solitons

Three-wave quadratic solitons obey Eqs. (3.16),(3.17),(3.18) and they are known in one, two and three dimensions, see e.g. [62, 79]. Main differences with degenerate model (3.14),(3.15) originate from the fact that Eqs. (3.16),(3.17),(3.18) have two phase symmetries:

$$(E_1, E_2, E_3) \to (E_1 e^{i\phi+i\psi}, E_2 e^{i\phi-i\psi}, E_3 e^{i2\phi}). \tag{3.61}$$

Stationary solutions now constitute two-parameter family. We seek solutions of Eqs. (3.16),(3.17),(3.18) in the form

$$\begin{aligned} E_1 &= A_1(x,y,\tau)e^{i(\kappa+\delta)z}, \\ E_2 &= A_2(x,y,\tau)e^{i(\kappa-\delta)z}, \\ E_3 &= A_3(x,y,\tau)e^{i2\kappa z}. \end{aligned} \tag{3.62}$$

Existence of bright solitary solutions with tails decaying in both space and time require $(\kappa \pm \delta) > 0$, $2\kappa > -\beta$ and $\gamma_m > 0$. In analogy with two-wave solitons we suppose that $\gamma_{1,2} = 2\gamma_3$ and rescale time, $\tau = \sqrt{\gamma_1}t$, then for spherically symmetric solutions Eqs. (3.16),(3.17),(3.18) become

$$\begin{aligned} \frac{d^2A_1}{d\rho^2} + \frac{D-1}{\rho}\frac{dA_1}{d\rho} &= 2(\kappa+\delta)A_1 - 2A_2A_3, \\ \frac{d^2A_2}{d\rho^2} + \frac{D-1}{\rho}\frac{dA_2}{d\rho} &= 2(\kappa-\delta)A_2 - 2A_1A_3, \\ \frac{d^2A_3}{d\rho^2} + \frac{D-1}{\rho}\frac{dA_3}{d\rho} &= 4(2\kappa+\beta)A_3 - 4A_1A_2. \end{aligned} \tag{3.63}$$

Exact analytical solution are again known for $D = 1$ and $\beta = -\frac{3}{2}\kappa$

$$A_{1,2} = \frac{3\kappa}{2\sqrt{2}} sech^2\sqrt{\frac{\kappa}{2}}x, \quad A_3 = \frac{3\kappa}{2} sech^2\sqrt{\frac{\kappa}{2}}x. \tag{3.64}$$

Stability analysis similar to described for degenerate case was presented in Ref. [62]. In first order approximation it reveals stability threshold, which in our notations is given by

$$\partial_\delta Q \partial_\kappa Q_u = \partial_\kappa Q \partial_\delta Q_u, \tag{3.65}$$

where

$$Q = Q_1 + Q_2 + 2Q_3 \tag{3.66}$$

is the total energy and

$$Q_u = Q_1 - Q_2 \tag{3.67}$$

is the energy unbalance. Because of the symmetry property (3.61), Q and Q_u or equivalent combinations of $Q_m = \int dV |E_m|^2$ are conserved quantities. Stability threshold (3.65) is typical for solitonic models with two phase symmetries and it was known in other branches of nonlinear science, for review see [82].

According to the results presented in Ref. [62] soliton dynamics near the threshold specified by the Eq. (3.65) is very similar to the degenerate case. There are certain peculiarities related to the existence of another branch of stable solitons [88]. This bistability happens in a very narrow parameter region close to the boundary of the soliton existence and it will not be discussed here.

Author's point of view is that the asymptotic theory of stability of two- and generally multi-parameter solitons is still far from to be completed. Some steps in the direction to solve this problem are presented in Appendix B.

3.5 Instabilities of ring-like solitons with bright central spot

Ground-state solitary solutions being the most important solitary solutions do not exhaust the set of solitary solutions due to three-wave mixing, see e.g. [56, 89, 90, 91, 92, 93, 94, 95, 96]. In this section we will consider the stability of two-dimensional higher-order solitary waves with bright central spots surrounded

by one or more rings. Such solutions were also known for NLS equation with pure Kerr [97] and saturable [81, 91, 98] nonlinearities. For quadratic nonlinear media their existence was reported in [90, 91, 92], see also Section 5.1 below. No universal stability criterion is known for higher-order bound states and their stability has to be studied individually in every case. It has been shown that for saturable nonlinearity higher-order bound states with bright central spots are stable with respect to purely radial perturbations, obeying to criteria for ground states, but unstable with respect to azimuthally dependent perturbations, showing breakup of their rings into filaments [98].

We consider Eqs. (3.20),(3.21) with $\gamma_{1,2} = 0$. In the whole region of the existence of the spatially localised solutions I was able to numerically find families of many-ring solutions with bright central peak. Examples of spatial profiles of one- and two-ring solutions are presented in Fig. 3.4(a). For any finite number of rings, the fundamental field has radial zeroes but the second harmonic field always remains positive, though having minima close to the zeros of the fundamental. For increasing β *(cascading limit)* the second harmonic field tends to carry less and less of the energy. The situation is opposite for negative β, when κ values are close to the boundary of soliton existence. Dependencies vs κ of the energy invariant Q are presented in Fig. 3.4(b).

We will consider in most detail stability of the solutions with only one ring outside the central peak. These show the main features of the dynamics of solutions with an arbitrary number of rings. First we focus symmetry-preserving perturbations, $J = 0$, see Eqs. (3.40)-(3.42). Asymptotic techniques described above can be applied to many ring solutions as well. However, the positiveness of M can not be proved analytically. But independently from the sign of M it is clear that the neutrally stable mode (3.31) branches at the point $\partial_\kappa Q = 0$ giving instability for either $\partial_\kappa Q < 0$ or $\partial_\kappa Q > 0$. Numerical investigation of EVP (3.27),(3.42) shows that instability happens for $\partial_\kappa Q < 0$, see Figs. 3.4(b),3.5, and it means that $M > 0$ in the vicinity of $\partial_\kappa Q = 0$. Thus we can conclude that the standard stability criterion for ground states [81, 60] is also a *necessary* condition for stability of higher-order bound-states. This instability is related to the existence for $\partial_\kappa Q > 0$

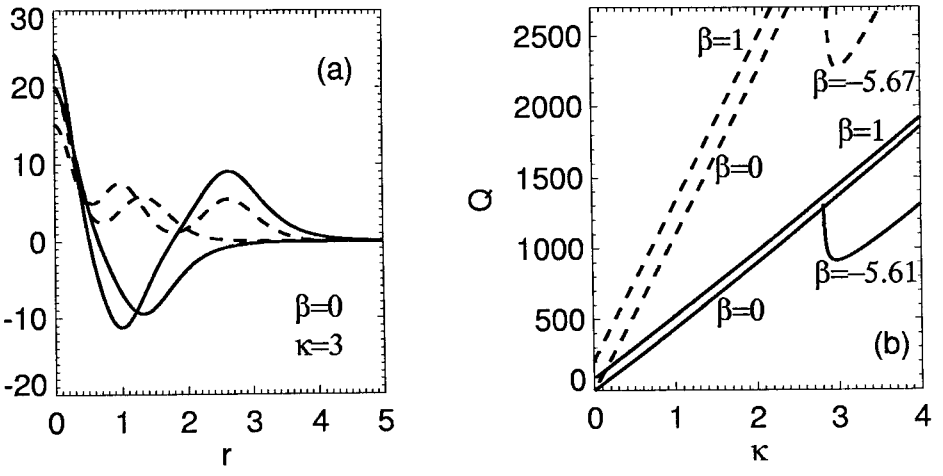

Figure 3.4: (a) Radial profiles of one- and two-ring solitary waves. Full (dashed) lines are for A_1 (A_2). (b) Total energy vs κ for one-ring (full lines) and two- ring (dashed lines) solitary waves. The negative values of β are chosen so as to give $\partial_\kappa Q = 0$ at $\kappa = 3$.

of a pair of eigenmodes with purely imaginary eigenvalues (with opposite signs) lying in the gap $(-i\Omega_c, i\Omega_c)$. At the point $\partial_\kappa Q = 0$ these eigenmodes coincide with the neutral mode and for more negative β appear again but with purely real eigenvalues of opposite sign, signifying instability. For the ground-state this is the only instability scenario and these modes disappear into the continuum for large $\beta > 0$.

However, detailed numerical investigation reveals that two pairs of discrete eigenmodes exist in $J = 0$ case. Interplay between them leads to a new bifurcation scenario, which is different from scenario known for ground state solutions. I will study this scenario varying β for fixed $\kappa = 3$. Changing κ at fixed β has no qualitative effect due to scaling properties of (3.25).

Real and imaginary parts of key eigenvalues from the discrete spectrum are plotted vs β in Fig. 3.5. In the limit of large β I found one internal eigenmode (line 1 in Fig. 3.5) but at $\beta \simeq 4.75$ another internal eigenmode (line 2) emerges from the continuum. On emergence mode 2 has $Im\lambda_0 = \kappa = 3$, but as β is decreased the eigenvalues of the two modes come together, as Fig. 3.5 shows. They fuse at $\beta \simeq -0.82$ to form two pairs of eigenfunctions with complex conjugate eigenval-

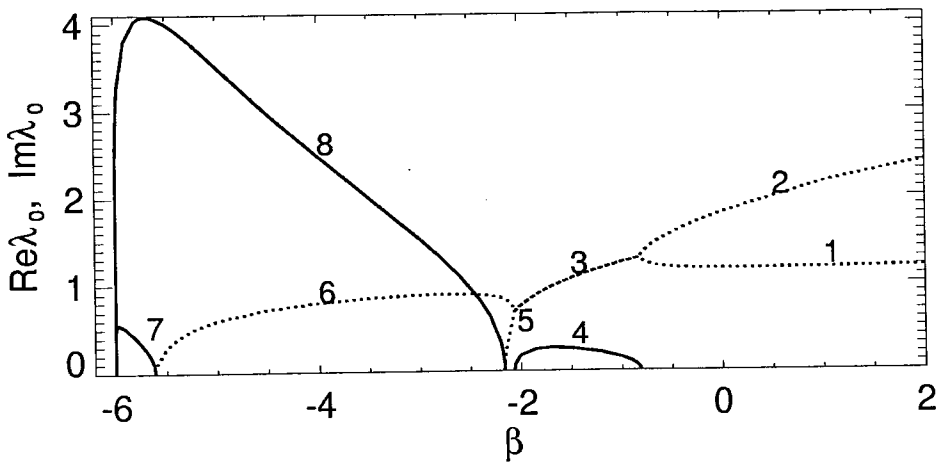

Figure 3.5: Real (full lines) and imaginary (dotted lines) parts of the eigenvalues of $J = 0$ eigenmodes vs β, $\kappa = 3$.

ues, giving onset of an instability (lines 3,4). At $\beta \simeq -2.06$ a reverse bifurcation takes place (lines 5,6). One eigenmode (Fig. 3.6(a)) then has a purely imaginary eigenvalue (line 6) until it loses its stability at $\beta \simeq -5.61$ (line 7) where $\partial_\kappa Q = 0$. This is the standard instability scenario described above. The other eigenmode undergoes a similar bifurcation, but at $\beta \simeq -2.17$ (lines 5,8) which is well before the point $\partial_\kappa Q = 0$. At this bifurcation the eigenfunction profiles, Fig. 3.6(b), are quite different from those of the neutrally stable eigenmode. Thus, unlike the previously-known case (lines 6,7 in Fig. 3.5) this new instability cannot be captured by asymptotic expansion around that neutral eigenmode. In both cases the unstable eigenvalues reach a maximum then go steeply to zero near the existence limit of solitary solutions, $\beta = -2\kappa$.

The cascade of symmetry preserving bifurcations presented in Fig. 3.5 is somewhat similar to that for TE_1 mode instability in a planar waveguide (1D geometry) with Kerr nonlinearity [99] where joint action of the refraction index discontinuities and field nodes leads to instability. In our situation the new symmetry-preserving instability develops in the region where the nodeless second harmonic starts to dominate over the fundamental, which has one or more nodes.

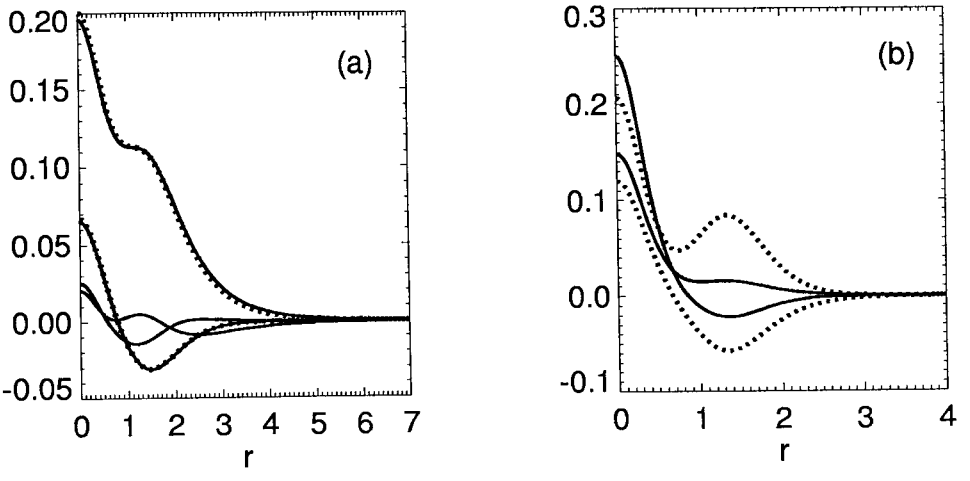

Figure 3.6: (a) The internal eigenfunction corresponding to branch 6 in Fig. 3.5 at the point $\beta = -5.58$, slightly before the bifurcation point $\partial_\kappa Q = 0$. (b) The internal eigenfunction corresponding to the bifurcation point at $\beta = -2.17$ where branches 5,8 in Fig. 3.5 meet. Dots mark the neutrally stable eigenmode. $\kappa = 3$.

For symmetry-breaking perturbations, $J \neq 0$, the stability properties are not so rich as for $J = 0$. For $J = 1$ numerics reveals the presence of a neutral mode and a pair of eigenmodes in the discrete spectrum with purely real eigenvalues, one of which is responsible for instability. I did not find any exchange of stability of these modes. For every J from 2 to 5 I find such a pair of discrete eigenmodes with purely real eigenvalues and all modes for $J > 5$ belong to the continuum. The unstable perturbations for $J = 3, 4$ are localised around the ring of the bound-state in a manner similar to what happens in saturable media [98].

To show how the character of instability of the one-ring solution depends on phase mismatch parameter I plot in Fig. 3.7 growth rates vs β for all unstable eigenmodes. For phase mismatches from the cascading limit down to $\beta \sim -3$ symmetry breaking instabilities with $J = 3, 4$ are dominant. However, sufficiently far from the NLS limit our new scenario, with azimuthally homogeneous perturbations dominant, is realised. I stress again (see discussion above) that this symmetry preserving instability is not related to violation of the criterion $\partial_\kappa Q > 0$. Note that in the limit $\beta \gg 1$ the $J = 0$ internal eigenmode exists and the $J = 1$ eigenmode has non-zero growth rate (Fig. 3.7(b)).

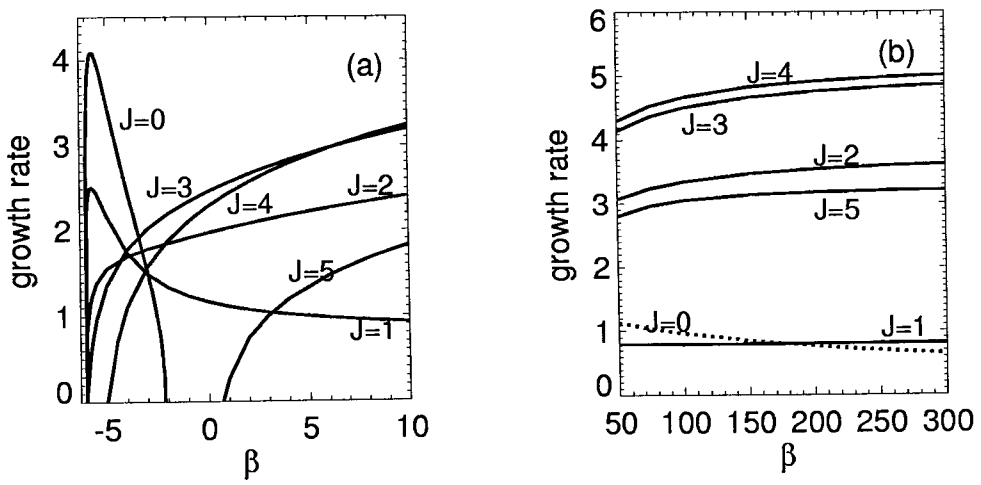

Figure 3.7: Growth rates of the maximally unstable eigenmodes vs β for one-ring solitary solutions. Dotted line in (b) displays $Im\lambda_0$ of the $J = 0$ internal eigenmode marked by Line 1 in Fig. 3.5. $\kappa = 3$.

One expects the propagation dynamics of solitary states to be mainly determined by the perturbation eigenmode with maximal growth rate. To examine this I performed an extensive series of numerical simulations of Eqs. (1), using both polar and cartesian grids. Predictions based on our stability analysis are in good agreement with the results of our simulations. An example of noise-stimulated break-up of a one-ring solution into three filaments is shown in Fig. 3.8(a). I plot the real part of the fundamental field profile rather than the intensity distributions to show that the daughter solitons formed from the ring are out of phase with the central one. Radiation losses in the break-up are quite small, so that the initial energy Q is mostly divided among the daughter solitons. Their diameters are comparable to the width of the initial ring. For β values where growth rates for $J = 3$ and $J = 4$ are almost equal the simulation results depended on the particular noise realisation, but I mostly observed the ring forming four filaments, one of which was usually less intense than the others.

Throughout the whole range of parameters where the symmetry-breaking instability is dominant we observed repulsion between the central spot and daughter filaments, which results from the fact they are out of phase [53, 100], see Fig. 3.8(a). This repulsive force makes the outer filaments move out along radii (Fig.

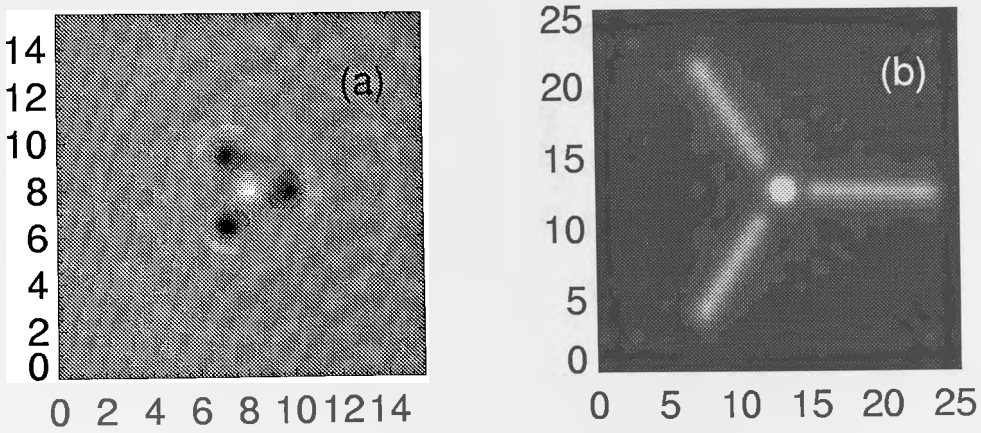

Figure 3.8: (a) Real part of the fundamental harmonic field at a late stage of a simulation of the symmetry-breaking process. (b) Superimposed images of its transverse intensity distribution at different values of z, showing radial trajectories of the daughter solitons. $\beta = -1$, $\kappa = 3$. Brightness and size of central spot in figure (b) are exaggerated by the superposition of multiple images.

3.8(b)), in contrast to the tangential motion of daughter solitons after breakup of one-ring solitary waves carrying non-zero orbital angular momentum [91], where inter-soliton forces are negligible in comparison to the need to conserve angular momentum.

Our stability analysis predicts a novel symmetry-preserving instability scenario where the $J = 0$ eigenmode dominates. This prediction is indeed confirmed by the simulations. For example, at $\beta = -4.2$, instead of fragmentation I observed coalescence of the ring with the central spot to form a single filament. After transient dynamics this filament forms an oscillating solitary wave, see Fig. 3.9. These undamped pulsations are related to the existence of an internal eigenmode of the ground-state solution [83].

Considering now two-ring solitary solutions, I present the growth rates for the dominant eigenmodes and an example of symmetry- breaking instability, see Fig. 3.10. General features of the dynamics are qualitatively similar to the one-ring situation.

The evolution of filaments following a symmetry breaking instability of peak-and-

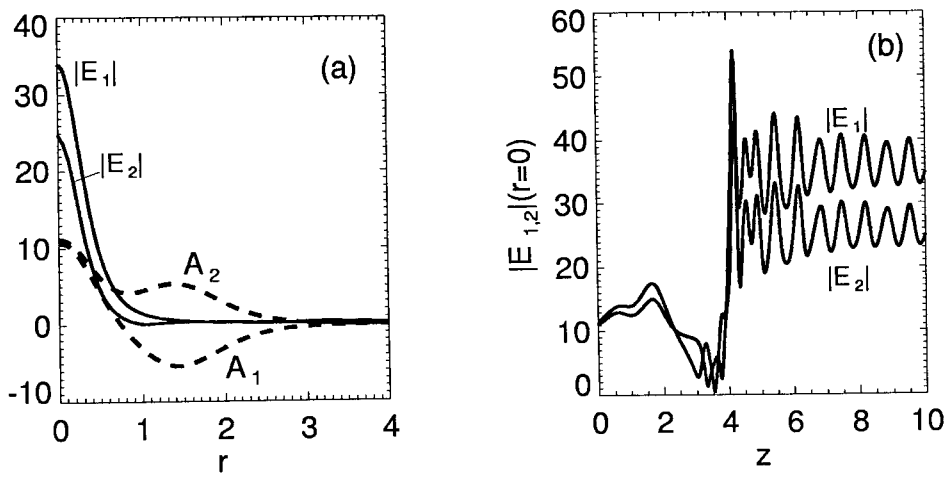

Figure 3.9: (a) Initial (dashed lines) and post-coalescence (solid lines) radial profiles of fundamental and second harmonics simulated where the symmetry-preserving instability is predicted to dominate. (b) Corresponding evolution of $|E_{1,2}|$ *at* $r = 0$ *vs propagation coordinate* z. $\kappa = 3$, $\beta = -4.2$

ring solitary solutions in saturable Kerr media [98] is a question which has not previously been examined. In simulations of this problem I observed the same sort of dynamics as described above for quadratic media, but with no coalescence phenomena. Note, also that higher-order one dimensional $\chi^{(2)}$ solitons are also known, see [56, 89, 96], but question of their stability has not yet been rigorously studied.

3.6 Summary

In this Chapter equations describing degenerate and nondegenerate three wave mixings in quadratic nonlinear media have been derived from the first principles. Review of the results and methods of the stability theory of the ground-state quadratic solitons has been presented. In particular, adiabatic theory of the soliton dynamics [60, 86] has been reproduced.

Detailed analysis of stability of cylindrically-symmetric higher-order solitary waves has been performed. For a wide range of positive mismatches, symmetry-breaking

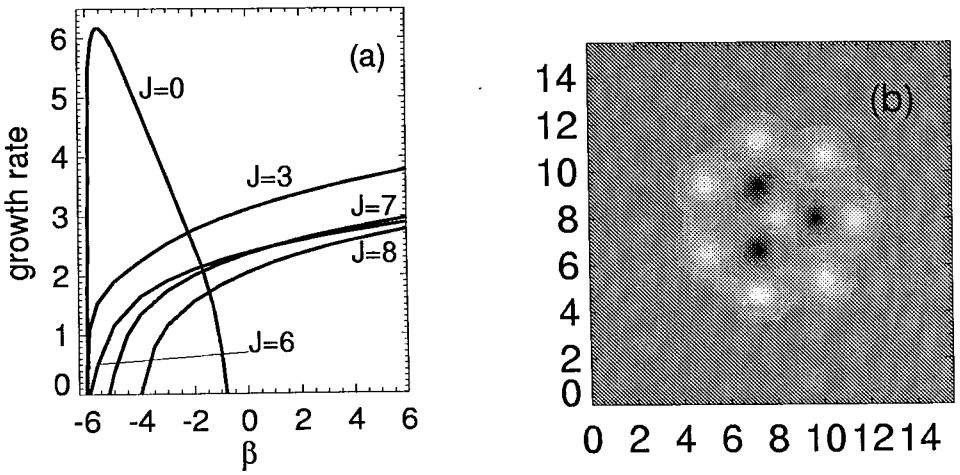

Figure 3.10: (a) Growth rates of the dominant unstable eigenmodes vs β for two-ring solitary solutions. (b) Real part of the fundamental field at a late stage of a simulation of the symmetry-breaking process. $\beta = 1$, $\kappa = 3$.

instability of the rings is predicted, and confirmed by simulations which show that the instability leads to filamentation into daughter solitons which are repelled radially from the central spot. For sufficiently negative phase mismatches I predict that a new symmetry- preserving instability becomes dominant. This is confirmed in simulations, in which the rings are found to coalesce with the central filament, forming an oscillating, single-peaked, solitary wave. Threshold of this novel instability is not given by the famous Vakhitov-Kolokolov formula (3.43).

Chapter 4

Modulational instability of solitary waves due to three-wave mixing

4.1 Introduction

In this Chapter I am going to present some of the analytical and numerical results related with modulational instability (MI) of quadratic solitons. This instability can happen for one- and two-dimensional spatial solitons due to group velocity dispersion terms, see Eqs. (3.14),(3.15) and (3.16),(3.17),(3.18). The case of MI of one-dimensional soliton in media with anomalous GVD for all harmonics is formally equivalent to the MI due to diffraction along second transverse dimension.

The problem of MI of $\chi^{(2)}$ solitons was pioneered by Kanashov and Rubenchik [101] in the context of degenerate three-wave mixing and during the $\chi^{(2)}$-boom of the last years it was re-explored and supported by numerical [102, 103, 59] and, in spatial case, by experimental [104] results. The nondegenerate case was studied in [105] and it reveals qualitatively different behaviour, which, as it should be already clear from the context of the Chapter 2, originates from the presence of

the extra symmetry in the differential phase ψ, see Eq. (3.61).

In first section of this Chapter I will present analytical results in low-frequency limit for one- and two-dimensional solitons. Peculiar and still unpublished points will be: showing presence of new unstable branch bifurcating from the continuum; and deriving analytical formulae for situation where MI of solitons happens close to the threshold of the longitudinal instability, specified by Eq. (3.43). Second section is devoted to nondegenerate situation and it is based on a recent paper [105].

4.2 Degenerate three-wave mixing

In degenerate case spatio-temporal evolution of the wave packet is governed by Eqs. (3.14),(3.15). For simplicity we will consider the case with $\partial_y = 0$, $\alpha_1 = 1/2$, $\alpha_2 = 1/4$ and $\delta_{1,2} = 0$:

$$\begin{aligned} i\partial_z E_1 + \frac{1}{2}\partial_x^2 E_1 + \gamma_1 \partial_\tau^2 E_1 + E_1^* E_2 = 0, \\ i\partial_z E_2 + \frac{1}{4}\partial_x^2 E_2 + \gamma_2 \partial_\tau^2 E_2 + \frac{1}{2}E_1^2 = \beta E_2. \end{aligned} \tag{4.1}$$

As was discussed in previous Chapter, Eqs. (4.1) with suppressed temporal derivatives have family of soliton solutions $E_m = A_m(x)e^{im(\kappa z+\phi)}$, $m = 1, 2$. To study MI of this solitons one can seek solutions of Eqs. (4.1) in the form of spatial solitons weakly modulated in time at frequency $\Omega \geq 0$:

$$E_m = (A_m(x) + (U_m(x,z) + iW_m(x,z))\cos\Omega t)e^{im(\kappa z+\phi)}. \tag{4.2}$$

Setting $U_m = u_m e^{\lambda z}$, $W_m = w_m e^{\lambda z}$, we obtain two adjoint eigenvalue problems

$$(\hat{\mathcal{L}}_0 + \Omega^2\hat{\gamma})(\hat{\mathcal{L}}_1 + \Omega^2\hat{\gamma})\vec{u} = -\lambda^2\vec{u}, \tag{4.3}$$

$$(\hat{\mathcal{L}}_1 + \Omega^2\hat{\gamma})(\hat{\mathcal{L}}_0 + \Omega^2\hat{\gamma})\vec{w} = -\lambda^2\vec{w}, \tag{4.4}$$

where $\vec{v} = (u_1, u_2)^T$, $\vec{w} = (w_1, w_2)^T$, $\hat{\mathcal{L}}_{0,1}$ are given by Eqs. (3.28), (3.29) and

$$\hat{\gamma} = \begin{pmatrix} \gamma_1 & 0 \\ 0 & \gamma_2 \end{pmatrix}. \tag{4.5}$$

In the general situation the stability problem can be solved only numerically, but for small absolute values of λ we can obtain analytical results.

Phase, translational and Galilean symmetries and infinitesimal variations of κ allow us to identify neutral eigenmodes of the adjoint operators $\hat{\mathcal{L}}_1\hat{\mathcal{L}}_0$ and $\hat{\mathcal{L}}_0\hat{\mathcal{L}}_1$. These eigenmodes are $\vec{w}_\phi = (A_1, 2A_2)^T$, $\vec{w}_v = x(A_1, 2A_2)^T$, $\vec{u}_\kappa = \partial_\kappa(A_1, A_2)^T$, and $\vec{u}_x = \partial_x(A_1, A_2)^T$. These four modes obey following identities: $\hat{\mathcal{L}}_0\vec{w}_\phi = 0$, $\hat{\mathcal{L}}_0\vec{w}_v = -\vec{u}_x$, $\hat{\mathcal{L}}_1\vec{u}_\kappa = -\vec{w}_\phi$ and $\hat{\mathcal{L}}_1\vec{u}_x = 0$.

Similarly to the previously studied cases branches of discrete spectrum produced by the spatially symmetric $\vec{w}_\phi$, $\vec{u}_\kappa$ and by the spatially asymmetric vectors $\vec{w}_v$, $\vec{u}_x$ can be considered as independent ones. To study the discrete spectrum arising due to branching of the symmetric/asymmetric modes it is naturally to consider EVP (4.4)/(4.3).

Let us start from the symmetric problem. We seek solution of the EVP (4.4) in the form

$$\vec{w} = \vec{w}_\phi + \vec{w}_1 + \ldots, \tag{4.6}$$

where $|\vec{w}_1| \sim \lambda^2 \sim \varepsilon \ll 1$. Generally, one must also specify order of Ω^2, but at this stage it is enough to assume that $\Omega^2 \sim \varepsilon^n$ $(n \geq 1)$. Using the identity $\hat{\mathcal{L}}_1\vec{u}_\kappa = -\vec{w}_\phi$ it is straightforward to show that

$$\vec{w}_1 = \hat{\mathcal{L}}_0^{-1}\left(\lambda^2\vec{u}_\kappa - \Omega^2\hat{\gamma}\vec{w}_\phi\right). \tag{4.7}$$

Multiplying (4.4) by $\vec{u}_\kappa$ and using Eqs. (4.6), (4.7) we get

$$\Omega^2\langle\hat{\gamma}\vec{w}_\phi, \vec{w}_\phi\rangle \simeq \lambda^2\left(\frac{1}{2}\partial_\kappa Q + \lambda^2 M - \lambda^2\Omega^2\langle\hat{\mathcal{L}}_0^{-1}\hat{\gamma}\vec{w}_\phi, \vec{u}_\kappa\rangle\right), \tag{4.8}$$

where $Q = \int dx(A_1^2 + 2A_2^2)$ and $M = \langle\hat{\mathcal{L}}_0^{-1}\vec{u}_\kappa, \vec{u}_\kappa\rangle$. It is time now to specify order of Ω^2 and $\partial_\kappa Q$. If we are far from the threshold of the longitudinal instability, $\partial_\kappa Q = 0$, we can assume $\partial_\kappa Q \sim \varepsilon^0$ and $\lambda^2 \sim \Omega^2 \sim \varepsilon$. In this situation in the leading order λ^2 is

$$\lambda^2 \simeq \frac{2\Omega^2\langle\hat{\gamma}\vec{w}_\phi, \vec{w}_\phi\rangle}{\partial_\kappa Q} = \frac{2\Omega^2}{\partial_\kappa Q}\int dx(\gamma_1 A_1^2 + 4\gamma_2 A_2^2). \tag{4.9}$$

In a particular case $\gamma_1 = 2\gamma_2$ Eq. (4.8) becomes

$$\lambda^2 \simeq 2\Omega^2\gamma_1 \frac{Q}{\partial_\kappa Q},$$

which coincides with the corresponding formula for single and coupled NLS equations, see Eqs. (2.41), (2.50).

If the point $\partial_\kappa Q = 0$ is close then to have self-consistent expression which incorporates branches of the spectrum due to both neutral and gap modes we should assume that $\partial_\kappa Q \sim \lambda^2 \sim \varepsilon$ and $\Omega^2 \sim \varepsilon^2$. In this situation λ^2 obeys the quadratic equation

$$\Omega^2\langle\hat{\gamma}\vec{w}_\phi, \vec{w}_\phi\rangle \simeq \lambda^2\left(\frac{1}{2}\partial_\kappa Q + \lambda^2 M\right), \tag{4.10}$$

which has roots

$$\lambda_\pm^2 = \frac{1}{2M}\left(-\frac{1}{2}\partial_\kappa Q \pm \sqrt{\frac{1}{4}(\partial_\kappa Q)^2 + 4M\Omega^2\langle\hat{\gamma}\vec{w}_\phi, \vec{w}_\phi\rangle}\right). \tag{4.11}$$

At $\Omega = 0$ Eq. (4.8) becomes

$$\lambda^2\left(\frac{1}{2}\partial_\kappa Q + \lambda^2 M\right) = 0 \tag{4.12}$$

and it now describes doubly degenerate neutral mode $\vec{w}_\phi$ and modes with eigenvalues

$$\lambda \simeq \pm\sqrt{-\frac{\partial_\kappa Q}{2M}}. \tag{4.13}$$

One of the last modes is responsible for instability happening at $\partial_\kappa Q < 0$. Looking at Eq. (4.13) one can easily recognise Eq. (3.59) obtained in the previous Chapter by the slightly more sophisticated adiabatic approach.

Now we turn our attention to the branching of the spatially asymmetric eigenmodes and seek solution of EVP (4.3) in the form

$$\vec{u} = \vec{u}_x + \vec{u}_1 + \ldots, \tag{4.14}$$

where $|\vec{u}_1| \sim \varepsilon$. Acting similarly to the symmetric case we find that

$$\vec{u}_1 = \hat{\mathcal{L}}_1^{-1}\left(\lambda^2\vec{w}_v - \Omega^2\hat{\gamma}\vec{u}_x\right). \tag{4.15}$$

In order to satisfy solvability condition of the first order problem we have to multiply (4.3) by $\vec{w}_v$, which after some algebra gives

$$\Omega^2\langle\hat{\gamma}\vec{u}_x,\vec{u}_x\rangle \simeq \lambda^2\left(\langle\vec{u}_x,\vec{w}_v\rangle + \lambda^2\langle\hat{\mathcal{L}}_1^{-1}\vec{w}_v,\vec{w}_v\rangle - \lambda^2\Omega^2\langle\hat{\mathcal{L}}_1^{-1}\hat{\gamma}\vec{u}_x,\vec{w}_v\rangle\right). \qquad (4.16)$$

Because of the fact that there are no spatially asymmetric modes inside the gap of the continuous spectrum for $\Omega = 0$ all inner products in Eq. (4.16) always have order of unity and therefore in the leading approximation λ^2 is given by

$$\lambda^2 \simeq \frac{\Omega^2\langle\hat{\gamma}\vec{u}_x,\vec{u}_x\rangle}{\langle\vec{u}_x,\vec{w}_v\rangle} = 2\Omega^2\frac{\langle\hat{\gamma}\vec{u}_x,\vec{u}_x\rangle}{Q}, \qquad (4.17)$$

which again should be compared with corresponding formula for NLS equations, see Eqs. (2.42), (2.51).

I have to say that the approach presented here is a modification of the approach which was applied Chapter 2 to the coupled NLS equations. It allows continuation into the region of small Ω not only neutrally stable modes, but also stable and unstable eigenmodes with eigenvalues close to zero. It is clear that the root λ_+^2 of Eq. (4.10) corresponds to the spectral branch produced by the neutral modes and that the root λ_-^2 corresponds to the branch produced by the stable ($\partial_\kappa Q > 0$) or unstable ($\partial_\kappa Q < 0$) modes which have nonzero eigenvalues.

Note, that at the point where the analytical solution is known the growth rates (4.9), (4.17) can be found in explicit form and values of Ω where instabilities disappear also can be calculated, see [102, 103]. Results of the similar calculation for the type II case will be presented in the next section. It is obvious that possibility to play with relative energies of first and second harmonics and signs of $\gamma_{1,2}$ gives quite a few possible scenarious of MI in $\chi^{(2)}$ model. However, below we will consider only the simplest but typical situations with γ_1 and γ_2 having the same signs.

Let us now to formulate conclusions, which can be made on the basis of the analytical formulas (4.9), (4.17), (4.11) describing the situation with small values of λ and Ω and compare these conclusions with results of numerical analysis.

The last is obviously always necessary to investigate the whole range of Ω and understand the competition between different instability branches.

Anomalous dispersion, $\gamma_{1,2} > 0$.
It is clear from (4.9), (4.11) that if $\partial_\kappa Q > 0$ then only the neutral mode $\vec{w}_\phi$ gives onset to the MI instability and that the eigenvalues corresponding to the stable gap modes (if they exist) remain within the gap of the continuum spectrum. For $\partial_\kappa Q < 0$ the situation is reversed. Namely, the eigenvalue corresponding to $\vec{w}_\phi$ shifts inside the gap with Ω increasing and eigenvalue corresponding to the eigenmode responsible for the longitudinal instability grows with Ω increasing.

In this case MI branches predicted by analytical analysis seem to be the only unstable branches of the spectrum. Numerically calculated growth rates and spatial profiles of unstable eigenmodes vs Ω are presented in Fig. 4.3. The nonlinear stage of modulational instability development was analysed by direct numerical solution of Eqs. (4.1). In the case when solitary stripe is stable with respect to longitudinal perturbation, $\partial_\kappa Q > 0$, the initially uniform stripe develops into multihump structure and each hump forms into a stable soliton-like filament oscillating with propagation, see Fig. 4.1. Such a scenario is typical not only for quadratic solitons, see [59, 103, 106], but also for solitons in media with saturable nonlinearity [107].

More intriguing problem is what happens with longitudinally unstable solitary stripe, $\partial_\kappa Q < 0$. Because of the fact that longitudinal instability is strongly suppressed by the modulational one, see Fig. 4.3(b), break up of the stripe into filaments is the dominating process compare to spreading or beating of the stripe as whole, see previous Chapter. Most of the energy of the filaments formed at the initial stage of the instability contains in the second harmonic but important that always there is a seeding at fundamental frequency. Thus according to the results reported in Ref. [108] conditions for formation of quadratic solitons are still satisfied. Indeed, numerical simulation shows that the filaments eventually form soliton-like entities which now carry more energy in the fundamental field, see Fig. 4.2. This redistribution of the energy through the cascading and mutual

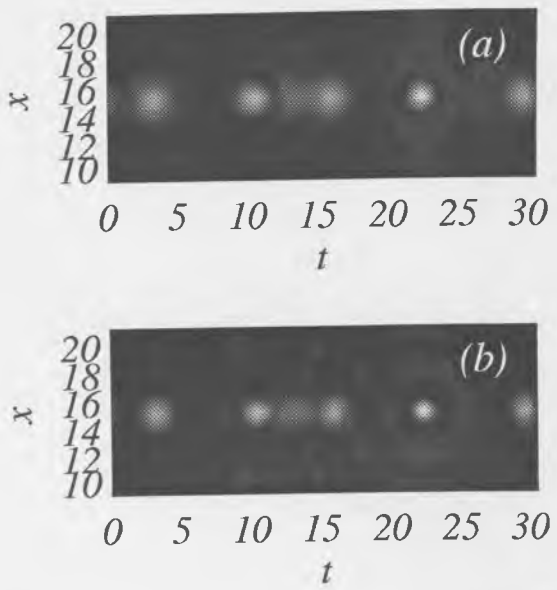

Figure 4.1: Development of the MI for $\beta = 0$ $(0 < \partial_\kappa Q \sim \varepsilon^0)$, $\kappa = 1$, $\gamma_1 = 2\gamma_2 = 0.5$. *(a)* $|E_1|$, *(b)* $|E_2|$ *for* $z = 25$.

trapping mechanisms leads to a quite large radiation into nonsolitary forms, see Fig. 4.2(b).

Note that, filaments are usually formed after propagation of 4-6 diffraction lengths for noise level $\sim 1-3\%$. Large propagation distances corresponding to the results presented in Figs. 4.1, 4.2 were taken to actually show that filaments indeed form quasi-stable soliton-like structures.

Normal dispersion $\gamma_{1,2} < 0$.

Eq. (4.17) indicates that spatially asymmetrical ('snake') instability is always presented in this case. Spatially symmetrical ('neck') instability starting from the neighborhood of $\Omega = 0$ is clearly impossible when $\partial_\kappa Q \sim \varepsilon^0$. However, if $\partial_\kappa Q \sim \varepsilon$ low-frequency neck MI becomes possible for either sign of $\partial_\kappa Q$, see Eq. (4.11). If $\partial_\kappa Q > 0$, than neck MI starts to grow from

$$\Omega_c^2 = \frac{(\partial_\kappa Q)^2}{16M\langle\hat{\gamma}\vec{w}_\phi, \vec{w}_\phi\rangle},$$

because at $\Omega = \Omega_c$ two stable gap modes collide and give onset to the complex conjugated eigenvalues. If $\partial_\kappa Q < 0$ than both λ_+^2 and λ_-^2 are positive. λ_-^2 increases and λ_+^2 decreases with Ω increasing and at $\Omega = \Omega_c$ they collide and

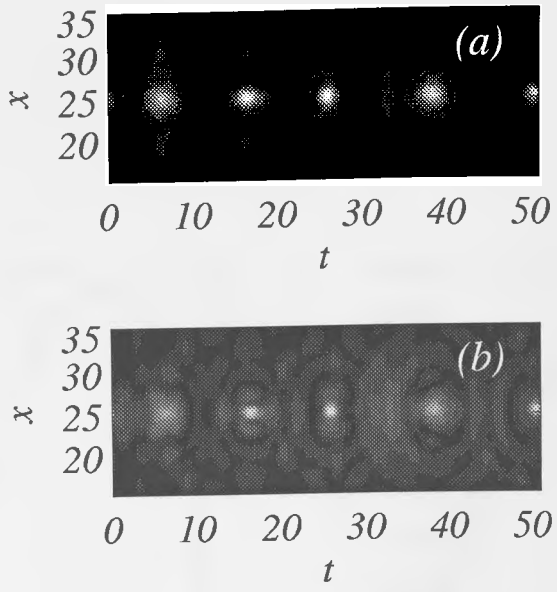

Figure 4.2: Development of the MI for $\beta = -1.93$ $(0 > \partial_\kappa Q \sim \varepsilon)$, $\kappa = 1$, $\gamma_1 = 2\gamma_2 = 0.5$. *(a)* $|E_1|$, *(b)* $|E_2|$ *for* $z = 50$.

transform into complex conjugate eigenvalues.

For normal GVD numerical analysis indicates presence not only MI branches predicted by the asymptotical analysis but also other branches which split form continuum at some critical values of Ω, see below for details.

Let us start from consideration of such β and κ values which are close to the bifurcation point $\partial_\kappa Q = 0$ from the right, i.e. $\partial_\kappa Q > 0$. Then there are two eigenmodes inside the gap of continuous spectrum at $\Omega = 0$ with the eigenvalues given by Eq. (4.13). With Ω increasing the eigenvalues corresponding to the continuation of the gap modes and of the neutral mode $\vec{w}_\phi$ start to approach each other and finally they collide at $\Omega = \Omega_c$ giving rise to the onset of the neck-type instability with complex conjugated eigenvalues. Details of this scenario are shown in Fig. 4.4. Note, that for normal GVD gap is narrowing with increasing Ω and it closes at $\Omega_g^2 = \min(\kappa/|\gamma_1|, (2\kappa + \beta)/|\gamma_2|)$. With further increase of Ω instability growth rate approaches its maximum, then decays and finally disappears inside the continuum at $\Omega > \Omega_g$, see Fig. 4.5 (full line). Slightly before this point but after the closure of the gap branch of discrete spectrum with purely real eigenvalues splits from continuum. When the corresponding growth rate, see

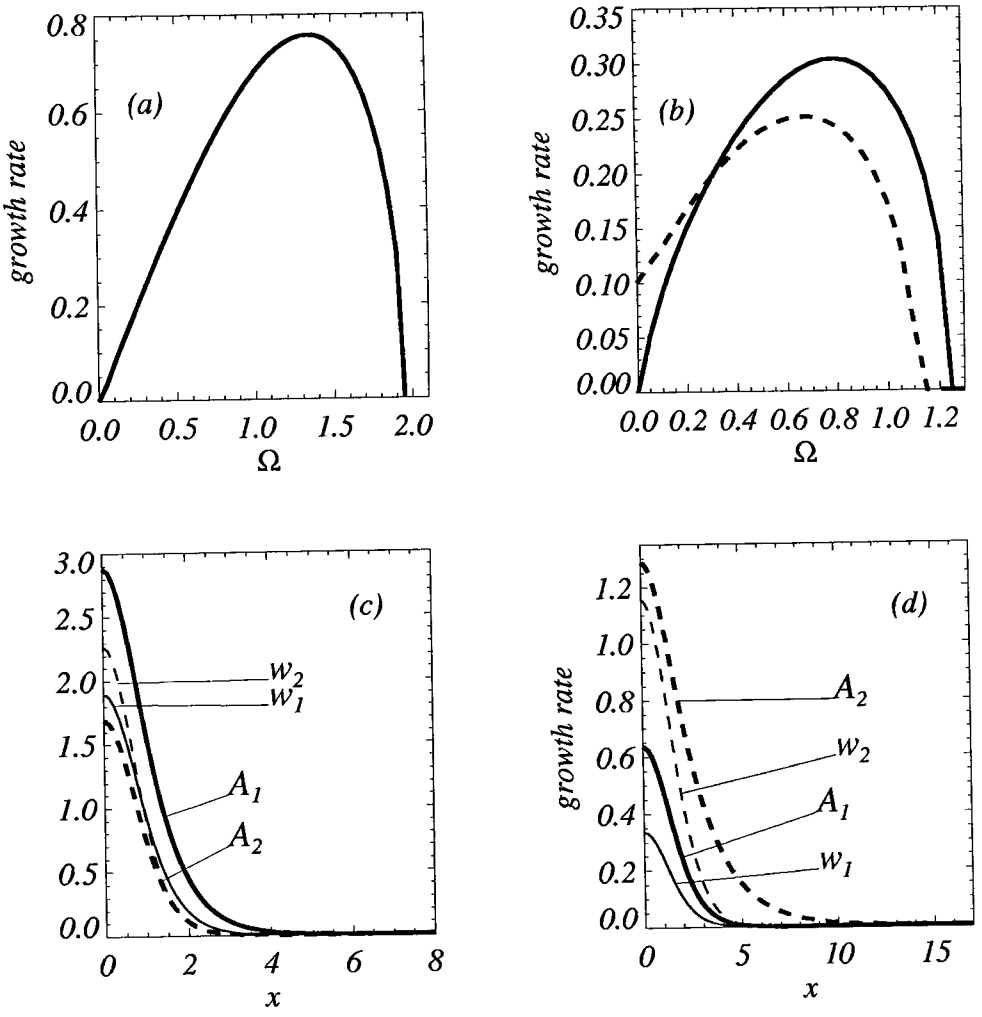

Figure 4.3: Instability growth rates, spatial profiles of the solitary solutions and of the unstable eigenmodes for $\kappa = 1$, $\gamma_1 = 2\gamma_2 = 0.5$. ($\partial_\kappa Q = 0$ at $\beta \simeq 1.9$) *(a), (b) MI growth rates vs* Ω: *(a)* $\beta = 0$; *(b)* $\beta = -1.87$ *(full line),* $\beta = -1.93$ *(dashed line). (c), (d) Components of the unstable eigenmodes: (c)* $\beta = 0$, $\Omega = 1.35$; $\beta = -1.93$, $\Omega = 0.65$.

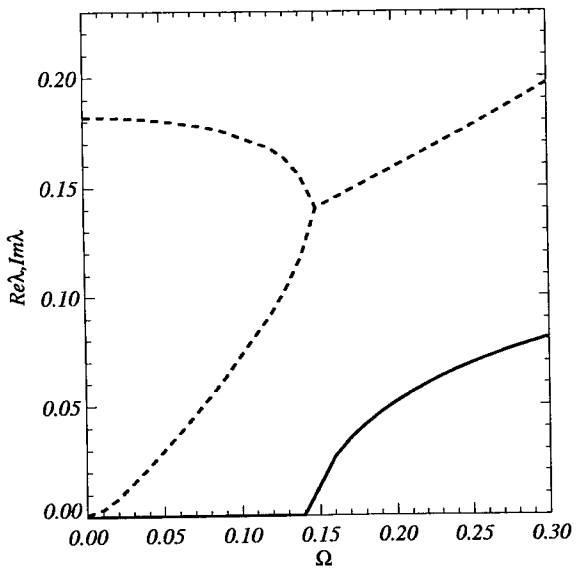

Figure 4.4: Bifurcation diagram showing collision of two gap modes and onset of neck-type instability with complex conjugated eigenvalues: $\beta = -1.8$, $\kappa = 1$, $\gamma_1 = 2\gamma_2 = -0.5$.

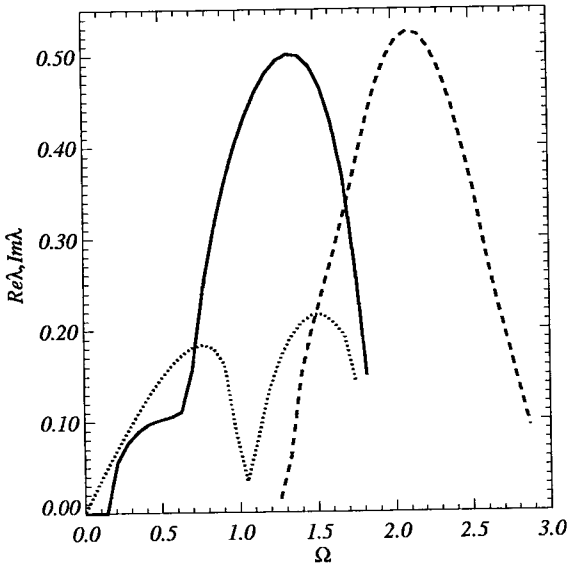

Figure 4.5: Instability growth rates for $\kappa = 1$, $\beta = -1.8$. *Full line corresponds to the neck MI with complex conjugated eigenvalues, dashed line to the neck MI with real eigenvalue and dotted line to snake MI. For the snake MI first maximum belongs to the branch with real eigenvalue and second one to the branch with conjugated eigenvalues.*

dashed line in Fig. 4.5, approaches its maximum, it appears to be slightly larger than growth rate associated with unstable band linked to the complex conjugated eigenvalues. Considering snake instability we also found two unstable bands of Ω. First band bifurcates from translational mode at $\Omega = 0$ and second band bifurcates from continuum having complex conjugated eigenvalues. Comparing growth rates due to these two neck-type instabilities and growth rate due to snake instability, see Fig. 4.5, one can see that the latter is strongly suppressed. Note, that maximal growth rates of the secondary MI branches happen at $\tilde{\Omega}_{max}$, which are approximatly twice the frequency Ω_{max} giving maximum of the primary instabilities.

Increasing wave-vector mismatch β and keeping $\kappa = 1$, i.e. moving away from the point $\partial_\kappa Q = 0$, secondary branches of the neck and snake instabilities quickly decay and finally disappear. At the same time neck instability with complex conjugate eigenvalues survives for wide range of β and remains dominant over snake instability up to $\beta \sim 0$, see Fig. 4.6. Typical spatial profiles of the most unstable neck and snake eigenvectors are presented in Fig. 4.7. I have to note that scenario of appearance of the complex conjugated eigenvalues changes with increasing β. After disappearence of the gap modes at $\Omega = 0$ [83], branch of MI with complex conjugated eigenvalues splits from continuum after the gap closure. Direct numerical simulation of Eqs. (4.1) with initial conditions in the form of a soliton stripe perturbed only by noise fully supports the presented stability analysis, see Figs. 4.8,4.9,4.10.

4.3 Nondegenerate three-wave mixing

Considering MI due to non-degenerate 3WM one can expect that at least formally situation should be very similar to the case of the coupled NLS equations considered in Chapter 2, because symmetry properties of these two models are the same.

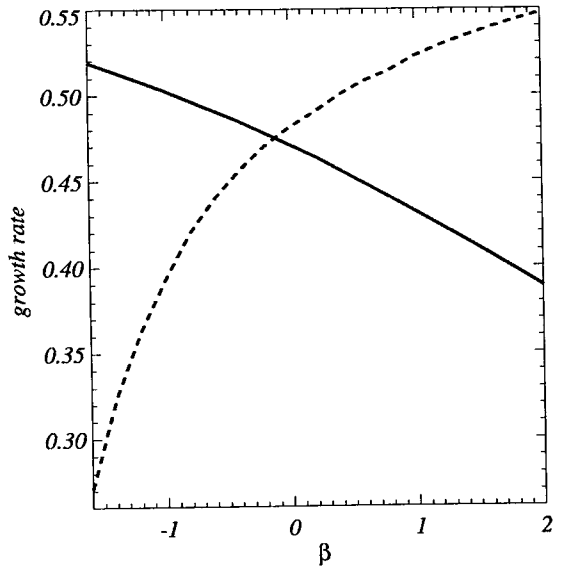

Figure 4.6: Maximal growth rates of the neck (full line) and snake (dashed line) instabilities. $\gamma_1 = \gamma_2 = -0.5$, $\kappa = 1$.

Let us rewrite here for convenience model equations (3.16), (3.17), (3.18) describing three wave interaction choosing $\alpha_{1,2} = 2\alpha_3 = 1/2$:

$$\begin{aligned} i\partial_z E_1 + \frac{1}{2}\partial_x^2 E_1 + \gamma_1 \partial_t^2 E_1 + E_2^* E_3 &= 0, \\ i\partial_z E_2 + \frac{1}{2}\partial_x^2 E_2 + \gamma_2 \partial_t^2 E_2 + E_1^* E_3 &= 0, \\ i\partial_z E_3 + \frac{1}{4}\partial_x^2 E_3 + \gamma_3 \partial_t^2 E_3 + E_1 E_2 &= \beta E_3. \end{aligned} \tag{4.18}$$

The stability boundary against purely spatial perturbations boundary of 3-wave solitons is given by the condition (3.65). Spatially stable domain is in fact almost the entire domain of soliton existence, excluding only a small range of κ, δ values with $\beta < 0$ [61, 62]. To study MI due to GVD we seek solutions of Eqs. (4.18) in the form of spatial solitons weakly modulated in time at frequency $\Omega \geq 0$:

$$E_m = (A_m(x) + (U_m(x,z) + iW_m(x,z))\cos\Omega t)e^{i(\kappa_m z + \phi_m)},$$

where $m = 1, 2, 3$, $\kappa_{1,2} = \kappa \pm \delta$, $\kappa_3 = 2\kappa$, $\phi_{1,2} = \phi \pm \psi$, $\phi_3 = 2\phi$, ϕ and ψ are arbitrary constants. Setting $U_m = u_m e^{\lambda z}$, $W_m = w_m e^{\lambda z}$, we obtain two eigenvalue problems

$$(\hat{\mathcal{L}}_0 + \Omega^2\hat{\gamma})(\hat{\mathcal{L}}_1 + \Omega^2\hat{\gamma})\vec{u} = -\lambda^2\vec{u} \tag{4.19}$$

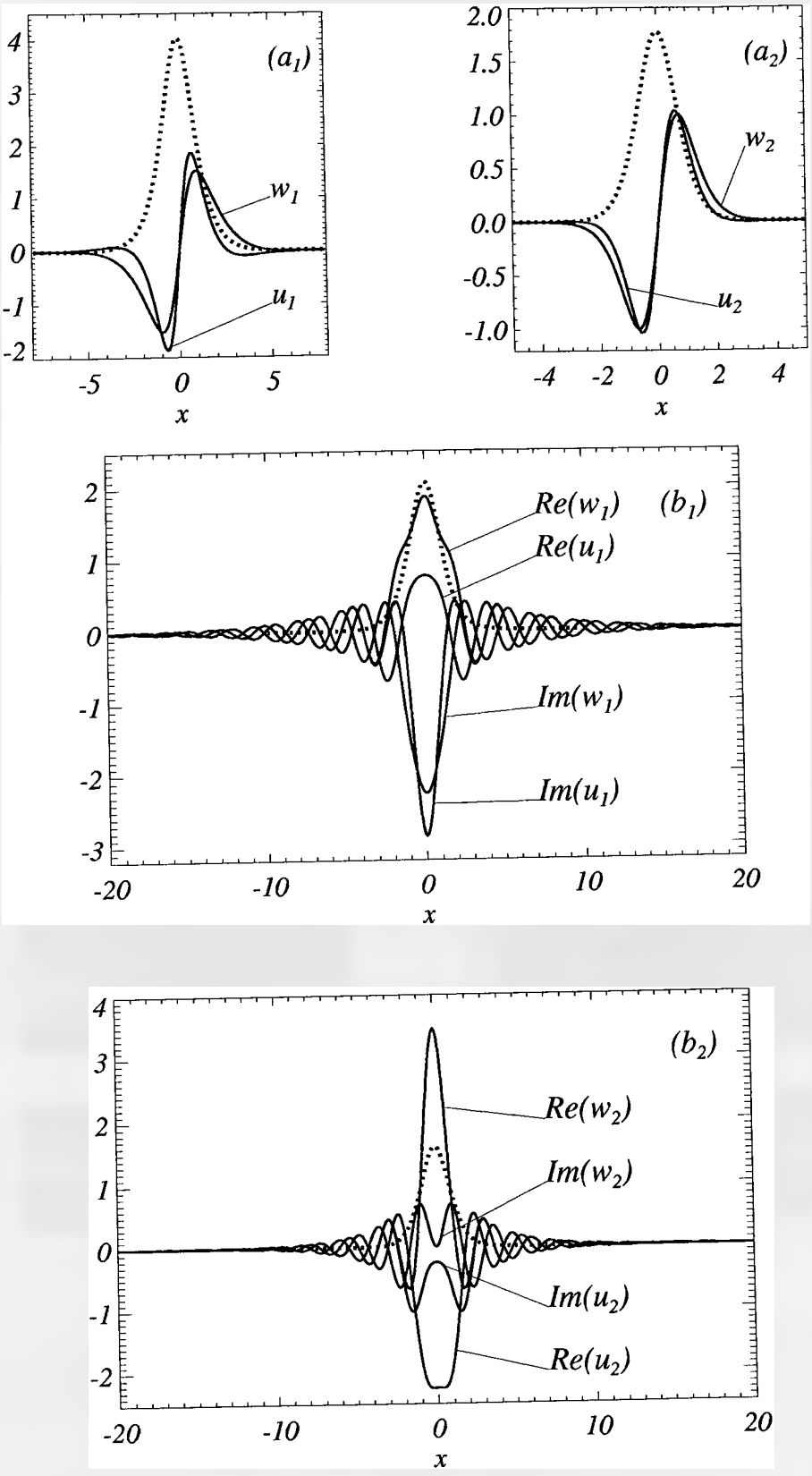

Figure 4.7: Spatial profiles of the most unstable eigenvectors: $\gamma_1 = \gamma_2 = -0.5$, $\kappa = 1$. $(a_{1,2})$ $\beta = 2$, $\Omega = 0.9$; $(b_{1,2})$ $\beta = -1$, $\Omega = 1.9$. *Dotted lines mark corresponding profiles of the solitary waves.*

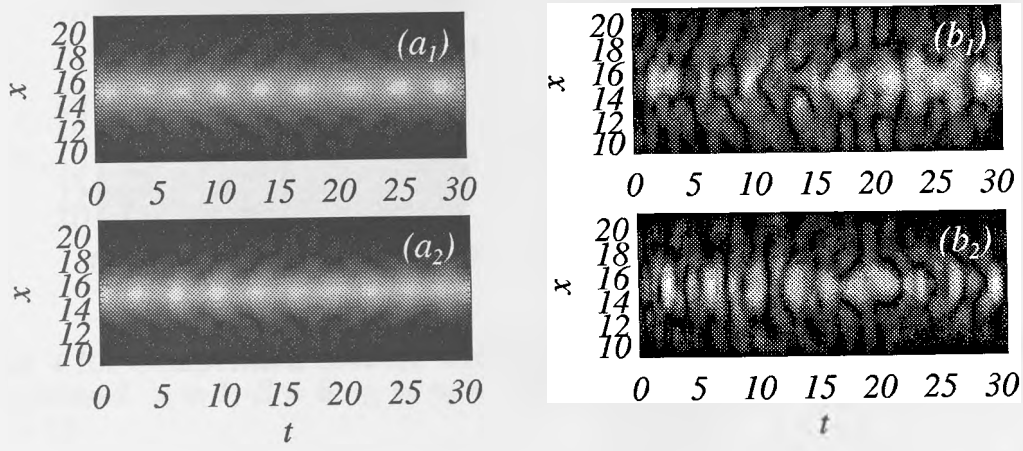

Figure 4.8: Competition between neck and snake instabilities. Snake instability is suppressed. $\kappa = 1$, $\beta = -1$, $\gamma_1 = \gamma_2 = -0.5$. $(a_{1,2})$ $|E_{1,2}|$ *at* $z = 10$, $(b_{1,2})$ $|E_{1,2}|$ *at* $z = 15$

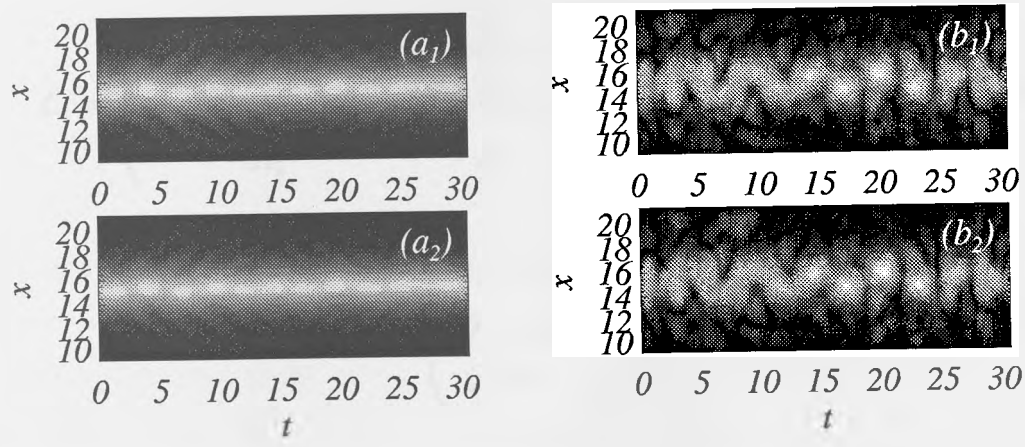

Figure 4.9: Competition between neck and snake instabilities. Neck and snake instabilities have approximatly equal growth rates. $\kappa = 1$, $\beta = 0$, $\gamma_1 = \gamma_2 = -0.5$. $(a_{1,2})$ $|E_{1,2}|$ *at* $z = 10$, $(b_{1,2})$ $|E_{1,2}|$ *at* $z = 15$

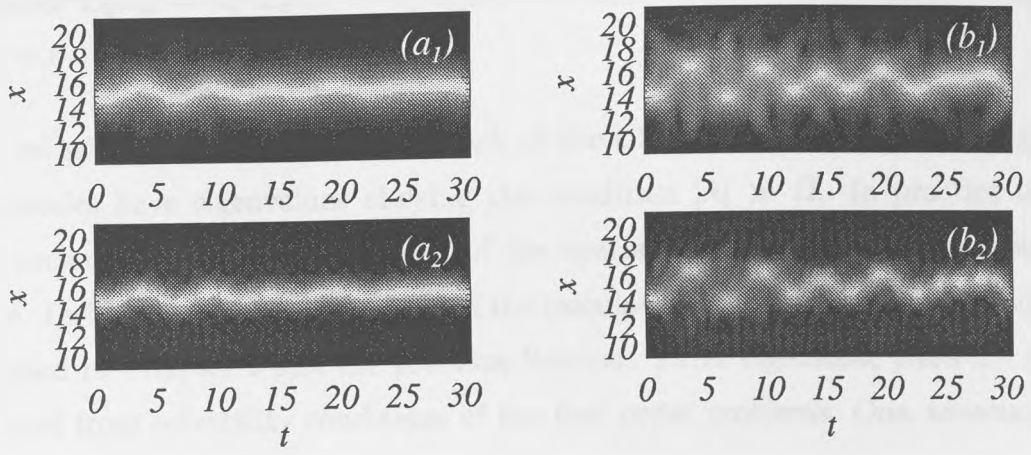

Figure 4.10: Competition between neck and snake instabilities. Neck instability is suppressed. $\kappa = 1$, $\beta = 5$, $\gamma_1 = \gamma_2 = -0.5$. $(a_{1,2})$ $|E_{1,2}|$ *at* $z = 10$, $(b_{1,2})$ $|E_{1,2}|$ *at* $z = 12$

$$(\hat{\mathcal{L}}_1 + \Omega^2\hat{\gamma})(\hat{\mathcal{L}}_0 + \Omega^2\hat{\gamma})\vec{w} = -\lambda^2\vec{w} \tag{4.20}$$

where $\vec{u} = (u_1, u_2, u_3)^T$, $\vec{w} = (w_1, w_2, w_3)^T$ and

$$\hat{\mathcal{L}}_0 = \begin{pmatrix} -\frac{1}{2}\vec{\nabla}_\perp^2 + \kappa + \delta & A_3 & -A_2 \\ A_3 & -\frac{1}{2}\vec{\nabla}_\perp^2 + \kappa - \delta & -A_1 \\ -A_2 & -A_1 & -\frac{1}{4}\vec{\nabla}_\perp^2 + 2\kappa + \beta \end{pmatrix}, \tag{4.21}$$

$$\hat{\mathcal{L}}_1 = \begin{pmatrix} -\frac{1}{2}\vec{\nabla}_\perp^2 + \kappa + \delta & -A_3 & -A_2 \\ -A_3 & -\frac{1}{2}\vec{\nabla}_\perp^2 + \kappa - \delta & -A_1 \\ -A_2 & -A_1 & -\frac{1}{4}\vec{\nabla}_\perp^2 + 2\kappa + \beta \end{pmatrix}, \tag{4.22}$$

$$\hat{\gamma} = \begin{pmatrix} \gamma_1 & 0 & 0 \\ 0 & \gamma_2 & 0 \\ 0 & 0 & \gamma_3 \end{pmatrix}. \tag{4.23}$$

Phase and Galilean symmetries generate three neutral eigenmodes of the operator $\hat{\mathcal{L}}_1\hat{\mathcal{L}}_0$. These modes are $\vec{w}_\phi = (A_1, A_2, 2A_3)^T$, $\vec{w}_\psi = (A_1, -A_2, 0)^T$, and $\vec{w}_v = x(A_1, A_2, 2A_3)^T$. Infinitesimal variations of κ and δ, and translational symmetry generate neutral modes of the adjoint operator $\hat{\mathcal{L}}_0\hat{\mathcal{L}}_1$: $\vec{u}_\kappa = \partial_\kappa(A_1, A_2, A_3)^T$, $\vec{u}_\delta = \partial_\delta(A_1, A_2, A_3)^T$, and $\vec{u}_x = \partial_x(A_1, A_2, A_3)^T$. These six modes obey the following

identities $\hat{\mathcal{L}}_0\vec{w}_\phi = 0$, $\hat{\mathcal{L}}_0\vec{w}_\psi = 0$, $\hat{\mathcal{L}}_0\vec{w}_v = -\vec{u}_x$, $\hat{\mathcal{L}}_1\vec{u}_\kappa = -\vec{w}_\phi$, $\hat{\mathcal{L}}_1\vec{u}_\delta = -\vec{w}_\psi$, $\hat{\mathcal{L}}_1\vec{u}_x = 0$.

Here we will apply asymptotic approach of the Chapter 2 assuming that all gap eigenmodes have eigenvalues obeying the condition $|\lambda| \gg \Omega$. In practice this only excludes a small neighborhood of the spatial stability boundary discussed above. I will omit most of the details of the calculations because they were already discussed in Chapter 2 and the previous Section. Three eigenvalue pairs $\pm\lambda$ are obtained from solvability conditions of the first order problems. One, associated with the asymmetric eigenvector $\vec{w}_x$, obeys

$$\lambda_x^2 \simeq -\frac{2\Omega^2}{Q}\int dx \sum_{m=1}^{3} \gamma_m (\partial_x A_m)^2. \tag{4.24}$$

Clearly the asymmetric mode is unstable for *normal* GVD, which corresponds to the snake instabilities found in NLS, see Chapter 2, and degenerate 3WM [101, 102, 103] models. In particular, for the above-quoted exact solution we find

$$\lambda_x^2 \simeq -\frac{4\kappa}{15}\left(\frac{1}{2}(\gamma_1+\gamma_2)+\gamma_3\right),$$

which coincides with the corresponding formula for the Type I case [102] on putting $\gamma_1 = \gamma_2$ and rescaling.

The other two eigenvalue pairs are associated with linear combinations of the spatially symmetric vectors $C_\varphi\vec{w}_\varphi + C_\psi\vec{w}_\psi$, and thus with neck-type instabilities. They are the roots of

$$a\lambda^4 + b\Omega^2\lambda^2 + c\Omega^4 = 0, \tag{4.25}$$

where $2a = (\partial_\delta Q \partial_\kappa Q_u - \partial_\kappa Q \partial_\delta Q_u)$, $b = \partial_\kappa Q(\gamma_1 Q_1 + \gamma_2 Q_2) + \partial_\delta Q_u(\gamma_1 Q_1 + \gamma_2 Q_2 + 4\gamma_3 Q_3) + (\partial_\kappa Q_u + \partial_\delta Q)(\gamma_2 Q_2 - \gamma_1 Q_1)$, $c = -8(\gamma_1\gamma_2 Q_1 Q_2 + \gamma_2\gamma_3 Q_2 Q_3 + \gamma_1\gamma_3 Q_1 Q_3)$ and a was specified earlier. These expressions are quite complicated, but yield some important general results. Clearly c is negative when all γ_m of the same sign. Since $a > 0$ throughout the spatially monostable domain, it follows that the two roots λ^2 are always real and of opposite sign, so that there is *always* an unstable neck-type mode. Thus similarly to the case of the coupled NLS equations we establish *coexistence and competition of neck and snake instabilities for normal GVD.*

Simple analytic expressions for growth rates of these neck modes can be obtained in several special cases, e.g. in the case of second harmonic generation ($\omega_1 = \omega_2$). Setting $\gamma_1 = \gamma_2$ and $\delta = 0$ the two eigenmodes have either $C_\varphi = 0$ or $C_\psi = 0$, with eigenvalues

$$\lambda_\psi^2 \simeq 2\gamma_1\Omega^2 \frac{Q_1}{\partial_\delta Q_1}, \qquad \lambda_\phi^2 \simeq \frac{4\Omega^2}{\partial_\kappa Q}(\gamma_1 Q_1 + 2\gamma_3 Q_3). \tag{4.26}$$

For $\delta = 0$, $\partial_\kappa Q$ is positive and $\partial_\delta Q_1$ is negative in the spatially monostable domain. Thus the ('anti-phase') neck instability for $\gamma_1 < 0$ can be directly attributed to the gauge symmetry in the differential phase ψ and its associated neutral mode $\vec{w}_\psi$. On the other hand λ_ϕ is associated with the usual ('in-phase') neck MI for anomalous GVD in models with a single gauge symmetry. Explicit expression for λ_ϕ^2 can be found for $\beta = -\frac{3}{2}\kappa$

$$\lambda_\phi^2 = \frac{4\kappa}{9}\left(\frac{\gamma_1\gamma_2}{\gamma_1+\gamma_2} + 2\gamma_3\right).$$

Solving the eigenvalue problem numerically, we find that in low-frequency limit the instability growth rates precisely match those predicted by our perturbation theory, see Fig. 1(a), (b). As Ω is increased each MI gain curve reaches a maximum and then decreases. A typical example of the maximal MI growth rate vs β is presented in Fig. 1(c). Similar plots for $Q_u \neq 0$ and across wide range of γ_m values show the same behaviour. Thus we conclude that *for normal GVD the new neck instability strongly dominates the snake one.* Note that its growth rate is maximised, as Fig. 1(a), (b) illustrate, for $Q_u = 0$. For normal GVD the unstable eigenfunctions become weakly confined and develop oscillating tails as Ω increases.

Spatial profiles of the symmetric eigenfunctions at maximum gain ($\Omega = \Omega_{max}$) are presented in Fig. 2. Despite this being well beyond the perturbative limit in which expressions (4) apply, the novel neck MI eigenmode still has qualitatively the same form as $\vec{w}_\psi$, i.e. $w_1 = -w_2$, $w_3 = 0$, indicating that the ψ phase symmetry underlies the instability through the whole range of Ω. Similarly, the unstable neck mode for anomalous GVD is evidently associated with the ϕ symmetry.

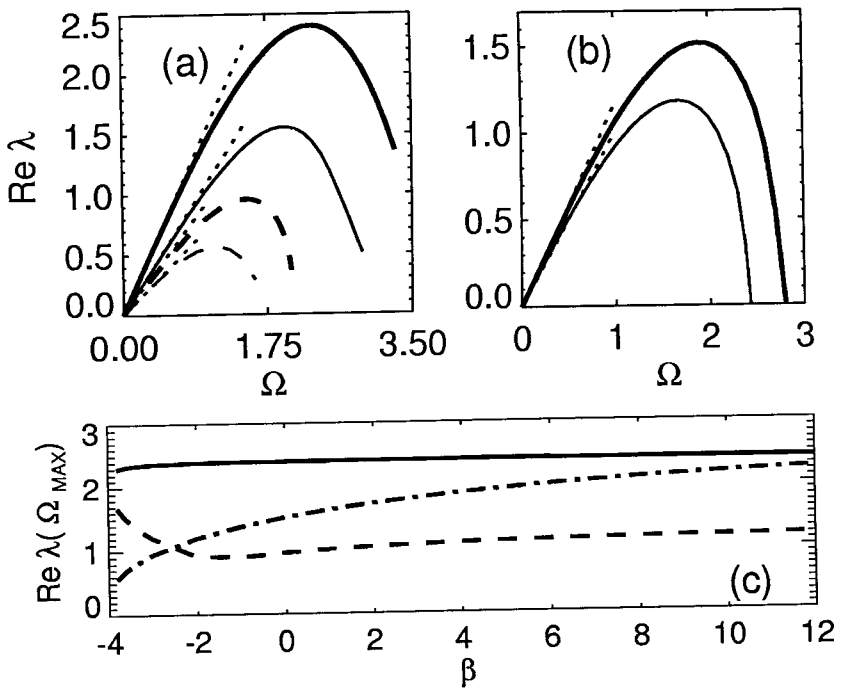

Figure 4.11: (a-b) Instability growth rate vs Ω*:* $Q = 65$*,* $\beta = 0$*. Thick (thin) lines are for* $\kappa = 2$*,* $\delta = 0$*,* $Q_u = 0$ *(*$\kappa = 2.075$*,* $\delta = 1.525$*,* $Q_u = -36$*). Full (dashed) lines correspond to neck (snake) MI. Dotted lines are perturbative results. (a) Normal dispersion:* $\gamma_{1,2} = 2\gamma_3 = -0.5$*. (b) Anomalous dispersion:* $\gamma_{1,2} = 2\gamma_3 = 0.5$*. (c) MI growth rate at* $\Omega = \Omega_{max}$ *vs* β *for* $\kappa = 2$*,* $\delta = 0$*. Full (dashed) lines correspond to neck (snake) MI for* $\gamma_{1,2} = 2\gamma_3 = -0.5$*; dot-dashed line to neck MI for* $\gamma_{1,2} = 2\gamma_3 = 0.5$

Note that there are different scenarious of the termination of the MI branches for large values of Ω. One scenario is that the unstable branch terminates in the gap at some $\Omega = \Omega_c$. This scenario occurs for anomalous dispersion because the gap gets wider with increasing Ω. However in the case of normal dispersion the gap narrows with increasing Ω, and close at $\Omega_g^2 = \min_m(\xi_m/|\gamma_m|)$ while MI may still exist, here $\xi_{1,2} = \kappa \pm \delta$, $\xi_3 = 2\kappa + \beta$. It means that no eigenmodes of discrete spectrum with $Re\lambda = 0$ exist for $\Omega \geq \Omega_g$. After the disappearance of the gap the unstable eigenfunctions develop oscillating tails. Both in degenerate and nondegenerate cases the band of unstable frequencies of the snake branch is narrow for negative β and therefore it may terminate before the gap closes. In particular providing the solitary solution is known analytically *exact* expressions for the cutoff frequency Ω_c can be found for the case $\gamma_{1,2} = 2\gamma_3$. For snake instability $\Omega_c^2 = -3\kappa/(4\gamma_1)$, with eigenvectors $\vec{v}_c = 0$, $\vec{w}_c = (1, 1, \sqrt{2})^T th\sqrt{\frac{\kappa}{2}}x \ sech\sqrt{\frac{\kappa}{2}}x$, while for the neck instability in the anomalous dispersion $\Omega_c^2 = 5\kappa/(4\gamma_1)$, with eigenvectors $\vec{v}_c = (1, 1, \sqrt{2})^T sech^3\sqrt{\frac{\kappa}{2}}x$, $\vec{w}_c = 0$. Branch corresponding to the anti-phase neck instability terminates after the gap closes.

To test our linear stability analysis and study the nonlinear evolution we performed an extensive series of computer simulations of the system (1) with initial conditions in form of a soliton stripe perturbed by spatio-temporal white noise of order 1%. Typical simulation results are presented in Fig. 3 and they fully support our predictions. We chose the size of the computational window in the time domain to be $18\pi/\Omega_{max}$, and the initial soliton stripe rapidly develops nine humps, in accord with the stability analysis. During further evolution the modulated stripe forms into a train of pulses which either spread (normal GVD) or form a persistent chain of three-wave optical bullets (anomalous GVD). Due to the initial noise, modes from a band of frequencies close to Ω_{max} are able to grow and compete, and hence the modulations in Fig. 3 are somewhat irregular.

A striking difference between Figs. 3(a,c) is that the initially imposed translational symmetry of the solitary stripe along the time dimension is broken in different ways. For normal GVD interleaved intensity peaks of E_1 and E_2 are formed, while for anomalous GVD the intensity peaks coincide. (Each amplitude

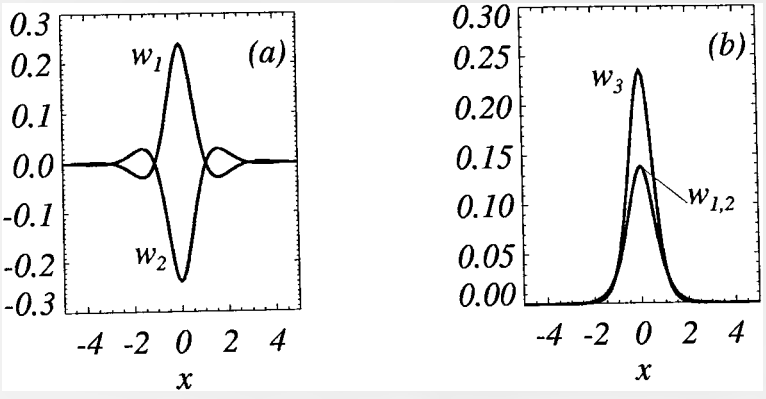

Figure 4.12: Most unstable eigenmodes ($\Omega = \Omega_{max}$) for $\beta = \delta = 0$, $\kappa = 2$. (a) Normal dispersion: $\gamma_{1,2} = 2\gamma_3 = -0.5$; (b) Anomalous dispersion: $\gamma_{1,2} = 2\gamma_3 = 0.5$.

is modulated with period $\simeq 2\pi/\Omega_{max}$.)

This difference is directly related with the spatial form of the most unstable eigenvectors. In the case of normal GVD w_1 and w_2 are out of phase and $w_3 = 0$, see Fig. 2(a), leading to the interleaving. Since E_1E_2 drives E_3, the intensity profile of the second harmonic becomes modulated with period π/Ω_{max}, see Fig. $3(a_3)$. Because the overlap of the three fields is diminished by this evolution, mutual trapping becomes impossible and the whole structure eventually spreads through diffraction and dispersion, see Fig. 3(b). For anomalous GVD, all three components of most unstable eigenvector are in phase, see Fig. 2(b), and thus all three intensities become modulated with the same temporal period, see Fig. 3 (c_1), (c_2), (c_3). This provides conditions for mutual self-trapping of the filaments, see Fig. 3(d).

4.4 Summary and discussion

In this Chapter we have analysed and described dispersive MI of spatial solitons due to degenerate and non-degenerate 3WM. For anomalous GVD soliton stripe

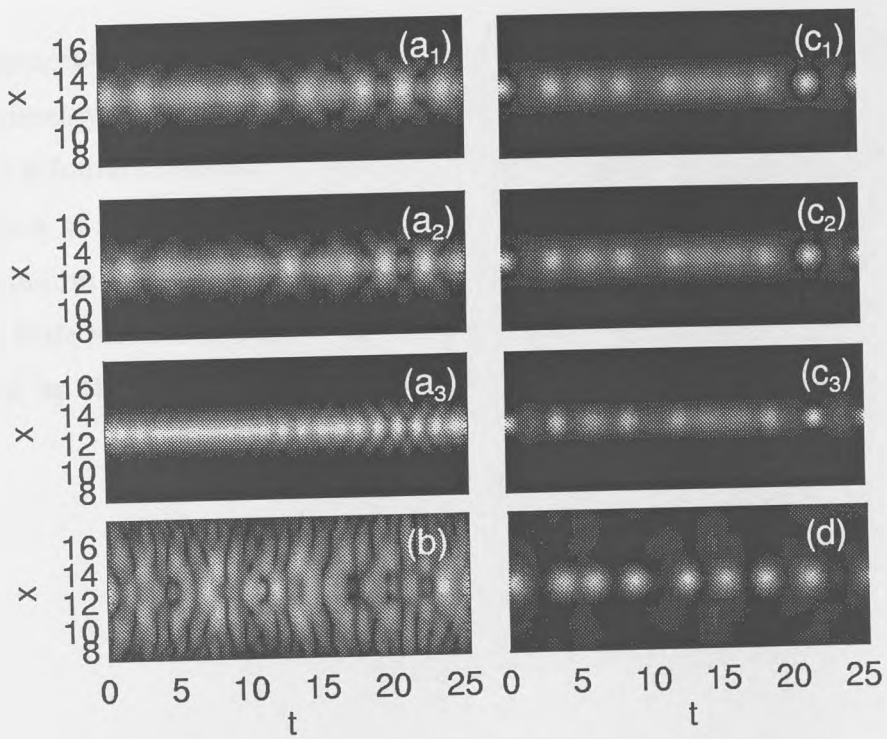

Figure 4.13: Development of noise-induced instability of spatial soliton stripe: $\kappa = 2$, $\delta = \beta = 0$. Left (right) panels for $\gamma_{1,2} = 2\gamma_3 = -0.5$ ($\gamma_{1,2} = 2\gamma_3 = 0.5$). (a_m) $|E_m|$ at $z = 2.7$, (b) $|E_1|$ at $z = 4.5$, (c_m) $|E_m|$ at $z = 5.4$, (d) $|E_1|$ at $z = 10.8$.

typically breaks into a chain of of soliton-like long-lived filaments. New and nontrivial results have been found for normal GVD. In degenerate case the snake MI is found to be dominant for positive wavevector mismatch. For negative wave vector mismatch the neck instability with complex eigenvalues originating either from the continuus spectrum or from internal modes is the dominant instability. This instability has its analogy for plane wave solutions [109, 110, 111]. However, secondary MI branches described above are probably pure solitonic effect, because they have not been found for plane waves [109, 110, 111].

In nondegenerate case the extra neutral mode associated with the additional phase symmetry gives rise to a new branch of MI. This is symmetric (of neck type), and is found to dominate the asymmetric (snake) instability throughout the whole region of soliton existance. It is noteworthy that MI branches bifurcating from continuum also have been found in non-degenerate case, but detail study of them has little sense because the corresponding instability growth rate is mainly suppressed by the instability due to symmetry in the differential phase.

typically breaks into a chain of of soliton-like long-lived filaments. New and nontrivial results have been found for normal GVD. In degenerate case the snake MI is found to be dominant for positive wavevector mismatch. For negative wave vector mismatch the neck instability with complex eigenvalues originating either from the continuus spectrum or from internal modes is the dominant instability. This instability has its analogy for plane wave solutions [109, 110, 111]. However, secondary MI branches described above are probably pure solitonic effect, because they have not been found for plane waves [109, 110, 111].

In nondegenerate case the extra neutral mode associated with the additional phase symmetry gives rise to a new branch of MI. This is symmetric (of neck type), and is found to dominate the asymmetric (snake) instability throughout the whole region of soliton existance. It is noteworthy that MI branches bifurcating from continuum also have been found in non-degenerate case, but detail study of them has little sense because the corresponding instability growth rate is mainly suppressed by the instability due to symmetry in the differential phase.

Chapter 5

Azimuthal modulational instability of self-trapped beams with phase dislocation in saturable Kerr and quadratic nonlinear media

The present Chapter deals with 2D propagation of electromagnetic waves in self-focusing saturable and in quadratically nonlinear media. In particular, we will consider azimuthal modulational instability of higher-order solitons in such media. Bright solitary waves decaying monotonically with distance from the axis (ground-states) are the most important solitary solutions in these media, but do not exhaust the set of self-trapped solutions. Considering 2D NLS with pure cubic nonlinearity Gagnon and Paré [112] built two remarkable sets of analytic solutions. These sets are analogs of Hermite-Gaussian and Laguerre-Gaussian modes of the propagation equation in linear media. In a certain limit these 'nonlinear modes', which generally depend on the longitudinal coordinate, transform into self-trapped solutions [112]. Several types of solitary wave reported by dif-

ferent authors, e.g. with a bright central spot and one or more radial nodes [97], 'doughnut' solutions with a nested phase dislocation [113], the 'dipole' solution [114], and solutions with both radial and azimuthal nodes [115, 116], are apparently special cases of these 'nonlinear modes' built by Gagnon and Paré. It is natural to expect that analogues of these solutions can exist in models which in certain limits are close to the NLS. Indeed, solutions with a *bright* central spot and radial nodes have been studied in saturable [81, 107] and quadratic nonlinear media [90, 92, 94]. Solutions with a *dark* central spot and nested phase dislocation have been also reported in both saturable [117, 118, 119, 91, 120] and quadratic [91, 92] media.

The stability of these solutions is a non-trivial issue because the standard stability criterion for ground-states [81] is only a necessary condition for the internal stability of higher-order solutions with nodes, and has no relevance to MI. It was first shown for saturable nonlinearity [107] that many-ring solutions with a bright central spot are stable with respect to purely radial perturbations but unstable with respect to azimuthally dependent perturbations, showing break-up of their rings into filaments. Similar solutions in quadratic nonlinear media show not only symmetry-breaking azimuthal instability, in analogy with saturable media, but also a novel symmetry-preserving decay scenario which is absent for the ground-state quadratic solitons, see Chapter 3 and [94].

Our special interest here is in self-trapped solutions with a phase dislocation, surrounded by one or more bright rings. Break-up of these rings into filaments has been reported in [117, 118, 119, 91, 120, 92]. Note that in Ref. [118] this break-up was interpreted not as an intrinsic property of the solutions but as due to interaction with another beam. Experimental observations of filamentation of finite beams with a nested phase dislocation has been recently reported for the self-focusing saturable [121, 122], photorefractive [123] and quadratic [124] media. The spatial profiles of the input beams used in these experiments did not correspond to self-trapped solutions but we believe that the dynamics of filaments elaborated below can provide valuable physical insight and reflects key features underlying evolution from more general initial conditions. This conclu-

sion is supported by similarities between the numerical simulations of Torner and Petrov [125] in which they observed break-up in quadratic nonlinear media of input Laguerre-Gaussian modes with phase dislocation, and the evolution of the corresponding self-trapped solutions studied below.

Note that the solutions discussed above are assumed to be linearly polarised in the transverse plane. Based on the Maxwell equations for a purely azimuthal field propagating in Kerr-like media, the existence of a family of many-ring solutions with a dark central spot [126, 127] and its azimuthal instability [128] have been reported. The model equation studied is like the NLS, but with an additional term of the form r^{-2} (r is the radial coordinate) argumenting the usual transverse laplacian operator. This model has some formal resemblance to the case of a scalar field with a singly-charged vortex, but the analogy has not been developed by these authors, and we will not pursue it here.

5.1 Self-trapped beams with phase dislocation in saturable media

5.1.1 Model and stationary solutions

The evolution of the slowly varying electric field envelope $\mathcal{E}$ in the nonlinear medium is governed by the equation, see e.g. [121],

$$2ik\partial_Z\mathcal{E} + \partial_X^2\mathcal{E} + \partial_Y^2\mathcal{E} + 2k\frac{\omega_0}{c}n_{NL}(I)\mathcal{E} = 0, \tag{5.1}$$

Z and X, Y are the longitudinal and transverse coordinates, ω_0 is the carrier frequency, $k = n_0\omega_0/c$ is the carrier wave number in the medium, n_0 is the (linear) refractive index and c the velocity of light in vacuum. The field is scaled such that $I = |\mathcal{E}|^2$ is the intensity, and $n_{NL}(I)$ is the intensity dependent part of the refractive index. The form of n_{NL} depends on the medium: e.g. for a Kerr medium $n_{NL} = n_2 I$. In most media the index change shows some form of saturation. For example, in a two-level medium excited well off resonance

the nonlinear index can be described by $n_{NL} = n_2 I/(1 + I/I_{sat})$, with I_{sat} the saturation intensity. This is the model we will use in the present work. Such a medium is self-focusing $n_2 > 0$ (or more generally $dn_{NL}/dI > 0$) and self-defocusing in the opposite situation.

We now re-scale our variables so as to reduce (5.1) to the dimensionless form

$$i\partial_z E + \frac{1}{2}\vec{\nabla}_\perp^2 E + f(|E|^2)E = 0. \tag{5.2}$$

through the following substitutions: $Z = zl_d$, $X = wx$, $Y = wy$, $\mathcal{E} = E\sqrt{I_{sat} l_{NL}/l_d}$, where $l_d = kw^2$ and $l_{NL} = c/(\omega_o |n_2| I_{sat})$ are the diffraction and nonlinear lengths, w is a characteristic transverse length scale, $\vec{\nabla}_\perp = \vec{i}\partial_x + \vec{j}\partial_y$. We will concentrate henceforth on the model with self-focusing ($n_2 > 0$) saturable nonlinearity

$$f(|E|^2) = \frac{|E|^2}{1 + \alpha|E|^2}, \quad \alpha = \frac{l_{NL} I_0}{l_d}, \tag{5.3}$$

which describes, e.g., nonlinear response of a two-level medium excited well off resonance. Here α is a saturation parameter, and clearly the Kerr limit is simply given by $\alpha = 0$. For this reason, and also for computational convenience, we retain α as a scaling parameter, even though it can clearly be scaled away.

It is well known, and qualitatively clear, that under an appropriate balance between diffractive stretching and nonlinear focusing ($l_d \sim l_{NL}$) the electromagnetic radiation can be self-trapped forming a self-induced waveguide. Formally this means that Eq. (5.2) has non-diffracting solutions of the form

$$E(x, y, z) = \mathcal{A}(x, y) e^{i\kappa z}, \tag{5.4}$$

Here κ has sense of the eigenvalue of the corresponding waveguide mode which many authors term as the nonlinear wave-vector shift. The transverse profile $\mathcal{A}(x, y)$ is can be chosen to be real, and obeys

$$\vec{\nabla}_\perp^2 \mathcal{A} = 2\left(\kappa - f(|\mathcal{A}|^2)\right)\mathcal{A}. \tag{5.5}$$

Beam confinement demands exponential decay of $|\mathcal{A}|$ at infinity, which requires $\kappa > 0$. Multiplying (5.5) by $\mathcal{A}^*$ and integrating the left-side by parts one gets

$$-\int dxdy |\vec{\nabla}_\perp \mathcal{A}|^2 = \int dxdy(\kappa - f(|\mathcal{A}|^2))|\mathcal{A}|^2 > (\kappa - \max f)\int dxdy|\mathcal{A}|^2. \tag{5.6}$$

Since $f < \alpha^{-1}$, any self-trapped solutions of our model must have $0 < \kappa < \alpha^{-1}$.

Below we will concentrate on one particular class of self-trapped solutions of Eq. (5.5) namely those with a phase singularity at the center, which have the form:

$$\mathcal{A}(x, y) = A(r)e^{il\theta}, \tag{5.7}$$

where $r = \sqrt{x^2 + y^2}$, θ is the polar angle and therefore Eq. (5.5) becomes

$$\frac{d^2A}{dr^2} + \frac{1}{r}\frac{dA}{dr} - \frac{l^2}{r^2}A = 2(\kappa - f(A^2))A, \tag{5.8}$$

Physically l must be an integer (there is no phase singularity for $l = 0$), while $A(r)$ must obey the following boundary conditions

$$\begin{aligned} r \to 0 \qquad & A(r) \to r^{|l|}c_0, \\ r \to \infty \qquad & A(r) \to \frac{c_\infty}{\sqrt{r}}e^{-r\sqrt{2\kappa}} \end{aligned} \tag{5.9}$$

where $c_{0,\infty}$ are real constants. There is redundancy in Eq. (5.8), since either κ or α can be scaled away. We prefer to keep them both: α to provide transition to the pure cubic nonlinearity and κ to retain the traditional form of the Vakhitov-Kolokolov stability criterion [81] (for more details see next subsection).

Eq. (5.8) with boundary conditions (5.9) was solved numerically using a second-order finite differences method. We found that for any non-zero integer l one-, two- and many-ring solutions with a central phase singularity exist in the entire region $0 < \kappa, \alpha^{-1}$ specified above. Typical radial profiles of A for different values of l are presented in Fig. 5.1. While these profiles can be obviously be approximated by analytical techniques, see e.g. [112, 119], here we confine ourselves to numerical solutions, which have, in principle, arbitrarily high accuracy.

5.1.2 Stability

Having found these stationary solutions, their stability is a natural question to study. Consider small complex perturbations $\varepsilon(z, r, \theta)$ of the stationary solution (5.7),

$$E(z, r, \theta) = (A(r) + \varepsilon(z, r, \theta))e^{i\kappa z + il\theta}. \tag{5.10}$$

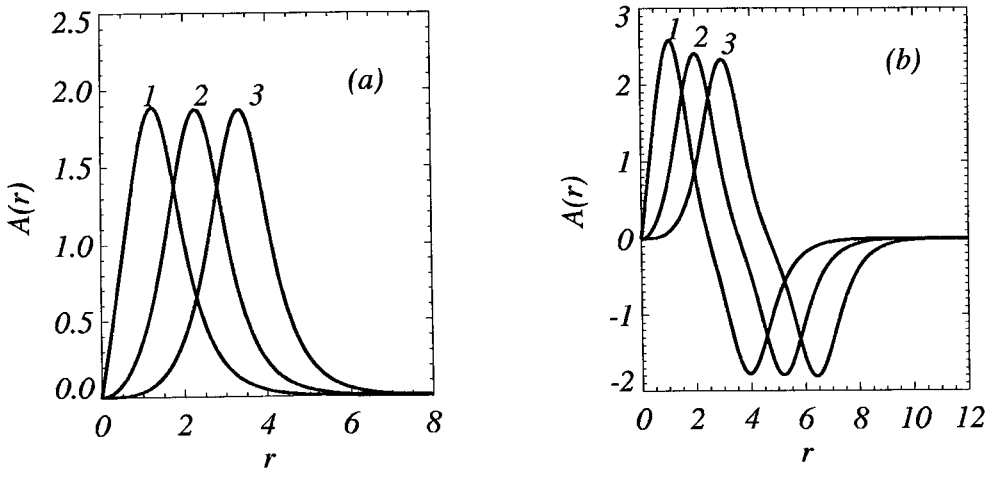

Figure 5.1: Plots of the field amplitude $A(r)$ for $l = 1, 2, 3$, $\kappa = 1$ and $\alpha = 0.1$. (a) One-ring and (b) two-ring solutions of Eq. (5.8). The labels in Figs. 1, 2 denote l values.

The general solution of the linearised problem for ε can be expressed as a superposition of azimuthal Fourier modes $e^{\pm iJ\theta}$ ($J = 0, \pm 1, \pm 2 \ldots$) with complex coefficients dependent on r and z. Therefore looking for the exponentially growing perturbations which characterise instability, we set

$$\varepsilon(z, r, \theta) = g_J^+(r) e^{\lambda_J z + iJ\theta} + g_J^{-*}(r) e^{\lambda_J^* z - iJ\theta} \tag{5.11}$$

and obtain the following non-self-adjoint eigenvalue problem:

$$i\lambda_J \vec{g}_J = \begin{bmatrix} \hat{L}_J^+ & A^2 f' \\ -A^2 f' & -\hat{L}_J^- \end{bmatrix} \vec{g}_J, \tag{5.12}$$

where $\vec{g}_J = (g_J^+, g_J^-)^T$, $f' = df/dA^2$ and

$$\hat{L}_J^{\pm} = \frac{1}{2}\left[\frac{1}{r}\frac{d}{dr} r \frac{d}{dr} - \frac{1}{r^2}(l \pm J)^2\right] - \kappa + f + A^2 f'.$$

Note that Eq. (5.12) is obviously valid also for $l = 0$, i.e. for the solitary waves with finite intensity at $r = 0$. It can be shown that for $l = 0$ perturbations proportional to $\cos J\theta$ and $\sin J\theta$ are equivalent and can be treated independently. This fact was implicitly used in Refs. [107, 128]. Therefore the dimension of the eigenvalue problem in the space of real functions can be reduced from 4×4 to 2×2 when $l = 0$. This also follows from the fact that if $l = 0$ then Eq. (5.12) has

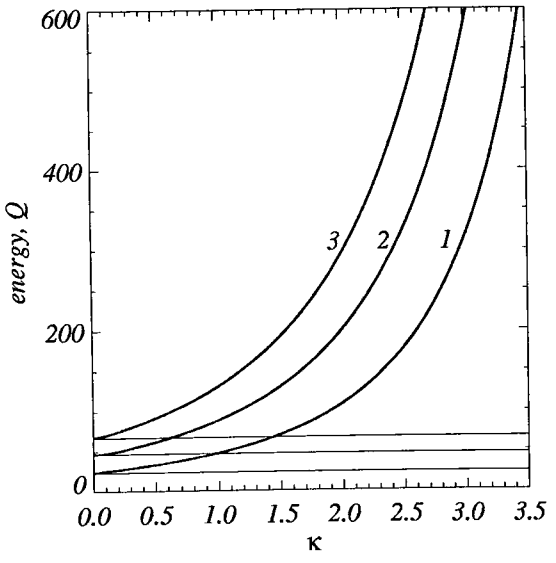

Figure 5.2: Energy Q vs κ for one-ring solutions with $l = 1, 2, 3$ and $\alpha = 0.2$. Horizontal lines correspond to a pure Kerr medium, $\alpha = 0$

the solutions $g_J^- = \pm g_J^{+*}$. Presence of a phase singularity destroys this symmetry property and cosine and sine perturbations cannot be decoupled.

The symptotic behaviour of the eigenvectors $\vec{g}_J$ is

$$\begin{aligned} r \to 0 \qquad & g_J^{\pm}(r) \to r^{|l \pm J|} b_0^{\pm}, \\ r \to \infty \qquad & g_J^{\pm}(r) \to \frac{b_\infty^{\pm}}{\sqrt{r}} e^{-r\sqrt{2(\kappa \pm i\lambda_J)}}, \end{aligned} \tag{5.13}$$

where $b_{0,\infty}^{\pm}$ are complex constants and the branch of the square root in the exponent must be chosen such that the eigenfunctions are square-integrable. The eigenvalues of the discrete spectrum corresponding to such eigenfunctions can lie anywhere in the complex plane outside the rays $(i\kappa, i\infty)$ and $(-i\kappa, -i\infty)$. These rays belong to the continuous spectrum with unbounded eigenfunctions. Unstable eigenmodes have eigenvalues with $Re\lambda_J > 0$. They must always have a counterpart with $Re\lambda_J < 0$ because of the hamiltonian nature of our problem, see Section IV.

Due to the symmetries of the our model (phase $(E \to Ee^{i\phi})$ and translational $(E(x,y) \to E(x+\delta x, y+\delta y))$) Eq. (5.12) has neutrally stable modes, i.e. modes

with zero eigenvalues. The corresponding eigenvectors are

$$\vec{g}_0^{(0)} = \begin{bmatrix} A \\ -A \end{bmatrix}, \quad \vec{g}_{\pm 1}^{(0)} = \begin{bmatrix} \frac{dA}{dr} \mp \frac{l}{r} A \\ \frac{dA}{dr} \pm \frac{l}{r} A \end{bmatrix}. \tag{5.14}$$

These eigenmodes can be associated with $J = 0, \pm 1$ respectively.

Neutral modes are important for analytic approaches to stability problems of this type. Asymptotic techniques, see Section 3.3.3, can be used to show that the neutrally stable mode $\vec{g}_0^{(0)}$ branches at the point $\partial_\kappa Q = 0$ giving instability of any bound solution of Eq. (5.8) if

$$\partial_\kappa Q < 0, \tag{5.15}$$

here Q is the energy flux

$$Q = \int dxdy|E|^2. \tag{5.16}$$

Thus the standard stability criterion for the ground states [81] is also a *necessary* condition for the stability of self-trapped beams with a phase dislocation.

For pure Kerr media ($\alpha = 0$) $\partial_\kappa Q = 0$ and a collapse instability is present [117]. The evolution of this collapse in z is of polynomial type, therefore it can easily be suppressed by an exponential instability if there is one. This is indeed the case in our situation due to the exponential instabilities for $J \neq 0$ described below. In case of single-ring solutions with $l \neq 0$, which have no nodes for $r > 0$, a variational approach to the eigenvalue problem (5.12) can be applied in a manner similar to that done in Refs.[81, 128]. It shows that $\partial_\kappa Q > 0$ is also *sufficient* for stability against *symmetry-preserving* perturbations ($J = 0$). Plots of the energy vs κ for the one-ring solutions are presented in Fig. 5.2. We conclude that the one-ring solitary waves are stable with respect to $J = 0$ perturbations in saturable media. For many-ring solutions there is no comparable approach, nor any simple criterion which is sufficient for symmetry-preserving stability and numerical checks are always necessary [94].

The above analytic criterion says nothing about stability against *symmetry breaking* perturbations, i.e. MI is not excluded even where $\partial_\kappa Q > 0$ holds. Azimuthal

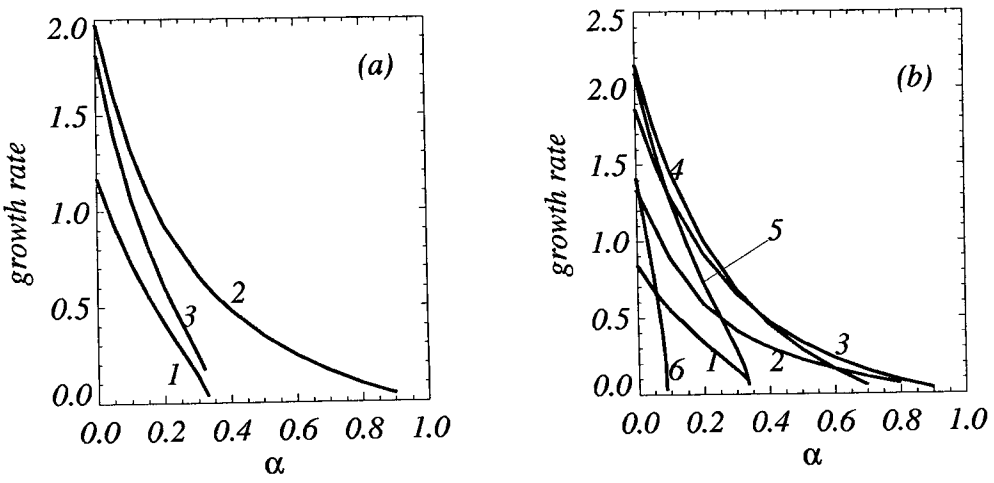

Figure 5.3: Growth rates of the unstable eigenmodes of the one-ring solution vs α for $\kappa = 1$. (a) $l = 1$, (b) $l = 2$. Here and in Figs. 5.4,5.8,5.13,5.15 numbers denote J values.

MI corresponds to modes with $J \neq 0$ having exponential growth, in general leading to J-fold intensity modulation around the ring, breaking the cylindrical symmetry of the intensity of the stationary solution. For $J = 1$ we might hope for an analytic result linked to the $g_1^{(0)}$ neutral mode, but asymptotic expansion shows that this neutral mode is not linked to the appearance of any instability. However this obviously does not forbid presence of instability for any $J \neq 0$ including $J = 1$ and we are obliged to study the eigenvalue problem (5.12) with some different method. There are several possible numerical approaches to solve such problems, see e.g. [107, 129]. We chose to reduce (5.12) to an algebraic eigenvalue problem by replacing the differential operators with the second order-finite differences. We apply zero boundary conditions for some large value of r and appropriate conditions at $r = 0$, as given in (5.13). 100 to 200 grid points was usually enough to get good precision. Zero boundary conditions for large r is a potential source of problems because weakly decaying eigenvectors require large numbers of grid points to maintain accuracy. However we did not meet such a situation in any of the investigations described in this paper. Furthermore, numerical results for the neutrally stable modes were always in good agreement with Eqs. (5.14).

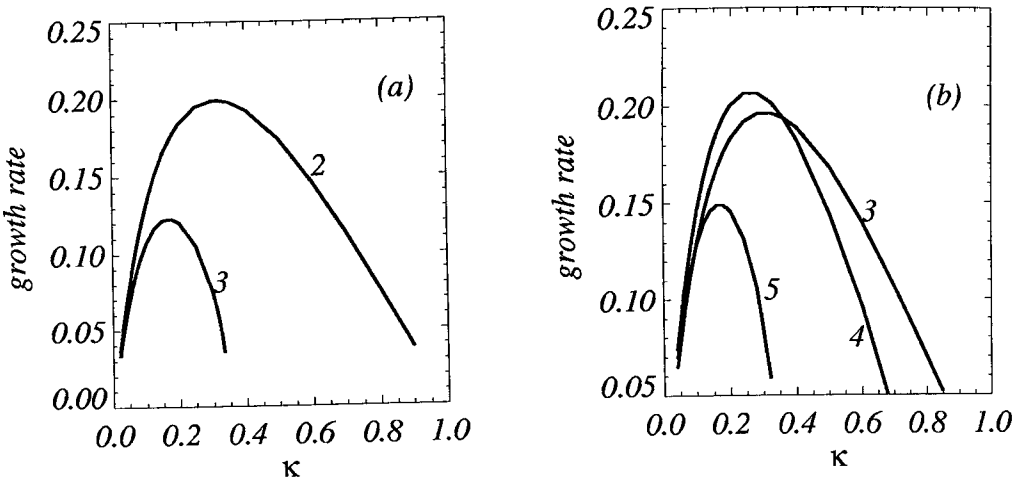

Figure 5.4: Growth rates vs κ of the most unstable eigenmodes of the one-ring solution for $\alpha = 1$. (a) $l = 1$, (b) $l = 2$.

Numerical analysis of symmetry-breaking perturbations ($J \neq 0$) shows the presence of instabilities over a finite range of values of J in every case. The results for the one-ring solutions with $l = 1, 2, 3$, $\kappa = 1$ and $\alpha = 0.1$ were presented earlier in Letter format [91]. Here we study in detail how variations of the parameters and of the initial noise level influence symmetry breaking instabilities of the one-ring solitary waves with $l = 1, 2$ and two-ring wave with $l = 1$. These cases are typical of the break-up of ring stationary waves in saturable Kerr media which carry orbital angular momentum.

Let us first describe the one-ring solutions. Although, because of the above-mentioned scaling, all possible situations can in fact be captured varying just one parameter keeping the other fixed, for convenience and ease of interpretation we plot the growth rates ($Re\lambda_J$) of the unstable eigenmodes vs both parameters, see Figs. 5.3,5.4. For $l = 1$ just three unstable eigenmodes ($J = 1, 2, 3$) appear, with $J = 2$ mode dominating through the whole range of α and κ. For $l = 2$ either of the two modes $J = 3, 4$ can be dominant depending on the parameter values. Generally the instability gets stronger for $\alpha \to 0$ and it is practically suppressed for $\alpha \to 1/\kappa$. Suppression of MI (of any nature) with increasing saturation is a common phenomenon which has also been reported for the fundamental bright and dark solitons in saturable media [12, 129]. Considering variations of κ, for

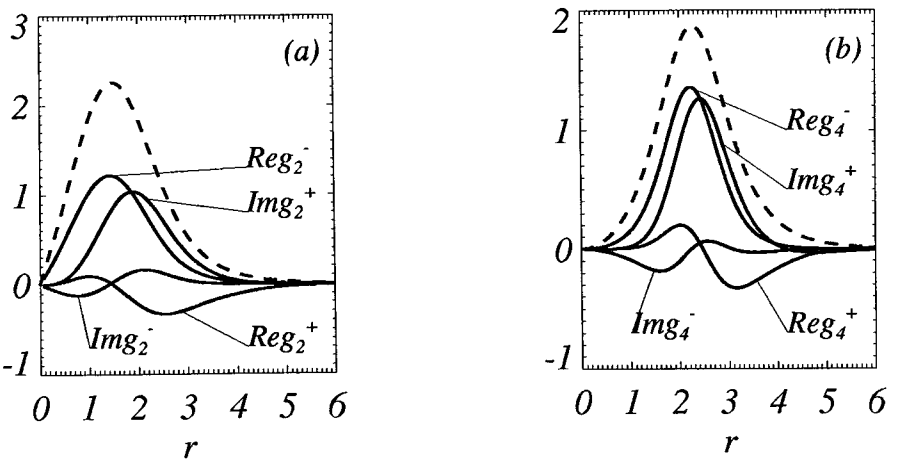

Figure 5.5: Real and imaginary parts of the maximally unstable eigenmodes for one-ring solutions. (a) $l = 1$, $J = 2$, $\alpha = 0.3$, $\kappa = 1$ and (b) $l = 2$, $J = 4$, $\alpha = 0.1$, $\kappa = 1$. Dashed lines mark the radial profile of the self-trapped solution $A(r)$.

κ close to 0 or to $1/\alpha$ the instability is again practically suppressed. This is also typical for the symmetry-breaking instabilities of other kinds of the ring-structures [107, 119, 128].

We found that the unstable eigenvalues are generally complex. If the instability for an eigenmode disappears within the existence region of the solitary solution the imaginary part of the corresponding λ_J usually remains finite as its real part goes through zero. In particular this holds for the unstable eigenmode with $J = 1$, and is the reason why instability for this mode cannot be captured by asymptotic expansion near the neutral mode $\vec{g}_1^{(0)}$.

We found that the radial profiles of the most unstable eigenfunctions mainly concentrate around the rings of the stationary solutions, see Fig. (5.5). Because $A(r)$ is real, it is the real part of the perturbations which determines the field amplitude modulation pattern which develops around an unstable ring. Therefore we expect the initially uniform ring will develop J_{max} minima and J_{max} maxima on propagation, where J_{max} is the azimuthal index of the perturbation eigenmode with the maximal growth rate. As a consequence, the ring should break up into J_{max} filaments. However other eigenmodes, in particular those with $J = J_{max} \pm 1$, can have comparable growth rates, which can affect the filamentation process and

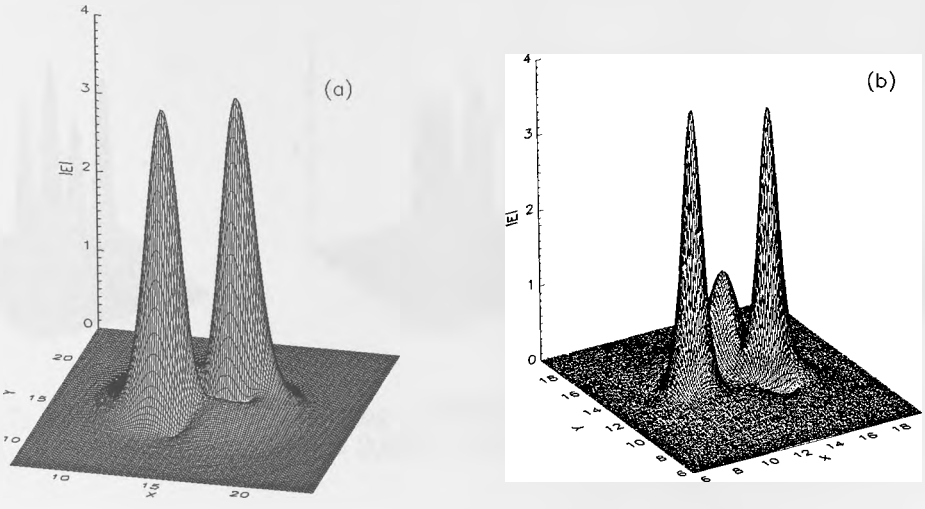

Figure 5.6: Breakup of the one-ring solution with $l = 1$, $\kappa = 1$. (a) $\alpha = 0.3$, $s = 0.01$, $z = 14$; (b) $\alpha = 0.1$, $s = 0.05$, $z = 7$.

make the output pattern depend somewhat on the particular realisation of the initial noise.

To test the results of our stability analysis we performed an extensive series of numerical simulations of Eq.(5.2) with initial conditions in the form

$$E(r,\theta) = (1 + s(q_r(r,\theta) + iq_i(r,\theta)))\, A(r)e^{il\theta}, \tag{5.17}$$

where $q_{r,i}$ are real functions modeling gaussian noise in the interval $(-1,1)$ and s is a constant. Simulation was done on the polar grid with 128 and $100-200$ grid points along the angular and radial coordinates respectively. The polar grid prevents the numerical noise effects of discretising a ring onto a rectangular grid from unduly influencing the number of filaments formed. For low noise level (s of the order 0.01 or less) the most unstable eigenmode was clearly dominant in the majority of simulations. Increasing the noise to $s \sim 0.1$ led to the occasional appearance of $J = J_{max} \pm 1$ filaments. In most of the simulations the filaments formed from the same ring had similar intensities. This suggests that the unstable eigenmode dominating at the beginning of the instability suppresses all the others. (For an exception see Fig. 5.6(b).)

Examples of the break-up of one-ring solutions with $l = 1$ into 2 and 3 filaments and with $l = 2$ into $4, 5$ and 3 filaments are presented in Figs. 5.6, 5.7. Parameters

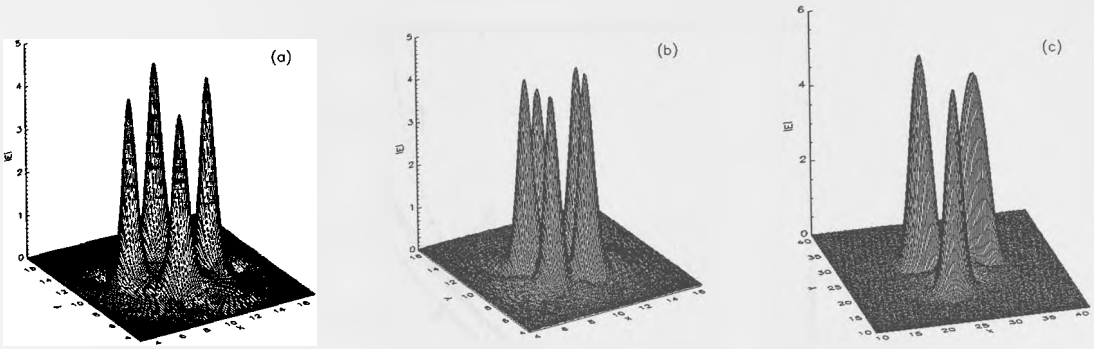

Figure 5.7: Breakup of the one-ring solution with $l = 2$, $\kappa = 1$. (a) $\alpha = 0.1$, $s = 0.005$, $z = 7$; (b) $\alpha = 0.1$, $s = 0.08$, $z = 4$; (c) $\alpha = 0.6$, $s = 0.08$, $z = 26$.

and level of the initial noise are specified in the figure captions. There is excellent agreement between the predictions of the stability analysis, see Fig. 5.3, and the results of these direct numerical simulation of the original model.

In case of a pure Kerr medium ($\alpha = 0$) the exponential growth of the symmetry-breaking perturbations should dominate over the algebraic growth of the symmetry-preserving collapse instability. In the simulations for the Kerr case we indeed first observed filamentation of the ring and subsequently collapse of the filaments.

For the two-ring solitary solutions with $l = 1$, we present just the growth rates for the dominant eigenmodes vs α, see Fig. 5.8. All unstable eigenmodes can be naturally separated into two groups. The radial profiles of the eigenmodes from one group concentrate around the first ring and from the other around the second ring, see Fig. 5.9. Because of this each ring develops its own modulated pattern and breaks up into the different number of filaments. We present here, see Fig. 5.10, results of the numerical simulation for $\alpha = 0.05$ (when $J = 2$ and $J = 6$ modes dominate for the first and second ring respectively) and for $\alpha = 0.6$ with dominant $J = 2$ and $J = 5$ modes. For $\alpha = 0.05$ first ring is more unstable and for $\alpha = 0.6$ second ring is more unstable. For the latter situation the instability of the first ring is so weak that its break up did not occur within the propagation distance simulated.

The examples presented in Figs. 5.6,5.7,5.10 show that filamentation happens

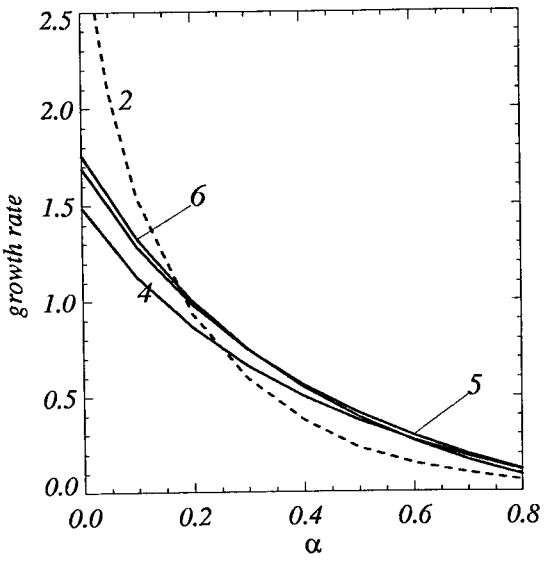

Figure 5.8: Growth rates of selected unstable eigenmodes of the two-ring solution vs α for $\kappa = 1$ and $l = 1$. Dashed (full) lines are for the modes concentrated around the first (second) ring.

over propagation distances from several to several tens of diffraction lengths. For small values of α and optimal initial energy, i.e. adjusting κ to maximise the instability, we were able to observe filamentation within one or two diffraction lengths.

Finally, regarding the possibility of analytical study of the stability with respect to symmetry-breaking perturbations we suggest that a proper generalisation of the averaging techniques developed originally in [107] may be the most efficient way to do it.

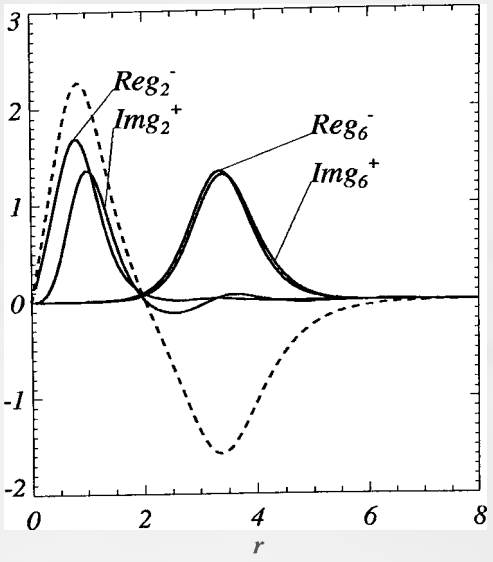

Figure 5.9: Real and imaginary parts of the maximally unstable eigenmodes for the two-ring solution. $l = 1$, $\alpha = 0.05$, $\kappa = 1$. $J = 2$ *and* $J = 6$ *for the eigenmodes concentrated around the 1st and 2nd ring respectively. Dashed line: radial profile of the self-trapped solution* $A(r)$.

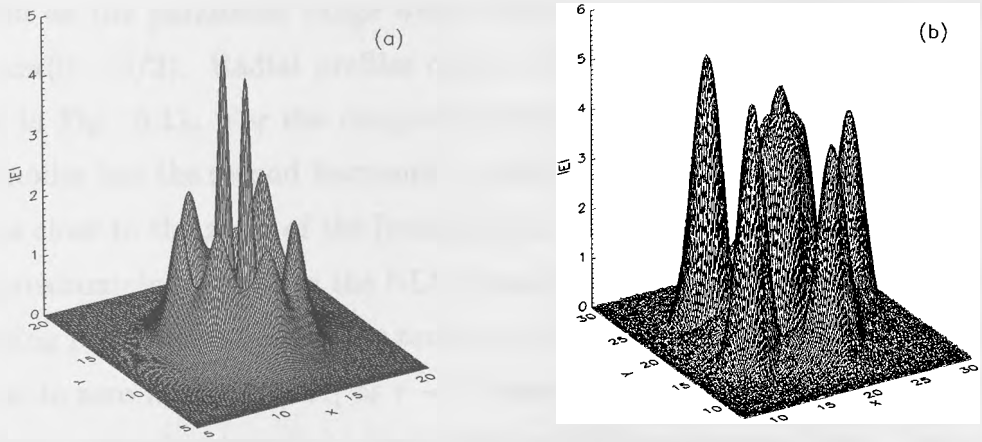

Figure 5.10: Breakup of the two-ring solution with $l = 1$ *and* $\kappa = 1$. *(a)* $\alpha = 0.05$, $s = 0.005$, $z = 4$; *(b)* $\alpha = 0.6$, $s = 0.1$, $z = 26$.

5.2 Self-trapped beams with phase dislocation in quadratic media

5.2.1 Model and stationary solutions

The evolution of the slowly varying envelopes of the fundamental ($\mathcal{E}_1$) and second harmonic ($\mathcal{E}_2$) electric fields in a noncentrosymmetric crystal is governed by the Eqs. (3.20), (3.21) with $\gamma_{1,2} = 0$. We look for stationary solutions of these equations in the form

$$E_m = A_m(r)e^{im(l\theta+\kappa z)}, \quad m = 1, 2. \tag{5.18}$$

The real amplitudes $A_{1,2}$ obey the equations

$$\begin{aligned} \frac{d^2A_1}{dr^2} + \frac{1}{r}\frac{dA_1}{dr} - \frac{l^2}{r^2}A_1 &= 2(\kappa - A_2)A_1, \\ \frac{d^2A_2}{dr^2} + \frac{1}{r}\frac{dA_2}{dr} - \frac{4l^2}{r^2}A_2 &= 4(2\kappa + \beta)A_2 - 2A_1^2. \end{aligned} \tag{5.19}$$

Eqs. (5.19) have a family of the ring-like solutions similar to the case of the saturable medium. However there is no condition similar to Eq. (5.6) and therefore just the requirement of exponential decay of the tails. This imposes a restriction on the parameter range where the solitary solutions can exist, namely $\kappa > \max(0, -\beta/2)$. Radial profiles of $A_{1,2}$ for one- and two-ring cases are presented in Fig. 5.11. For the many-ring solutions the fundamental field A_1 has radial nodes but the second harmonic A_2 always remains positive, though having minima close to the zeros of the fundamental. For large β Eqs. (3.20)-(3.21) can be approximately reduced to the NLS equation for the fundamental field and for increasing β the second harmonic tends to carry less and less of the total energy. A_2 goes to zero faster than A_1 as $r \to 0$ because the order of the phase singularity for the second harmonic is double that of the fundamental one. One of the parameters either κ or β can be scaled away from Eqs. (5.19) [57]. However we like to keep them both: β is not very natural parameter for scaling because it can be positive, negative or zero and we keep κ because of its physical interpretation

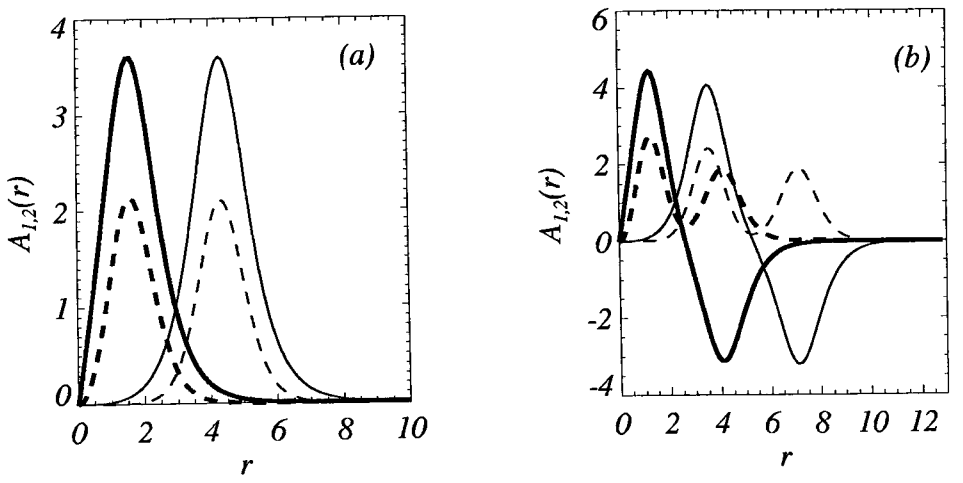

Figure 5.11: Plots of the field amplitudes $A_1(r)$ (full lines) and $A_2(r)$ (dashed lines) of (a) one-ring and (b) two-ring solutions of Eq. (5.19) for $l = 1$ (thick lines), $l = 3$ (thin lines). $\kappa = 1$ and $\beta = 0$.

as a nonlinear wave vector correction, and also, as remarked above, because it is the natural parameter for investigation of stability.

5.2.2 Stability

Considering small perturbations of the stationary solutions (5.18) in the form

$$\varepsilon_m(z,r,\theta) = g^+_{Jm}(r)e^{\lambda_J z + iJ\theta} + g^{-}_{Jm}{}^*(r)e^{\lambda^*_J z - iJ\theta},\ m = 1,2 \tag{5.20}$$

we get the following non-self-adjoint eigenvalue problem

$$i\lambda_J \vec{g}_J = \begin{bmatrix} \hat{L}^+_{J1} & A_2 & A_1 & 0 \\ -A_2 & -\hat{L}^-_{J1} & 0 & -A_1 \\ A_1 & 0 & \hat{L}^+_{J2} & 0 \\ 0 & -A_1 & 0 & -\hat{L}^-_{J2} \end{bmatrix} \vec{g}_J, \tag{5.21}$$

where $\vec{g}_J = (g^+_{J1}, g^-_{J1}, g^+_{J2}, g^-_{J2})^T$ and

$$\hat{L}^{\pm}_{J1} = \frac{1}{2}\left[\frac{1}{r}\frac{d}{dr}r\frac{d}{dr} - \frac{1}{r^2}(l \pm J)^2\right] - \kappa,$$

$$\hat{L}^{\pm}_{J2} = \frac{1}{4}\left[\frac{1}{r}\frac{d}{dr}r\frac{d}{dr} - \frac{1}{r^2}(2l \pm J)^2\right] - 2\kappa - \beta,$$

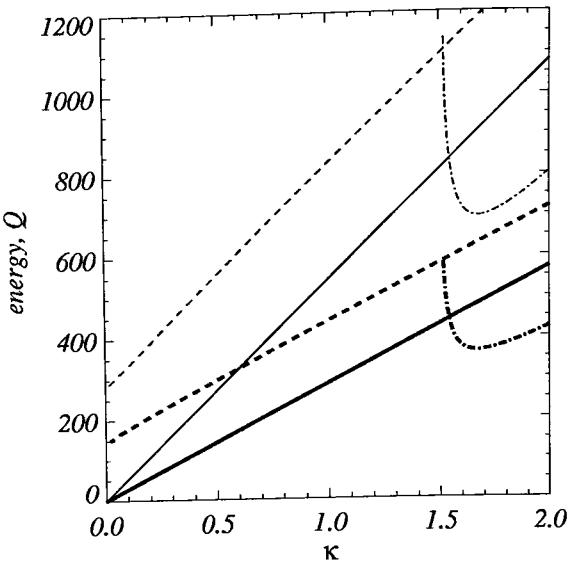

Figure 5.12: Energy Q vs κ for one-ring solutions with $l = 1$ (thick lines) and $l = 2$ (thin lines): $\beta = -3$ (dash-dotted lines), $\beta = 0$ (full lines) and $\beta = 3$ (dashed lines).

Pure imaginary λ_J belonging to the continuous spectrum lie in the rays $(i\Omega_c, i\infty)$ and $(-i\Omega_c, -i\infty)$, where $\Omega_c = \min(\kappa, 2\kappa+\beta)$ (5.21). Neutrally stable eigenmodes for $J = 0$ and $J = \pm 1$ are

$$\vec{g}_0^{(0)} = \begin{bmatrix} A_1 \\ -A_1 \\ 2A_2 \\ -2A_2 \end{bmatrix}, \quad \vec{g}_{\pm 1}^{(0)} = \begin{bmatrix} \frac{dA_1}{dr} \mp \frac{l}{r}A_1 \\ \frac{dA_1}{dr} \pm \frac{l}{r}A_1 \\ \frac{dA_2}{dr} \mp \frac{2l}{r}A_2 \\ \frac{dA_2}{dr} \pm \frac{2l}{r}A_2 \end{bmatrix}. \tag{5.22}$$

Symmetry-preserving ($J = 0$) perturbations of the one-ring solutions are damped for

$$\partial_\kappa Q = \partial_\kappa \int dxdy(|E_1|^2 + 2|E_2|^2) > 0, \tag{5.23}$$

where Q is the energy flux. Representative plots of Q vs κ are presented in Fig. 5.12. The instability for negative β is related to the existence for $\partial_\kappa Q > 0$ of a pair of the eigenmodes with purely imaginary eigenvalues (with opposite signs) lying in the gap $(-i\Omega_c, i\Omega_c)$. At the point $\partial_\kappa Q = 0$ these eigenmodes coincide with the neutral mode $\vec{g}_0^{(0)}$ and for larger $|\beta|$ appear again but with real eigenvalues of opposite signs. For the one-ring solitary solution this is the only route to a symmetry-preserving instability. We found that it is always suppressed

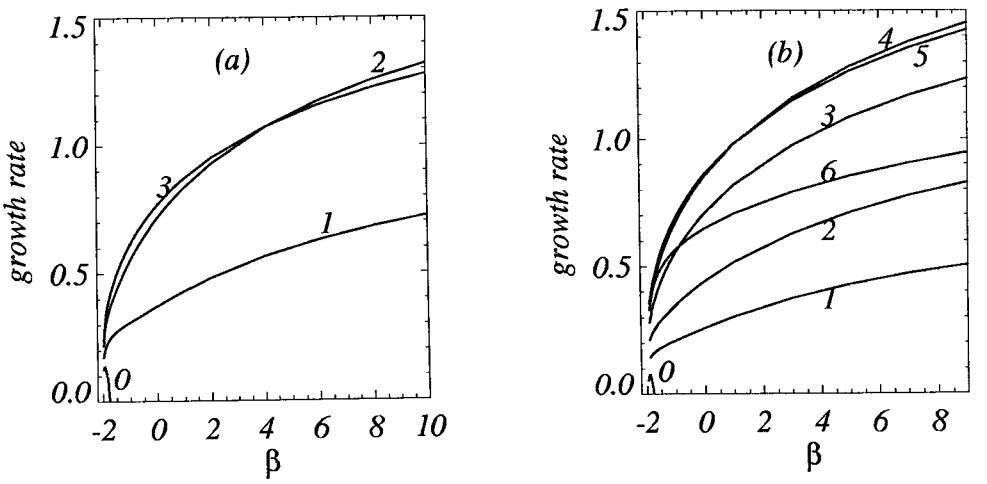

Figure 5.13: Growth rates of the maximally unstable eigenmodes of the one- ring solution vs β for $\kappa = 1$. (a) $l = 1$, (b) $l = 2$.

by stronger symmetry-breaking instabilities, i.e. MI is always dominant in this case.

For cases where $A_1(r)$ changes its sign (i.e. two or more rings), the criterion (5.23) is just a necessary condition and we found a new scenario of symmetry-preserving instability. It appears in a manner similar to that which we have described for solutions with a bright central spot and one or more rings [94]. However we found that this instability dominates the symmetry-breaking one only in a very narrow range of β values, close to the boundary of the solitary wave existence. This contrasts with the case described in Ref. [94] (zero angular momentum), where the symmetry- preserving scenario is a major factor for a significant region of β values.

Plots of the growth rates of the unstable eigenmodes vs β for the one-ring solutions with $l = 1, 2$ presented in Fig. 5.13. In the limit of $\beta \gg 1$ the dominating mode is the same as the one in the saturable medium for small saturation values, i.e for α close to 0. The growth rates of the dominating eigenmodes increase linearly with increasing of κ, see Ref. [92] and Fig. 5.19. An example of the radial profiles of the components of the most unstable eigenmode is presented in Fig. 5.14.

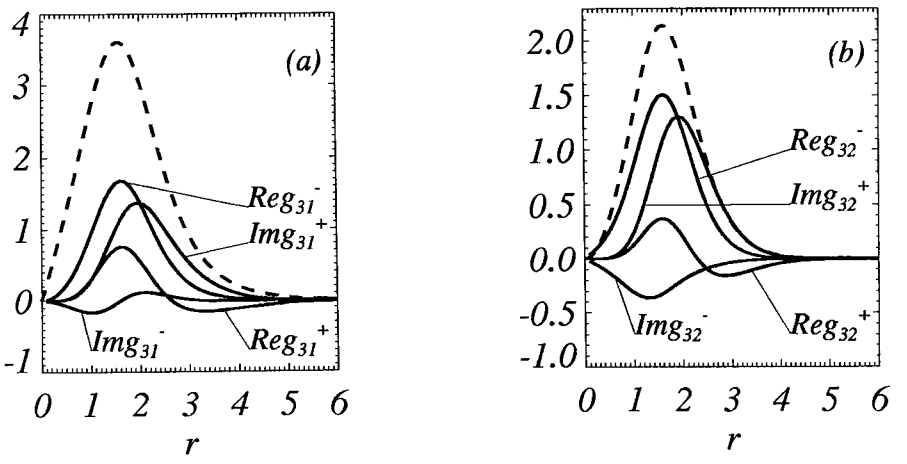

Figure 5.14: Real and imaginary parts of the maximally unstable eigenmodes of the one-ring solution. $l = 1$, $J = 3$, $\beta = 0$, $\kappa = 1$. (a) is for the fundamental field and (b) is for the second harmonic. Dashed lines mark the radial profiles of the self-trapped solution, $A_{1,2}(r)$.

The growth rates of the essential eigenmodes vs β for the two-ring solution with $l = 1$ are presented in Fig. 5.15. (These results are restricted to $\beta > -1.9$ because for increasingly negative β the many-ring solitary solutions become very wide and extra care is needed in the stability analysis.) Again the localisation of the eigenmodes on the rings suggests that during propagation any ring will break up into J_{max} filaments, where J_{max} shows maximum gain on that particular ring.

These predictions of our stability analysis are fully supported by simulations of Eqs. (3.20)-(3.21) and our comments in the previous section about saturable media, e.g. about the influence of noise on the symmetry-breaking instabilities, are also valid in quadratic media. An example of the break-up of the one-ring solution with $l = 2$ to four filaments is presented in Fig. 5.16.

5.3 Dynamics of filaments

As was shown above, self-trapped beams with a phase dislocation at the center and with varying numbers of rings exist as stationary solutions in both saturable and quadratic nonlinear media. They are unstable against symmetry-breaking perturbations, breaking up into a set of filaments during propagation. In this section we extend the analysis of the dynamics of the filaments outlined by us in [91]. This analysis is based on the conservation laws. Given initial values of the conserved quantities we show how to predict featues of the trajectories of the filaments, and even how to estimate their number.

The conserved hamiltonian and momenta which are essential to our present purposes are introduced by a Lagrangian reformulation of the problems. This also makes it possible to develop analogies between solitary waves and particles.

Eqs. (3.20)-(3.21) can be written as Euler-Lagrange equations

$$\frac{\partial}{\partial z}\frac{\partial \mathcal{L}}{\partial(\partial_z E_m^*)} = \frac{\partial \mathcal{L}}{\partial E_m^*} - \sum_{i=x,y} \partial_i \frac{\partial \mathcal{L}}{\partial(\partial_i E_m^*)}, \; m = 1,2, \tag{5.24}$$

where the Lagrangian density $\mathcal{L}$ is

$$\mathcal{L} = \frac{i}{2}\sum_{m=1,2}(E_m^*\partial_z E_m - c.c.) - \mathcal{H}. \tag{5.25}$$

The corresponding formulae for Eq. (5.2) can be obtained by simply omitting the subscript m, and this procedure will be implied in most formulae below, exceptions being stated explicitly.

In the above, $\mathcal{H}$ is the corresponding hamiltonian density, which for Eqs. (3.20)-(3.21) takes the form:

$$\mathcal{H} = \frac{1}{2}|\vec{\nabla}_\perp E_1|^2 + \frac{1}{4}|\vec{\nabla}_\perp E_2|^2 + \beta|E_2|^2 - \frac{1}{2}(E_1^2 E_2^* + c.c.), \tag{5.26}$$

while for Eq. (5.2)

$$\mathcal{H} = \frac{1}{2}|\vec{\nabla}_\perp E|^2 - \int_0^{|E|^2} du\; f(u) \tag{5.27}$$

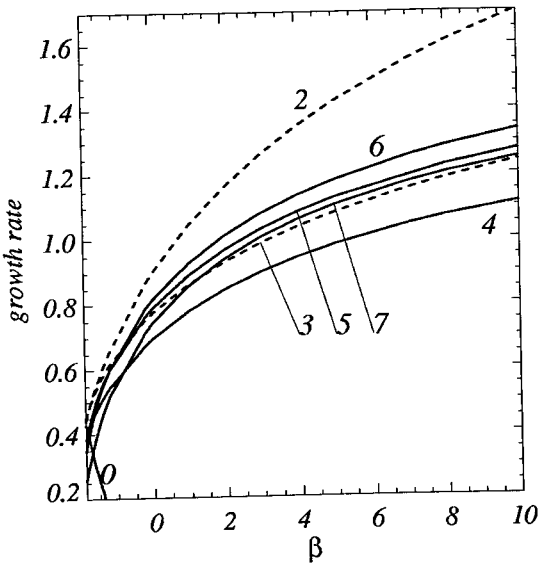

Figure 5.15: Growth rates of selected unstable eigenmodes of the two-ring solution vs β for $\kappa = 1$ and $l = 1$. Dashed (full) lines are for the modes concentrated around first (second) ring.

Considering variations of the action integral $S = \int_{z_1}^{z_2} dz \int dxdy\mathcal{L}$ with respect to infinitesimal spatial translations and rotations it can be shown that if $\mathcal{L}$ is invariant under these transformations the following two quantities are integrals of motion

$$\vec{P} = \int dxdy\ \vec{\Pi}, \tag{5.28}$$

$$\vec{L} = \int dxdy\ \vec{r} \times \vec{\Pi}. \tag{5.29}$$

Here $\vec{r} = \vec{i}x + \vec{j}y$ and

$$\vec{\Pi} = -\sum_{m=1,2} \left(\frac{\partial \mathcal{L}}{\partial(\partial_z E_m)} \vec{\nabla}_\perp E_m + c.c. \right) = \frac{1}{2i} \sum_{m=1,2} \left(E_m^* \vec{\nabla}_\perp E_m - c.c. \right). \tag{5.30}$$

By definition $\vec{P}$ is the linear momentum of the field, $\vec{L}$ its angular momentum, both expressed in terms of $\vec{\Pi}$, its linear momentum density. Solitary wave solutions (5.7), (5.18) carry zero linear momentum, $\vec{P} = 0$, and nonzero angular momentum, $|\vec{L}| = |l|Q_0$, where Q_0 are the energy invariants, see (5.16) and (5.23), evaluated at these stationary solutions.

Eq. (5.29) for the angular momentum is just the paraxial approximation for the optical orbital angular momentum per unit length [130]. The angular momentum

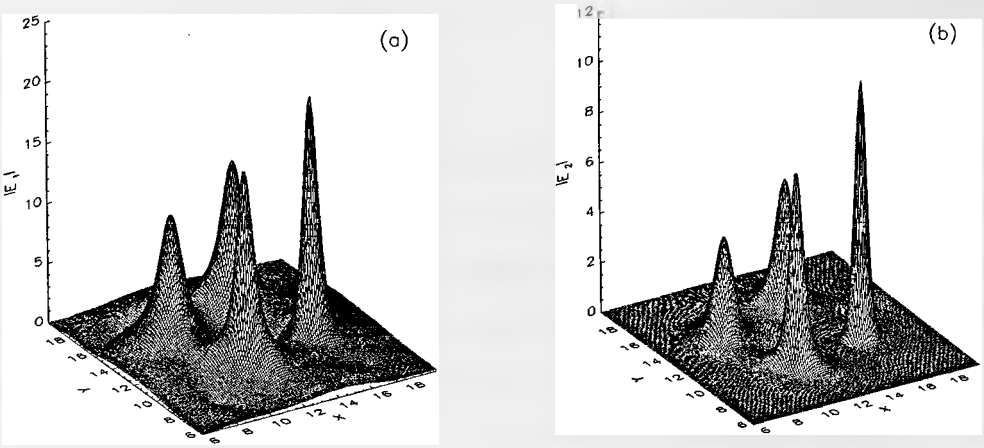

Figure 5.16: Breakup of the one-ring solution with $l = 2$, $\beta = 5$, $\kappa = 1$, $s = 0.05$, $z = 6$. (a) first harmonic, (b) second harmonic.

carried by light beams has attracted much recent interest. It has been predicted, and proved experimentally, that Laguerre-Gaussian beams with azimuthal mode index l carry orbital angular momentum $l\hbar$ per photon [131]. Frequency doubling of such a beam has been shown [132] to generate a second harmonic with doubled azimuthal mode index $2l$. Note that the present 'nonlinear modes' also obey this relation, because of the factor 2 in (5.23).

Both our models (5.2), (3.20)-(3.21) have the property of Galilean invariance, e.g. in the quadratic medium:

$$(E_1, E_2, \vec{r}) \to (E_1 e^{i\Phi}, E_2 e^{2i\Phi}, \vec{\xi}), \tag{5.31}$$

where

$$\Phi = \vec{v}(\vec{r} - \frac{1}{2}\vec{v}z),\ \vec{\xi} = \vec{r} - \vec{v}z,\ \vec{v} = \vec{i}v_x + \vec{j}v_y,$$

Under this transformation, a structure with zero linear momentum is boosted to $\vec{P} = Q\vec{v}$, therefore we can expect analogies with Newtonian mechanics with Q playing the role of mass. In particular, a fundamental soliton, which has no intrinsic angular momentum, will have orbital angular momentum $\vec{L} = \vec{r} \times Q\vec{v}$ about the origin, provided $|\vec{r}|$ is larger than the soliton size. It follows that if the total field can be regarded as a superposition of several separate localised

structures, e.g. solitons, we can expect the dynamics of these structures (while they remain well localised) to be somewhat similar to the dynamics of mechanical particles.

Because our model systems are not integrable, numerical methods are necessary to study the creation and dynamics of soliton filaments. For simulation of the soliton dynamics we used a split-step algorithm on a cartesian grid with initial conditions obtained on the polar grid as described in Section II. Once the number of filaments is established the transition from one grid to the other does not cause any significant loss of precision. As a further check, conservation of energy, hamiltonian and momenta was monitored during the simulations.

We found numerically that filaments formed due to the azimuthal modulational instability do not diffract with propagation, but remain well localised and soliton-like. Superimposing images of the transverse intensity distribution at different z values we found that *these filaments move out along tangents to the initial ring, carrying away its angular momentum as orbital angular momentum*, see Fig. 5.17 for the case of a saturable medium. Several figures in Ref. [91] show this behaviour for both saturable and quadratic media and different values of l.

Because, once fully formed, the filaments seem to behave like simple, *free* Newtonian particles, we now examine whether their number and dynamics can be predicted on the basis of the quasi-mechanical considerations. We consider only the dynamics of the filaments formed after the break-up of the one-ring structures. This is because an essential condition to apply the 'mechanical' approaches developed below is that the initial structures which undergo filamentation have to produce during their evolution a set of well separated filaments. Break-up of the many-ring solutions results generally in strong interaction between filaments from different rings, and so is too complex to consider in the present approach.

Let us represent the fields in the form

$$E_m \simeq \sum_{n=1}^{N} B_{mn}(x,y) e^{i\vec{v}_n\vec{r} - \frac{i}{2}|\vec{v}_n|^2 z}, \; m = 1,2 \tag{5.32}$$

here $\vec{v}_n$ have a sense of the 'transverse velocities' of the filaments. In other words

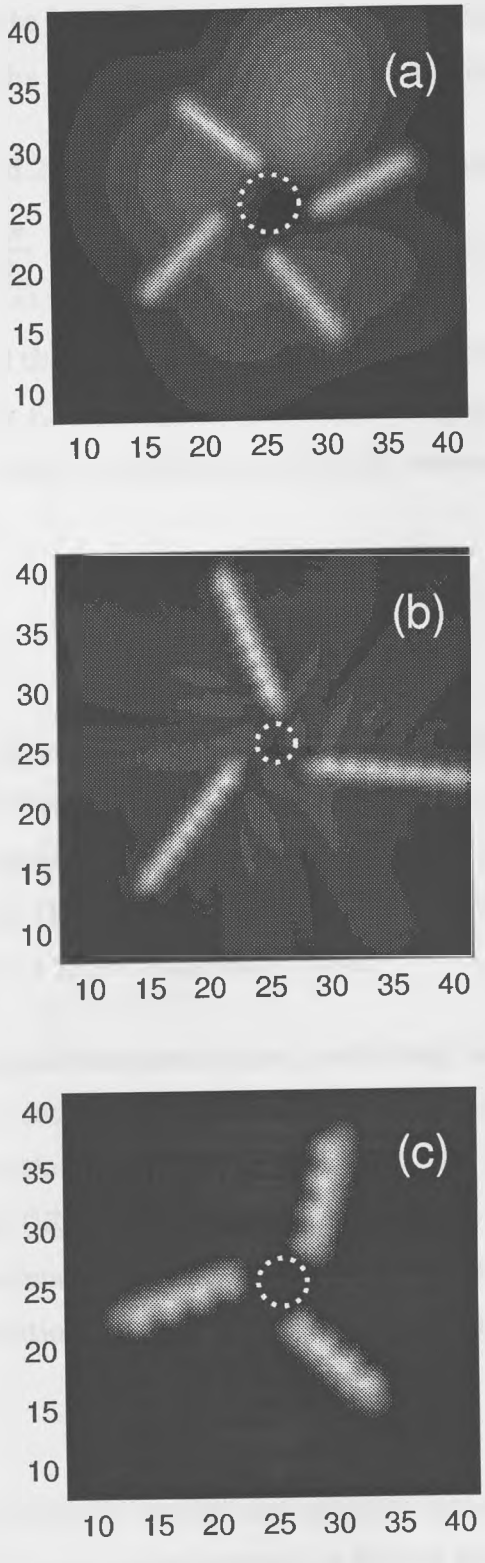

Figure 5.17: Superimposed images of the transverse intensity distribution at different z values showing soliton trajectories in a saturable medium: $\alpha = 0.1$, $l = 2$. (a) $\kappa = 1$, (b) $\kappa = 5$, (c) $\kappa = 8$. Propagation distance is $\Delta z = 10$ for (a)-(c).

$\vec{v}_n$ characterize the propagation directions of the solitary waves with respect to z axis. B_{mn} are assumed to be bell-shaped complex functions characterising the filaments, localised near the points $\vec{r}_n = \vec{v}_n z$. N is the number of these filaments.

Substituting (5.32) into (5.29) gives for the angular momentum

$$\vec{L} \simeq \sum_{n=1}^{N} \int dxdy[\vec{r} \times \vec{v}_n](|B_{1n}|^2 + 2|B_{2n}|^2). \tag{5.33}$$

To get (5.33) we neglected the overlap of the tails of the filaments. We now assume that $\vec{r}$ can be replaced by $\vec{r}_n$ and taken outside the integral, which then reduces to q_n, the total energy of the filament, and so (5.33) becomes, for well-localized, well separated filaments:

$$\vec{L} \simeq \sum_{n=1}^{N} \vec{r}_n \times q_n \vec{v}_n. \tag{5.34}$$

This is just the angular momentum of a set of spinless Newtonian particles with masses given by q_n. Under the same assumptions, $\vec{P} \simeq \sum_{n=1}^{N} q_n \vec{v}_n$, also the Newtonian form. If the initial linear and angular momenta are wholly transferred to the daughter filaments, these expressions for $\vec{L}$ and $\vec{P}$ must equate to those of the original ring soliton, i.e $|\vec{L}| = |l|Q_0$ and $\vec{P} = 0$.

We now make another simplifying assumption, restricting ourselves to cases where the break-up results in a set of the filaments with approximately equal energies. In this situation conservation of the two momenta obliges the filaments to move with nearly equal speeds ($|\vec{v}_n| \simeq v$) along paths tangent to the initial ring. Then in Eq. (5.34) we can estimate $|\vec{r}_n \times \vec{v}_n| = Rv$, where R characterises the initial radius of the solitary solution. In practice we assigned R by an energy-weighted mean:

$$R = \frac{\int r dr \; r(A_1^2 + 2A_2^2)}{\int r dr \; (A_1^2 + 2A_2^2)}. \tag{5.35}$$

Finally, assuming that the entire energy and angular momentum are transferred to the filaments we get a very simple expression for the escape speed:

$$v \simeq \frac{|l|}{R}. \tag{5.36}$$

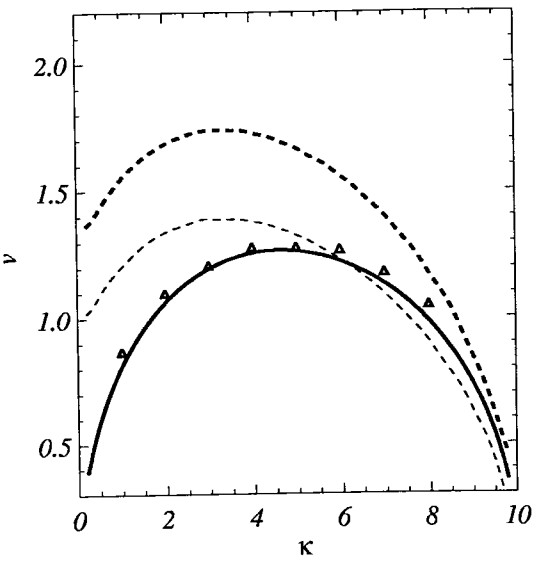

Figure 5.18: 'Transverse velocities' of filaments in saturable media vs κ for $l = 2$, $\alpha = 0.1$. Triangles mark results of the numerical simulation. Full line marks results gained through the angular momentum formula, Eq. (5.36). Dashed lines mark results gained through the hamiltonian formula, Eq. (5.40). Dash-dotted lines mark the growth rates of the perturbation eigenmodes. Thik and thin versions of the dashed and dash-dotted lines correspond to the cases of 3 and 4 filaments respectively.

This expression holds, under the stated assumptions, for both saturable and quadratic media. Before comparing it with numerical results, we consider an alternative hamiltonian-based approach.

Conservation of the hamiltonian $H = \int dxdy\ \mathcal{H}$ suggests another way to estimate v. Substitution of Eq. (5.32) into H, under the same approximations as were used to get Eq. (5.34), gives

$$H_0 \simeq \sum_{n=1}^{N} h_n + \frac{1}{2}\sum_{n=1}^{N} q_n v_n^2. \tag{5.37}$$

Eq. (5.37) links the initial hamiltonian H_0 with the sum of the 'intrinsic' hamiltonians h_n of the individual filaments calculated in their rest frames and of the 'kinetic energies' arising from their transverse motion, the latter again conforming to the particle analogue.

The hamiltonians of the initial stationary solutions (5.7), (5.18) are respectively

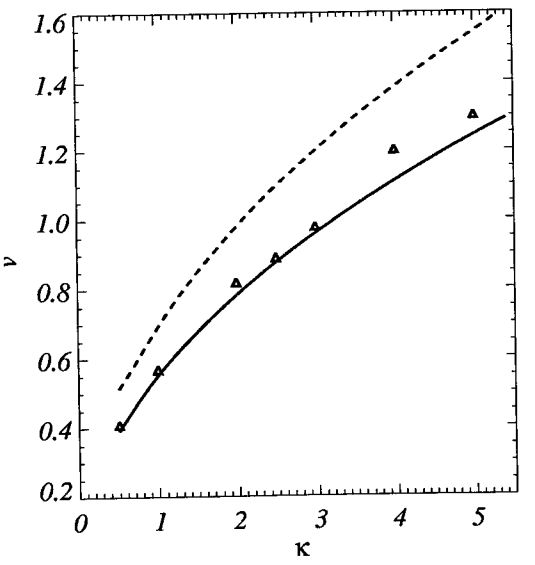

Figure 5.19: 'Transverse velocities' of filaments in quadratic media vs κ for $l = 1$, $\beta = 0$. Triangles mark results of the numerical simulation. Full line marks results gained through the angular momentum formula, Eq. (5.36). Dashed line marks results gained through the hamiltonian formula, Eq. (5.40). Dash-dotted line marks the growth rate of the maximally unstable perturbation eigenmode with J=3.

given by

$$H_0 = -\kappa Q_0 + 2\pi \int r dr \Big(f(A^2)A - \int_0^{A^2} du\, f(u) \Big), \tag{5.38}$$

$$H_0 = -\kappa Q_0 + \pi \int r dr A_1^2 A_2. \tag{5.39}$$

Considering the initial state as a composite of the final one, the last term in Eq. (5.37) can be interpreted as a 'negative binding energy' which induces break-up and transforms to kinetic energy of the fragments.

Supposing again that there are N identical filaments, i.e. $h_n \simeq h$, $q_n \simeq q$, we get the following formula for the speed:

$$v^2 \simeq 2 \left(\frac{H_0}{Q_0} - \frac{h}{q} \right). \tag{5.40}$$

For practical use of Eq. (5.40) we choose N which fixes $q \simeq Q_0/N$, and then we can find h for this q by using energy-hamiltonian diagrams, see e.g. [11], assuming the filaments to be ground-state solitons. Note that in Eq. (5.40) the first term

inside the bracket is fully defined by the initial conditions, but the second is an implicit function of N. Since Eq. (5.36) does not depend on N, comparison between Eq. (5.36) and Eq. (5.40) leads to a direct estimate of the number N of daughter solitons without numerical simulation or stability analysis.

For our two model systems we present in Figs. (5.18), (5.19) respectively examples of v vs κ obtained from the numerical simulation compared to the formulae given by Eqs. (5.36), (5.40). In both models there is near-perfect agreement of Eq. (5.36), based on angular momentum conservation, with numerical simulation. There is less good agreement with Eq. (5.40), based on the conservation of the hamiltonian, though the qualitative behaviour is correctly predicted. One reason for the discrepancy could be radiation, which we neglected in making these estimates. If so, it would seem that the radiation carries away energy and hamiltonian more efficiently than linear or angular momentum. Alternatively, the daughter solitons may be in an excited state. Certainly, internal shape oscillations are apparent in the simulations and also in Fig. 17 (though exaggerated by the superposition of a finite number of images at discrete times). These questions demand more detailed investigation, which we postpone to future work.

The approaches presented above can be in fact be applied to any initial field distribution which produces a set of well separated filaments with close intensities, e.g. they can be used to analyse break-up of Laguerre-Gaussian beams carrying orbital angular momentum.

In physical units Eq. (5.36) states that the angular divergence of the filaments is just the diffraction angle of a beam with radius Rw multiplied by the order $|l|$ of the phase singularity,

$$v \simeq \frac{|l|\lambda}{2\pi w}, \tag{5.41}$$

where λ is the wavelength of the light (for the quadratic case, the SH field has half the wavelength but double the order, and so the divergence is the same for both fields). This link between a linear quantity, the diffraction angle, and the nonlinear phenomenon of azimuthal instability suggests an analogy with the linear approach to soliton theory developed in [133].

5.4 Summary and discussion

Ring-like solutions with a phase dislocation nested at the center and exponentially decaying tails exist in self-focusing saturable and in quadratic media. They are quite different from the 'classical' optical vortex soliton supported by a defocusing nonlinearity [12], which is a dark spot with a phase dislocation on a broad, stable, bright background. Dynamics of the solutions studied here is characterised by azimuthal modulational instability which leads to break-up of the rings into a set of the filaments. This sort of dynamics has already been experimentally observed, in a saturable alkali vapour [121, 122], in photorefractive media [123] and in quadratically nonlinear crystal [124]. This shows that these solitary solutions, some properties of which can be more or less rigorously studied theoretically, reflect the main features of the dynamics of input beams used in experiments.

Solitons have been observed to spiral around each other because of a balance between either in-phase [134] or incoherent [135] attraction and repulsion due to nonzero angular momentum. Here, in contrast, we have nearly free quasi-solitons, with dynamics dominated by angular momentum conservation. Interaction forces may play a minor role in partitioning the energy among the filaments, but the daughter solitons rapidly cease to interact and fly off along straight- line trajectories without any spiraling. Note that a side view of the filaments in [121] shows rectilinear trajectories with no obvious evidence of any spiraling, so it seems possible to achieve such angular momentum dominated dynamics in practical experiments.

Initialising model equations (5.2), (3.20)-(3.21) with self-trapped beams with phase dislocation (plus noise) we demonstrated that their initial nonzero angular momentum transfers to the filaments and they fly out tangentially from the initial ring. We developed two semi-analytic approaches to the filament dynamics, in analogy with classical mechanics, one of them based on hamiltonian conservation and the other on conservation of angular momentum. Although both approaches give qualitatively valid estimates for the 'transverse velocity' (angular divergence)

of the filaments, the latter appears to be more general and gives also an excellent quantitative agreement with numerical results. The number N of daughter filaments is in most situations roughly twice the angular momentum index l, and thus depends relatively weakly on the other parameters. Taken together, the two approaches based on conservation laws yield an independent estimate for N in reasonable accord with estimates based on simulations and on stability analysis, both of which require considerable computational labour.

Chapter 6

Main results

Here I formulate two results which I consider as the most significant outcomes of my work on modulational instability of optical solitary waves.

- It is general feature of parametric processes to have a single phase symmetry, which is linked to the conservation of the total energy of the interacting waves. However, some of the parametric processes, e.g. non-degenerate three- and four-wave mixings, also have symmetry in the differential phase of two waves corresponding to the conservation of the energy imbalancing. If the parametric process can support bright solitary waves then symmetry in the differential phase strongly affects dispersive modulational instability of the solitary waves, alowing such phenomena as interleaving filament patterns and competion between neck and snake instabilities.

- Solitary waves with nested phase dislocation and carrying non-zero angular momentum propagating in media with different nonlinearities break up into soliton-like filaments. Subsequent dynamics of the filaments is strongly defined by the conservation of the angular momentum. It results in tangential motion of filaments and their angular divergence can be estimated as diffraction angle of the beam times the order of the phase singularity.

Appendix A

Variational approach

Variational approach is a poweful and relatively easy method, which allows to find approximation for profiles of solitary solutions and reduce partial differential equations describing soliton propagation to set of odinary differental equations. Here I show, following series of papers of other authors [55, 56, 57, 58, 59], how variational approach can be applied to approximate spatial profiles solitons due to degenerate three-wave mixing. Peculiar point of the calculations presented below is that I will not impose *a prior* restriction on the dimension of solitary solution.

As many others equations of physics, equations describing propagation of optical waves in nonlinear medium and in particular in quadratic nonlinear media can be obtained as conditions for extremum of the action integral: $S = \int_{z_1}^{z_2} dz \int dV \mathcal{L}$, where $\mathcal{L}$ is the Lagrangian density and $dV = dx_1 \dots dx_n$ is elementary volume. For Hamiltonian models Lagrangian density can be presented as

$$\mathcal{L} = \frac{i}{2}\left[\sum_s E_s^* \frac{\partial E_s}{\partial z} - c.c.\right] - \mathcal{H} \tag{A.1}$$

Here $s = 1, 2, \dots N$, N is the number of interacting fields and $\mathcal{H}$ is the hamiltonian density. Riquiring extrema of S one can find equations describing evolution of E_s, which have the form

$$i\partial_z E_s = \frac{\delta H}{\delta E_s^*}, \tag{A.2}$$

where H is the hamiltonian $H = \int dV\mathcal{H}$.

For Eqs. (3.14), (3.15) with $\alpha_1 = 2\alpha_2 = 1$ and $\delta_{1,2} = 0$ hamiltonian is

$$H = \int\int dxdydt\,[|\vec{\nabla}_\perp E_1|^2 + \frac{1}{2}|\vec{\nabla}_\perp E_2|^2 + \gamma_1|\partial_t^2 E_1|^2 + \gamma_2|\partial_t^2 E_2|^2 + \beta|E_2|^2 - \frac{1}{2}(E_1^2 E_2^* + c.c.)], \tag{A.3}$$

For simplicity we will again suppose that GVD of both field are anomalous and $\gamma_1 = 2\gamma_2$, $\tau = \sqrt{\gamma_1}t$. Application of variational approach in case of arbitary $\gamma_{1,2}$ was presented in Ref. [58].

I chose following trial functions

$$E_1 = A_1 e^{-\alpha_1\rho^2 + i\kappa z},\ E_2 = A_2 e^{-\alpha_2\rho^2 + i2\kappa z}, \tag{A.4}$$

where $\rho^2 = x^2$, or $\rho^2 = x^2 + y^2$, or $\rho^2 = x^2 + y^2 + \tau^2$. If one wants to reduce partial differential equations to a set of ordinary differential equations for free parameters of the trial functions, then $A_{1,2}, \alpha_{1,2}$ have to be some unknown functions of z. However, I only aim here to approximate shape of solitons, and therefore it is enough to put all unknown parameters to be constants.

For choosen trial functions Lagrangian is

$$-L = I_0\left[\frac{A_1^2\kappa}{(2\alpha_1)^{D/2}} + \frac{(2\kappa+\beta)A_2^2}{(2\alpha_2)^{D/2}} - \frac{A_1^2 A_2}{(2\alpha_1+\alpha_2)^{D/2}}\right] + I_2\left[\frac{A_1^2}{(2\alpha_1)^{D/2-1}} + \frac{A_2^2}{2(2\alpha_2)^{D/2-1}}\right]. \tag{A.5}$$

$I_0 = \sqrt{\pi}, \frac{1}{2}, \frac{1}{4}\sqrt{\pi}$ and $I_2 = \frac{1}{2}\sqrt{\pi}, \frac{1}{2}, \frac{3}{8}\sqrt{\pi}$, respectively, for one, two, and three dimensional geometries. Minimization of the Lagrangian gives four equations for four unknown parameters. Parameters $A_{1,2}$ and α_2 can be expressed as functions of α_1.

$$\alpha_2 = \frac{8\alpha_1^2 I_2}{I_0\kappa D + 2\alpha_1 I_2(D-2)}$$

$$A_2 = \frac{(2\alpha_1+\alpha_2)^{D/2+1}}{DI_0(2\alpha_1)^{D/2}}\left[\frac{D\kappa I_0}{2\alpha_1} - I_2(2-D)\right],$$

$$A_1^2 = \frac{(2\alpha_1+\alpha_2)^{D/2}2A_2}{I_0(2\alpha_2)^{D/2}}\left[(2\kappa+\beta)I_0 + \alpha_2 I_2\right].$$

α_1 and α_2 are linked by the equation

$$4\alpha_2 I_0(2\kappa+\beta) + 4\alpha_2^2 I_2 =$$

$$\frac{2}{D}(2\alpha_1+\alpha_2)(D(2\kappa+\beta)I_0-\alpha_2(2-D)I_2).$$

It is straightforward now to get cubic equation for α_1.

For $D=1$ we get

$$10\alpha_1^3-(4\kappa+3\beta)\alpha_1^2+4\kappa(2\kappa+\beta)\alpha_1-\kappa^2(2\kappa+\beta)=0. \tag{A.6}$$

Eq. (6) has exact solution $\alpha_1=\frac{\kappa}{5}$ if $\beta=-\frac{3}{2}\kappa$. This solution is in an excelent agreement with analytical solution (3.25), see [55].

For $D=2$ and $D=3$ we get, respectively,

$$16\alpha_1^3+2\kappa(2\kappa+\beta)\alpha_1-\kappa^2(2\kappa+\beta)=0, \tag{A.7}$$

and

$$18\alpha_1^3+\beta\alpha_1^2-\kappa^2(2\kappa+\beta)=0. \tag{A.8}$$

The Eq. (A.8) has obvious exact solution for $\beta=0$.

It can be shown, see e.g. [55], that Eqs. (A.6), (A.7), (A.8) have only one physically relevant root. Accordingly to [55, 58, 59] there is a tendency for variational-gaussian approximations to give poorer results with increasing dimension, presumably because the Lagrangian integral weights large radii more heavily as D increases.

Appendix B

On stability of multi-parameter vector solitons

The purposes of this Appendix are to formulate general asymptotical approach to stability of multi-parameter solitons in Hamiltonian models, to show how it can be used to find expressions for the instability growth rates with arbitrary accuracy and to demonstrate that under the certain conditions the first order approximation of this approach describes not only stationary, but also oscillatory instabilities of solitons.

We will consider Hamiltonian equations in the form

$$i\frac{\partial E_n}{\partial z} = \frac{\delta H}{\delta E_n^*},\ n = 1, 2 \ldots N, \tag{B.1}$$

which describes wide range of physical phenomena related with self-action and interaction of slowly varying along z wave envelopes in various nonlinear media. Here E_n are the complex fields, z is the propagation direction of the interacting waves, x is the coordinate characterising dispersion or diffraction, $H = H(\partial_x E_n, E_n, \partial_x E_n^*, E_n^*)$ is the Hamiltonian and * means complex conjugation. We will assume that H is invariant with respect to the set of $(L-1)$ phase transformations:

$$E_n \to E_n \exp(i\gamma_{nl}\phi_l),\ l = 1, 2, \ldots (L-1), \tag{B.2}$$

ϕ_l are arbitrary real phases and γ_{nl} are some constants. Because H does not depend from x explicitly, Eqs. (B.1) are invariant with respect to arbitrarily translations along x:

$$E_n(x,z) \to E_n(x-x_0,z). \tag{B.3}$$

Symmetry properties (B.2), (B.3) together with Hamiltonian nature of our problem imply presence of L conserved quantities, which are $(L-1)$ energy invariants

$$Q_l = \int dx \sum_{n=1}^{N} \gamma_{nl}|E_n|^2,\ l = 1,2,\ldots(L-1), \tag{B.4}$$

and momentum

$$Q_L = \frac{1}{2i}\int dx \sum_{n=1}^{N}(E_n^*\partial_x E_n - E_n\partial_x E_n^*). \tag{B.5}$$

Another important consequence of the invariances (B.2), (B.3) is that certain class of solutions of Eqs. (B.1) can be sought in a form when x_0 and ϕ_l are z dependent. In a simplest case they are just linear functions of z

$$E_n(x,z) = a_n(x-\kappa_L z)\exp(i\sum_{l=1}^{L-1}\gamma_{nl}\kappa_l z), \tag{B.6}$$

where κ_l are real parameters characterising phase velocities and angle of propagation with respect to z axis. Functions $a_n(\tau)$ obey following differential equations

$$(i\kappa_L\partial_\tau + \alpha_n)a_n = -\frac{\delta H_a}{\delta a_n^*}, \tag{B.7}$$

where $H_a \equiv H(\partial_\tau a_n, a_n, \partial_\tau a_n^*, a_n^*)$, $\tau = x - \kappa_L z$ and $\alpha_n = \sum_{l=1}^{L-1}\gamma_{nl}\kappa_l$. We assume now that in a certain domain of the parameter space $(\kappa_1, \kappa_2, \ldots \kappa_L)$ Eqs. (B.7) have family of solitary solutions such that $|a_n| \to 0$ for $\tau \to \pm\infty$.

To study stability of the solitons we seek solutions of the Eqs. (B.1) in the form

$$E_n = (a_n(\tau) + \varepsilon_n(\tau,z))\exp(i\sum_{l=1}^{L-1}\gamma_{nl}\kappa_l z), \tag{B.8}$$

where $\varepsilon_n(\tau,z)$ is small complex perturbations. Linearising Eqs. (B.1) and assuming that $\varepsilon_n(\tau,z) = \xi_n(\tau)e^{\lambda z}$, $\varepsilon_n^*(\tau,z) = \xi_{n+N}(\tau)e^{\lambda z}$ we get the following non-selfadjoint eigenvalue problem (EVP)

$$i\lambda\vec{\xi} = \hat{\mathcal{L}}\vec{\xi} \equiv \begin{pmatrix} \hat{S} & \hat{R} \\ -\hat{R}^* & -\hat{S}^* \end{pmatrix}\vec{\xi}, \tag{B.9}$$

where $\vec{\xi} = (\xi_1, \dots \xi_N, \xi_{N+1} \dots \xi_{2N})^T$, and $\hat{R}$, $\hat{S}$ are $N \times N$ matrix operators with elements given by

$$\hat{s}_{nl} = \delta_{nl}(\alpha_n + i\kappa_L \partial_\tau) + \frac{\delta^2 H_a}{\delta a_n^* \delta a_l}, \ \hat{r}_{nl} = \frac{\delta^2 H_a}{\delta a_n^* \delta a_l^*},$$

here δ_{nl} is the Kroneker symbol. Note, that the operator $\hat{S}$ is a selfadjoint one, i.e. $\hat{S} = \hat{S}^\dagger$, and $\hat{R}$ is a symmetric operator, i.e. $\hat{R} = \hat{R}^T$.

By infinitesimal variations of ϕ_l and x_0 or by direct substitution it can be shown that

$$\vec{u}_l = (\gamma_{1l} a_1, \dots \gamma_{Nl} a_N, -\gamma_{1l} a_1^*, \dots - \gamma_{Nl} a_N^*)^T, \ \vec{u}_L = \frac{\partial \vec{a}}{\partial \tau},$$
$$\vec{a} \equiv (a_1, \dots a_N, a_1^*, \dots a_N^*)^T, \ l = 1, \dots (L-1)$$

are neutral modes of $\hat{\mathcal{L}}$, i.e. $\hat{\mathcal{L}}\vec{u}_l = 0$ $(l = 1, \dots L)$. Operator $\hat{\mathcal{L}}$ also has L associated vectors $\vec{U}_l = \partial \vec{a}/\partial \kappa_l$ such that $\hat{\mathcal{L}}\vec{U}_l = -\vec{u}_l$, $l = 1, \dots L$.

It is straightforward to see that any solution of EVP (B.9) must obey L solvability conditions

$$\langle \vec{w}_l | \lambda \vec{\xi} \rangle = 0, \ l = 1, \dots L, \tag{B.10}$$

where $\langle \vec{y} | \vec{z} \rangle = \sum_{i=1}^{2N} \int dx y_i^* z_i$ and $\vec{w}_l$ are neutral modes of the operator $\hat{\mathcal{L}}^\dagger$, $\hat{\mathcal{L}}^\dagger \vec{w}_l = 0$,

$$\vec{w}_l = (\gamma_{1l} a_1, \dots \gamma_{Nl} a_N, \gamma_{1l} a_1^*, \dots \gamma_{Nl} a_N^*)^T, \ \vec{w}_L = i\frac{\partial \vec{b}}{\partial \tau},$$
$$\vec{b} = (-a_1, \dots - a_N, a_1^*, \dots a_N^*)^T, \ l = 1, \dots (L-1).$$

Associated vectors of $\hat{\mathcal{L}}^\dagger$ are $\vec{W}_l = \partial \vec{b}/\partial \kappa_l$ and they obey $\hat{\mathcal{L}}^\dagger \vec{W}_l = -\vec{w}_l$, $l = 1, \dots L$.

Close to instability threshold it is naturally to assume that $|\lambda| \sim \varepsilon \ll 1$. As was already discussed above we will consider a special class of the perturbations which in the leading approximation can be presented as a linear combination of the neutral modes. Therefore we seek asymptotical solution of EVP (B.9) in the following form

$$\vec{\xi} = \sum_{m=0}^{\infty} \varepsilon^m \vec{\xi}_m(x), \ \vec{\xi}_0 = \sum_{l=1}^{L} C_l \vec{u}_l \tag{B.11}$$

where constants C_l and vector-functions $\vec{\xi}_{m>0}$ have to be defined. Here and below $l = 1, 2, \ldots L$. Substitution (B.11) into EVP (B.9) gives recurrent system of equations for $\vec{\xi}_m$

$$\vec{\xi}_{m>0} = \left[\frac{i\lambda}{\varepsilon}\hat{\mathcal{L}}^{-1}\right]^m \vec{\xi}_0. \tag{B.12}$$

Substituting (B.11), (B.12) into conditions (B.10) one will find homogeneous system of L linear algebraic equations

$$\lambda^2\Big\langle \vec{w}_l \Big| \sum_{m=0}^{\infty}(-\lambda^2)^m \hat{\mathcal{L}}^{-2m} \sum_{l=1}^{L} C_l \vec{U}_l \Big\rangle = 0 \tag{B.13}$$

for L unknown constants C_l. System (B.13) has nontrivial solution providing that corresponding determinant is equal to zero. This determinant is an infinite-order polynomial with respect to λ^2. Zeros of this polynomial define spectrum of the solitary wave linked with the chosen class of the perturbations. Thus equation specifying soliton spectrum is

$$\lambda^{2L}\sum_{j=0}^{\infty}(-\lambda^2)^j D_j = 0, \tag{B.14}$$

where D_j are real constants. Eq. (B.14) always has zero root of the $2L$-order. It indicates that each of the zero eigenvalues corresponding to the neutral modes $\vec{u}_l$ is doubly degenerate one. This degeneracy originates from the presence of the associated vectors $\vec{U}_l$.

To write explicit expressions for D_j it is convenient to introduce vectors $\vec{\mathcal{M}}_l^{(m)} = (\mathcal{M}_{l1}^{(m)} \ldots \mathcal{M}_{lL}^{(m)})$, where,

$$\mathcal{M}_{ll'}^{(m)} = \langle \vec{w}_l | \hat{\mathcal{L}}^{-2m} \vec{U}_{l'} \rangle, \; m = 0, 1, \ldots \infty.$$

Now each D_j can be presented as

$$D_j = \sum_{m_1 + \ldots m_L = j} \mathcal{D}(\vec{\mathcal{M}}_1^{(m_1)}, \ldots \vec{\mathcal{M}}_L^{(m_L)}), \tag{B.15}$$

where $\mathcal{D}(\vec{\mathcal{M}}_1^{(m_1)}, \ldots \vec{\mathcal{M}}_L^{(m_L)})$ is the determinant of the $L \times L$ matrix consisting from the raws $\vec{\mathcal{M}}_l^{(m_l)}$ and sum is taken over all such combinations of $(m_1, \ldots m_L)$ that $\sum_{l=1}^{L} m_l = j$. $\mathcal{M}_{ll'}^{(0)}$ can be readily expressed via derivatives of the conserved

quantities with respect to the soliton parameters:

$$\mathcal{M}^{(0)}_{ll'} = \frac{\partial Q_l}{\partial \kappa_{l'}}, \tag{B.16}$$

and practical calculation of $\mathcal{M}^{(m)}_{ll'}$ for $m > 0$ can be simplified: $\mathcal{M}^{(m)}_{ll'} = -\langle \vec{W}_l | \hat{\mathcal{L}}^{(1-2m)} \vec{U}_{l'} \rangle$. Note, that in most of the cases solitary solution itself can be found only numerically using any of the well established methods for solving odinary differential equations, and recurrent calculations of $\hat{\mathcal{L}}^{(1-2m)}\vec{U}_l$ can be readily reduced to numerically equivalent problem.

Because $|\lambda|$ was assumed to be small, Eq. (B.14) has asymptotical character. Therefore to make it work some additional assumptions about orders of D_j must be made. In case if these assumptions are satisfied then Eq. (B.14) correctly describes soliton spectrum and predict bifurcations of the soliton. Corresponding eigenvalues can be found using Eq. (B.14) with any degree of accuracy. For example, let us assume that $D_0 \sim \varepsilon^2$ and $D_{j>0} \sim O(1)$. Then, presenting λ^2 as

$$\lambda^2 = \varepsilon^2 \sum_{j=0}^{\infty} \zeta_j, \ \zeta_j \sim \varepsilon^{2j}, \tag{B.17}$$

in the first order Eq. (B.14) gives linear equation for ζ_0,

$$D_0 - \varepsilon^2 \zeta_0 D_1 = 0, \tag{B.18}$$

which indicates threshold of stationary bifurcation at $D_0 = 0$. Continuing calculations into the next order one obtains

$$\lambda^2 = \frac{D_0}{D_1}\left(1 - \frac{D_0 D_2}{D_1^2} + O(\varepsilon^4)\right). \tag{B.19}$$

If $D_1 \sim \varepsilon^2$ then asymptotical expression (B.19) fails. This is because now to have balanced equation for ζ_0 one must assume that $D_0 \sim \varepsilon^4$, but in this case equation for ζ_0 changes from linear one to quadratic:

$$D_0 - \varepsilon^2 \zeta_0 D_1 + \varepsilon^4 \zeta_0^2 D_2 = 0. \tag{B.20}$$

Eq. (B.20) gives two threshold conditions $D_0 = 0$ and $D_1^2 = 4 D_0 D_2$, see Fig. B.1. The latter condition indicates onset of an oscillatory instability.

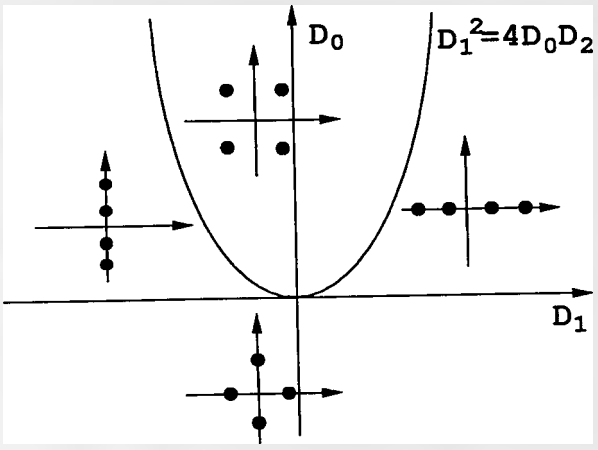

Figure B.1: Soliton bifurcation diagram in the neighbourhood of the point $D_0 = D_1 = 0$ *for* $D_2 > 0$. *Insets show* $(Re\lambda, Im\lambda)$*-plane with horizontal/vertical axes corresponding to* $Re\lambda/Im\lambda$ *and dots marking soliton eigenvalues described by Eq. (B.20).*

By recurrence it is clear that if $D_{j'>0} \sim \varepsilon^2$ then to have balanced equation for ζ_0 one must assume that $D_{j<j'} \sim \varepsilon^{2(1+j')}$. Other words asymptotical expansion near neutral modes can describe soliton spectrum in such regions of the parameter space which are close to the codimension-$(j'+1)$ bifurcation. If $j' = 0$ then only one condition must be satisfied and asymptotical approach predicts presence of either two purely imaginary or two purely real eigenvalues, which can collide at zero. If $j' = 1$ then two conditions must be satisfied and asymptotical approach predicts presence of two pairs of the eigenvalues which can be real, imaginary or complex. In this situation soliton becomes oscillatory unstable providing that two pairs of imaginary eigenvalues collided. For every further j' two new eigenvalues come into play.

It is now instructive, to consider two simplest situations of one- and two-parameter solitons and to compare results of the presented theory with previously published numerical and analytical results on stationary instabilities. For one parameter solitons: $D_0 = \partial_{\kappa_1} Q_1$, $D_1 = -\langle \vec{W}_1 | \hat{\mathcal{L}}^{-1} \vec{U}_1 \rangle$, $D_2 = -\langle \vec{W}_1 | \hat{\mathcal{L}}^{-3} \vec{U}_1 \rangle$. Using these formulas one can show that in case of when $D_1 \sim O(1)$ first term of Eqs. (B.19) gives the same expression for λ^2 which was obtained in Refs. [27, 60, 86]. If

$D_1 D_2 > 0$ then it can be concluded that second term in Eq. (B.19) indicates saturation of the growth rate when distance from the instability threshold, $D_0 = 0$, growthes, which agrees with numerical results [60, 94].

For two parameter solitons:

$$
\begin{aligned}
D_0 &= \begin{vmatrix} \frac{\partial Q_1}{\partial \kappa_1} & \frac{\partial Q_1}{\partial \kappa_2} \\ \frac{\partial Q_2}{\partial \kappa_1} & \frac{\partial Q_2}{\partial \kappa_2} \end{vmatrix}, \\
D_1 &= \begin{vmatrix} \frac{\partial Q_1}{\partial \kappa_1} & \frac{\partial Q_1}{\partial \kappa_2} \\ \mathcal{M}_{21}^{(1)} & \mathcal{M}_{22}^{(1)} \end{vmatrix} + \begin{vmatrix} \mathcal{M}_{11}^{(1)} & \mathcal{M}_{12}^{(1)} \\ \frac{\partial Q_2}{\partial \kappa_1} & \frac{\partial Q_2}{\partial \kappa_2} \end{vmatrix}, \\
D_2 &= \begin{vmatrix} \mathcal{M}_{11}^{(1)} & \mathcal{M}_{12}^{(1)} \\ \mathcal{M}_{21}^{(1)} & \mathcal{M}_{22}^{(1)} \end{vmatrix} + \begin{vmatrix} \frac{\partial Q_1}{\partial \kappa_1} & \frac{\partial Q_1}{\partial \kappa_2} \\ \mathcal{M}_{21}^{(2)} & \mathcal{M}_{22}^{(2)} \end{vmatrix} + \begin{vmatrix} \mathcal{M}_{11}^{(2)} & \mathcal{M}_{12}^{(2)} \\ \frac{\partial Q_2}{\partial \kappa_1} & \frac{\partial Q_2}{\partial \kappa_2} \end{vmatrix}.
\end{aligned}
\tag{B.21}
$$

Comparing first order approximation for eigenvalues given by Eqs. (B.19), (B.21) and those which can be calculated from the effective-particle Hamiltonians presented in [62] one will discover significant difference in the resulting formulae. Mapping asymptotical theory presented above to the method used in [62], it becomes clear that results of Refs. [62] can be recovered if one will try to calculate λ^2 in order ε^2 using ratio C_1/C_2 obtained from the solvability conditions (B.10) in the order $O(1)$, see Eqs. (7), (10) in [62].

In summary, general form of the asymptotical approach to the problem of the stability of the multi-parameter solitons in the Hamiltonian systems has been developed. It has been shown that asymptotical study of the soliton stability reduces to the calculation of a certain sequence of the determinants, where famous determinant of the matrix consisting from the derivatives of the system invariants with respect to the soliton parameters [82] is just the first in the series. In its first approximation presented approach gives criteria for both stationary and oscillatory instabilities. Higher order approximations allow to calculate corresponding eigenvalues with arbitrary accuracy.

Appendix C

Useful formulae

$$sechx = \frac{1}{chx} = \frac{2}{e^x + e^{-x}}$$

$$th^2x = 1 - sech^2x$$

$$\partial_x(sech^N x) = -N sech^N x\ thx$$

$$\partial_x^2(sech^N x) = N^2 sech^N x - N(1+N)sech^{N+2}x$$

$$\partial_x(thx\ sech^N x) = (1+N)sech^{N+2}x - N sech^N x$$

$$\partial_x^2(thx\ sech^N x) = N^2 sech^N x\ thx - (1+N)(2+N)sech^{N+2}x\ thx$$

Appendix D

Numerics

Here I give brief description of FORTRAN programmes which have been written and used to get most of the results described in this thesis

- To find stationary solitary profiles I have descretised one-dimensional systems of ordinary differential equations using 2nd order finite differences. Thus, reducing the differential equations to nonlinear set of algebraic equations which have been solved by NAG16 routine *c05nbf*. Shooting method also have been occasionally used. I have used upto 400 grid points with maximal spatial step 0.15.

- To study stability of the solitary solutions I have also used 2nd order finite differences to reduce corresponding eigenvalue problems for differential operator to the eigenvalue problems for matrix, which have been solved by NAG17 routine *f02ebf*.

- To numerically simulate propagation I used split-step method, for details see [80]. Nonlinear step was calculated by 2nd order Runge-Kutta method [80]. Linear step on Cartesian grid was calculated using two-dimensional fast Fourier transform (FFT). On polar grid linear operator was devided to radial and angular parts. Radial part was integrated by Crank-Nicholson method [80] and angular part by the one-dimensional FFT method.

Appendix E

Publications

Here is the full list of papers which author contributed into and which were either published or submitted prior submission of the thesis.

- D.V. Skryabin, *Asymptotical theory of stability of multi-parameter solitary waves*, Physica D (submitted).
- E.A. Ostrovskaya, Y.S. Kivshar, D.V. Skryabin, and W.J. Firth, *Stability of multi-hump optical solitons*, Physical Review Letters, 1999, vol. 83, No. 2 , pp. 296-299
- D.V. Skryabin and W.J. Firth, *Modulational instability of bright solitary waves in incoherently coupled nonlinear Schrödinger equations*, Physical Review E, 1999, vol. 60, No. 1, pp. 1019-1029
- D.V. Skryabin and W.J. Firth, *Modulational instability of solitary waves in non-degenerate three-wave mixing: The role of phase symmetries*, Physical Review Letters, 1998, vol. 81, No. 16, pp. 3379-3382
- D.V. Skryabin and W.J. Firth, *Dynamics of self-trapped beams with phase dislocation in saturable Kerr and quadratic nonlinear media*, Physical Review E, 1998, vol. 58, No. 3, pp. 3916-3930

- D.V. Skryabin and W.J. Firth, *Instabilities of parametric higher-order solitons. Filamentation vs coalescence*, Physical Review E, 1998, vol. 58, No. 2, pp. R1252-R1255.

- D.V. Skryabin and W.J. Firth, *Generation and stability of optical bullets in quadratic nonlinear media*, Optics Communications, 1998, Vol. 148, No. 1-3, pp. 79-84.

- W.J. Firth and D.V. Skryabin, *Optical solitons carrying orbital angular momentum*, Physical Review Letters, 1997, Vol.79, No.13, pp.2450-2453.

- D.V. Skryabin, A.G. Vladimirov, and A.M. Radin, *Phase and amplitude dynamics of TEM_{01} and TEM_{10} modes in a class-B laser*, Quantum Electronics, 1997, vol 27, No. 10, pp. 892-896 [originally published in russian: Kvantovaya Elektronika, 1997, vol 24, No. 10, pp. 918-922]

- A.G. Vladimirov and D.V. Skryabin, *Dynamical instabilities due to interaction of transverse modes in a class-B laser*, Quantum Electronics, 1997, vol 27, No. 10, pp. 887-891 [originally published in russian: Kvantovaya Elektronika, 1997, vol 24, No. 10, pp. 913-917]

- D.V. Skryabin, *Rotating and oscillating transverse patterns in an inhomogeneously broadened laser operating in a pair of doughnut modes*, Quantum & Semiclassical Optics, 1996, Vol.8, No.3, pp.485-493

- D.V. Skryabin, A.G. Vladimirov, and A.M. Radin, *Spontaneous phase symmetry-breaking due to cavity detuning in a class-A bidirectional ring laser*, Optics Communication, 1995, Vol.116, No.1-3, pp.109-115.

- D.V. Skryabin, A.G. Vladimirov, and A.M. Radin, *Self-oscillatory regimes in a gas ring laser*, Optics & Spectroscopy, 1995, Vol.78, No.6, pp. 896-905 [originally published in russian: Optika i Spectroskopiya, 1995, Vol.78, No.6, pp.989-998].

- D.V. Skryabin and A.M. Radin, *Passive optical cavity with backward scattering*, Optics & Spectroscopy, 1994, Vol.77, No.1, pp.96-102 [originally

published in russian: Optika i Spectroskopiya, 1994, Vol.77, No.1, pp.109-115]

- D.V. Skryabin and A.M. Radin, *The correction to the paraxial approximation for the laser cavity modes*, Laser Physics, 1994, Vol.4, No.1, pp.148-152

- D.V. Skryabin and A.M. Radin, *Optical rign resonator with a scattering inhomogeneity*, Optics & Spectroscopy, 1993, Vol.75, No.1, pp. 105-110 [originally published in russian: Optika i Spectroskopiya, 1993, Vol.75, No.1, pp.175-185]

- D.V. Skryabin and A.M. Radin, *On the high-frequency asymptotics of ring-cavity modes*, Optics & Spectroscopy, 1991, Vol.71, No.6, pp.612-614 [originally published in russian: Optika i Spectroskopiya, 1991, Vol.71, No.6, pp.1064-1068]

Bibliography

[1] V. E. Zakharov and A. B. Shabat, "*Exact theory of two dimensional self-focusing and one dimensional self-modulation of nonlinear waves in nonlinear media*", Zh. Eksp. Teor. Fiz., Vol. **61**, p.118 (1971) [Sov. Phys. JETP, Vol. **34**, p.62 (1971)].

[2] V. E. Zakharov and A. B. Shabat, "*Interaction between solitons in a stable medium*", Zh. Eksp. Teor. Fiz., Vol. **64**, pp.1627–1639 (1973) [Sov. Phys. JETP, Vol. **37**, p.823 (1973)].

[3] S. P. Novikov, S. V. Manakov, L. P. Pitaevskii, and V. E. Zakharov, *Theory of solitons. The inverse scattering method.* (Plenum Press, New York, 1984).

[4] J. J. Rasmussen and K. Rypdal, "*Blow-up in nonlinear Schroëdinger equations. 1. A general-review*", Physica Scripta, Vol. **33**, pp.481–497 (1986).

[5] G. Askar'yan, "*Effects of the gradient of a strong electromagnetic beam on electrons and atoms*", Zh. Eksp. Teor. Fiz., Vol. **42**, p.1567 (1962) [Sov. Phys. JETP **15**, 1088 (1962)].

[6] V. I. Bespalov and V. I. Talanov, "*Filamentary structure of light beams in nonlinear liquids*", Pis'ma Zh. Eksp. Teor. Fiz., Vol. **3**, p.471 (1966) [JETP Lett. **3**, 307 (1966)].

[7] T. B. Benjamin and J. E. Feir, "*The disintegration of wave trains on deep water. Part 1. Theory*", J. Fluid Mech., Vol. **27**, pp.417–430 (1967).

[8] N. F. Pilipetskii and A. R. Rustamov, "*Observation of self-focusing of light in liquids*", Pis'ma Zh. Eksp. Teor. Fiz., Vol. **2**, p.88 (1965) [JETP Lett. **2**, 55 (1965)].

[9] E. A. Kuznetsov, A. M. Rubenchik, and V. E. Zakharov, "*Soliton stability in plasmas and hydrodynamics*", Phys. Rep., Vol. **142**, pp.103–165 (1986).

[10] L. Berge, "*Wave collapse in physics: principles and applications to light and plasma waves*", Phys. Rep., Vol. **303**, p.259 (1998).

[11] N. N. Akhmediev and A. Ankievich, *Solitons: Nonlinear pulses and beams* (Chapman & Hall, London, 1997).

[12] Y. S. Kivshar and B. Luther-Davies, "*Dark optical solitons: physics and applications*", Phys. Rep., Vol. **298**, pp.81–197 (1998).

[13] R. K. Dodd, J. C. Eilbeck, J. D. Gibbon, and H. C. Morris, *Solitons and nonlinear wave equations.* (Academic Press, London, 1984).

[14] A. I. Dyachenko *et al.*, "*Soliton turbulence in nonintegrable wave systems*", Zh. Eksp. Teor. Fiz., Vol. **96**, pp.2026–2032 (1989) [Sov. Phys. JETP **69**, 1144 (1989)].

[15] N. N. Akhmediev, D. R. Heatley, G. I. Stegeman, and E. M. Wright, "*Pseudorecurrence in 2-dimensional modulation instability with a saturable self-focusing nonlinearity*", Phys. Rev. Lett., Vol. **65**, pp.1423–1426 (1990).

[16] A. L. Berkhoer and V. E. Zakharov, "*Self-excitation of waves with different polarizations in nonlinear media*", Zh. Eksp. Teor. Fiz., Vol. **58**, p.903 (1970) [Sov. Phys. JETP **31**, 486 (1970)].

[17] G. Roskes, "*Some nonlinear multiphase interactions*", Stud. Appl. Math., Vol. **55**, p.231 (1976).

[18] G. G. Luther and C. J. McKinstrie, "*Transverse modulational instability of collinear waves*", J. Opt. Soc. Am B, Vol. **7**, p.1125 (1990).

[19] G. P. Agrawal, "*Modulation instability induced by cross-phase modulation*", Phys. Rev. Lett., Vol. **59**, pp.880–883 (1987).

[20] G. P. Agrawal, "*Transverse modulation instability of copropagating optical beams in nonlinear kerr media*", J. Opt. Soc. Am B, Vol. **7**, pp.1072–1078 (1990).

[21] W. J. Firth and C. Paré, "*Transverse modulational instabilities for counterpropagating beams in Kerr media*", Opt. Lett., Vol. **13**, p.1096 (1988).

[22] W. J. Firth, A. Fitzgerald, and C. Paré, "*Transverse instabilities due to counterpropagation in Kerr media*", J. Opt. Soc. Am B, Vol. **7**, p.1087 (1990).

[23] J. E. Rosenberg, "*Modulational instability for normal dispersion*", Phys. Rev. A, Vol. **42**, pp.R682–R685 (1990).

[24] M. Haelterman and A. P. Sheppard, "*Vector soliton associated with polarization modulational instability in the normal-dispersion regime*", Phys. Rev. E, Vol. **49**, pp.3389–3399 (1994).

[25] V. E. Zakharov, "*Instability of self-focusing of light*", Zh. Eksp. Teor. Fiz., Vol. **53**, pp.1735–1743 (1967) [Sov. Phys. JETP **26**, 994-998 (1968)].

[26] B. B. Kadomtsev and V. I. Petviashvily, "*On the stability of solitary waves in weakly dispersing media*", Dokl. Acad. Nauk SSSR, Vol. **192**, pp.753–756 (1970) [Sov. Phys. Dokl. **15**, 539 (1970)].

[27] V. E. Zakharov and A. M. Rubenchik, "*Instability of waveguides and solitons in nonlinear media*", Zh. Eksp. Teor. Fiz., Vol. **65**, p.997 (1973) [Sov. Phys. JETP **38**, 494 (1974)].

[28] R. W. Boyd, *Nonlinear Optics* (Academic Press, Boston, 1992).

[29] P. N. Butcher and D. Cotter, *The elements of nonlinear optics* (Cambridge University Press, Cambidge, 1990).

[30] C. J. McKinstrie and D. A. Russel, "*Nonlinear focusing of coupled waves*", Phys. Rev. Lett., Vol. **61**, p.2929 (1988).

[31] T. Ueda and W. I. Kath, "*Dynamics of coupled solitons in nonlinear optical fibers*", Phys. Rev. A, Vol. **42**, pp.563–571 (1990).

[32] J. Yang and D. J. Benney, "*Some properties of nonlinear wave systems*", Stud. Appl. Math., Vol. **96**, pp.111–139 (1996).

[33] J. Yang, "*Vector solitons and their internal oscillations in birefringent nonlinear optical fibers*", Stud. Appl. Math., Vol. **98**, pp.61–97 (1997).

[34] J. K. Yang, "*Classification of the solitary waves in coupled nonlinear Schrodinger equations*", Physica D, Vol. **108**, pp.92–112 (1997).

[35] B. A. Malomed and R. S. Tasgal, "*Internal vibrations of a vector soliton in the coupled nonlinear Schrodinger equations*", Phys. Rev. E, Vol. **58**, pp.2564–2575 (1998).

[36] L. D. Landau and E. M. Lifshits, *Quantum Mechanics* (Pergamon Press, Oxford, 1965).

[37] S. V. Manakov, "*On the theory of two-dimensional stationary self-focusing of electromagnetic waves*", Zh. Eksp. Teor. Fiz., Vol. **65**, pp.505–516 (1973) [Sov. Phys. JETP **38**, 248-253 (1974)].

[38] J. K. Ranka, R. W. Schirmer, and A. L. Gaeta, "*Observation of pulse splitting in nonlinear dispersive media*", Phys. Rev. Lett, Vol. **77**, pp.3783–3786 (1996).

[39] S. A. Diddams, H. K. Eaton, A. A. Zozulya, and T. S. Clement, "*Amplitude and phase measurements of femtosecond pulse splitting in nonlinear dispersive media*", Opt. Lett., Vol. **23**, p.379 (1998).

[40] N. Belanger, A. Villeneuve, and J. S. Aitchison, "*Solitonlike pulses in self-defocusing AlGaAs waveguides*", J. Opt. Soc. Am. B, Vol. **14**, p.3003 (1997).

[41] J. S. Aitchison *et al.*, "*Power-dependent polarization dynamics of mixed-mode spatial solitary waves in AlGaAs waveguides*", J. Opt. Soc. Am. B, Vol. **14**, p.3032 (1997).

[42] Y. N. Karamzin and A. P. Sukhorukov, "*Nonlinear interaction of diffracted light beams in a medium with quadratic nonlinearity: mutual focusing of beams and limitation on the efficiency of optical frequency converters*", Pis'ma Zh. Eksp. Teor. Fiz., Vol. **20**, p.734 (1974) [JETP Lett. Vol. **20**, p.339 (1974)].

[43] Y. N. Karamzin and A. P. Sukhorukov, "*Mutual focusing of high-power light beams in media with quadratic nonlinearity*", Zh. Eksp. Teor. Fiz., Vol. **68**, p.834 (1975) [Sov. Phys. JETP Vol. **41**, p.414 (1976)] .

[44] R. Y. Chiao, E. Garmire, and C. H. Townes, "*Self-trapping of optical beams*", Phys. Rev. Lett., Vol. **13**, pp.479–480 (1964).

[45] M. J. Werner and P. D. Drummond, "*Simulton solitons for the parametric amplifier*", J. Opt. Soc. Am. B, Vol. **10**, pp.2390–2393 (1993).

[46] K. Hayata and M. Koshiba, "*Multidimensional solitons in quadratic nonlinear media*", Phys. Rev. Lett., Vol. **71**, pp.3275–3278 (1993).

[47] C. R. Menyuk, R. Schiek, and L. Torner, "*Solitary waves due to* $\chi^{(2)} : \chi^{(2)}$ *cascading*", J. Opt. Soc. Am. B, Vol. **11**, pp.2434–2443 (1994).

[48] A. V. Buryak and Y. S. Kivshar, "*Spatial optical solitons governed by quadratic nonlinearity*", Opt. Lett., Vol. **19**, pp.1612–1614 (1994).

[49] W. E. Torruellas *et al.*, "*Observation of 2-dimensional spatial solitary waves in a quadratic medium*", Phys. Rev. Lett., Vol. **74**, pp.5036–5039 (1995).

[50] W. Torruellas *et al.*, "*All-optical switching by spatial walkoff compensation and solitary-wave locking*", Appl. Phys. Lett., Vol. **68**, pp.1449–1451 (1996).

[51] R. A. Fuerst, M. T. G. Canva, D. Baboiu, and G. I. Stegeman, "*Properties of type II quadratic solitons excited by imbalanced fundamental waves*", Opt. Lett., Vol. **22**, pp.1748–1750 (1997).

[52] R. Schiek, Y. Baek, and G. Stegeman, "*One-dimensional spatial solitary waves due to cascaded second-order nonlinearities in planar waveguides*", Phys. Rev. E, Vol. **53**, p.1138 (1996).

[53] Y. Baek *et al.*, "*Interactions between one-dimensional quadratic solitons*", Opt. Lett., Vol. **22**, pp.1550–1552 (1997).

[54] P. Di Trapani *et al.*, "*Observation of temporal solitons in second-harmonic generation*", Phys. Rev. Lett., Vol. **81**, pp.570–573 (1998).

[55] V. Steblina, Y. Kivshar, M. Lisak, and B. Malomed, "*Self-guided beams in a diffractive $\chi^{(2)}$ medium - variational approach*", Opt. Commun., Vol. **118**, pp.345–352 (1995).

[56] A. D. Boardman, K. Xie, and A. Sangarpaul, "*Stability of scalar spatial solitons in cascadable nonlinear media*", Phys. Rev. A, Vol. **52**, pp.4099–4106 (1995).

[57] L. Torner *et al.*, "*Stationary trapping of light beams in bulk second-order nonlinear media*", Opt. Commun., Vol. **121**, pp.149–155 (1995).

[58] B. A. Malomed *et al.*, "*Spatiotemporal solitons in multidimensional optical media with a quadratic nonlinearity*", Phys. Rev. E, Vol. **56**, pp.4725–4735 (1997).

[59] D. V. Skryabin and W. J. Firth, "*Generation and stability of optical bullets in quadratic nonlinear media*", Opt. Commun., Vol. **148**, pp.79–84 (1998).

[60] D. E. Pelinovsky, A. V. Buryak, and Y. S. Kivshar, "*Instabilities of solitons governed by quadratic nonlinearities*", Phys. Rev. Lett., Vol. **75**, pp.591–595 (1995).

[61] U. Peschel, C. Etrich, F. Lederer, and B. A. Malomed, "*Vectorial solitary waves in optical media with a quadratic nonlinearity*", Phys. Rev. E, Vol. **55**, pp.7704–7711 (1997).

[62] A. V. Buryak, Y. S. Kivshar, and S. Trillo, "*Stability of three-wave parametric solitons in diffractive quadratic media*", Phys. Rev. Lett., Vol. **77**, pp.5210–5213 (1996).

[63] C. Etrich, U. Peschel, F. Lederer, and B. A. Malomed, "*Stability of temporal chirped solitary waves in quadratically nonlinear media*", Phys. Rev. E, Vol. **55**, pp.6155–6161 (1997).

[64] D. Mihalache, D. Mazilu, L. C. Crasovan, and L. Torner, "*Walking solitons in type II second-harmonic generation*", Phys. Rev. E, Vol. pp.R6294–R6297 (1997).

[65] D. Eimerl, J. Auerbach, and P. Milonni, "*Paraxial wave theory of second and third harmonic generation in uniaxial crystals. I. Narrowband pump fields*", J. Mod. Opt., Vol. **42**, pp.1037–1067 (1995).

[66] A. D. Boardman, P. Bontemps, and K. Xie, "*Transverse modulation instability of vector optical beams in quadratic nonlinear media*", J. Opt. Soc. Am., Vol. **14**, pp.3119–3126 (1997).

[67] L. Torner, D. Mazilu, and D. Mihalache, "*Walking solitons in quadratic nonlinear media*", Phys. Rev. Lett., Vol. **77**, pp.2455–2458 (1996).

[68] D. Mihalache, D. Mazilu, L. C. Crasovan, and L. Torner, "*Stationary walking solitons in bulk quadratic nonlinear media*", Opt. Commun., Vol. **137**, pp.113–117 (1997).

[69] H. He and P. Drummond, "*Ideal soliton environment using parametric band gaps*", Phys. Rev. Lett., Vol. **78**, pp.4311–4315 (1997).

[70] C. Conti, S. Trillo, and G. Assanto, "*Doubly resonant Bragg Simultons via second-hartmonic generation*", Phys. Rev. Lett., Vol. **78**, pp.2341–2344 (1998).

[71] J. A. Armstrong, N. Bloembergen, J. Ducuing, and P. S. Pershan, "*Interaction between light waves in a nonlinear dielectric*", Phys. Rev., Vol. **127**, pp.1918–1939 (1962).

[72] M. M. Fejer, G. A. Magel, D. H. Jundt, and R. L. Byer, "*Quasi-phase-matched second harmonic generation: Tuning and tolerance*", IEEE J. Quant. Electr., Vol. **28**, pp.2631–2654 (1992).

[73] C. B. Clausen, O. Bang, and Y. S. Kivshar, "*Spatial solitons and induced Kerr effects in quasi-phase-matched quadratic media*", Phys. Rev. Lett., Vol. **78**, pp.4749–4752 (1997).

[74] C. B. Clausen and L. Torner, "*Self-bouncing of quadratic solitons*", Phys. Rev. Lett., Vol. **81**, pp.790–793 (1998).

[75] A. Fiore *et al.*, "*Phase matching using an isotropic nonlinear optical material*", Nature, Vol. **391**, pp.463–466 (1998).

[76] J. P. Van der Ziel, "*Phase-matched harmonic generation in a laminar structure with wave propagation in the plane of the layers*", Appl. Phys. Lett., Vol. **26**, pp.60–62 (1975).

[77] A. G. Kalocsai and J. W. Haus, "*Nonlinear Schrödinger-equation for optical media with quadratic nonlinearity*", Phys. Rev. A, Vol. **49**, pp.574–585 (1994).

[78] H. Leblond, "*Propagation of optical localized pulses in $\chi^{(2)}$ crystals: a (3+1)-dimensional model and its reduction to the NLS equation*", J. Phys. A, Vol. **31**, pp.3041–3066 (1998).

[79] Y. Chen, "*Stability criterion of solitons in three wave mixing of $\chi^{(2)}$ nonlinear media*", Phys. Lett. A, Vol. **234**, pp.443–452 (1997).

[80] W. H. Press, S. A. Teukolsky, W. T. Vetterling, and B. P. Flannery, *Quantum Mechanics* (Cambridge University Press, Cambridge, 1992).

[81] N. G. Vakhitov and A. A. Kolokolov, "*Stationary solutions of the wave equation in a medium with nonlinearity saturation*", Izv. Vyssh. Uchebn. Zaved. Radiofiz., Vol. **16**, p.1020 (1973) [Sov. Radiophys. **16**, 783 (1975)].

[82] V. G. Makhankov, Y. P. Rybakov, and V. I. Sanyuk, "*Localized nontopological structures - construction of solutions and stability problems*", Usp. Fiz. Nauk, Vol. **164**, pp.121–148 (1994) [Physics-Uspekhi , Vol. **37**, pp.113 (1994)].

[83] C. Etrich *et al.*, "*Origin of the persistent oscillations of solitary waves in nonlinear quadratic media*", Phys. Rev. E, Vol. **54**, pp.4321–4324 (1996).

[84] D. Pelinovsky, "*Radiative effects to the adiabatic dynamics of envelope-wave solitons*", Physica D, Vol. **119**, pp.301–313 (1998).

[85] R. Courant and D. Hilbert, *Methods of mathematical physics* (John Wiley & Sons, New York, 1966).

[86] D. E. Pelinovsky, V. V. Afanasjev, and Y. S. Kivshar, "*Nonlinear theory of oscillating, decaying, and collapsing solitons in generalized nonlinear Schrödinger equation*", Phys. Rev. E, Vol. **53**, pp.1940–1953 (1996).

[87] D. E. Pelinovsky, Y. S. Kivshar, and V. V. Afanasjev, "*Internal modes of envelope solitons*", Physica D, Vol. **116**, pp.121–142 (1998).

[88] A. V. Buryak and Y. S. Kivshar, "*Multistability of three-wave parametric self-trapping*", Phys. Rev. Lett., Vol. **78**, pp.3286–3289 (1997).

[89] A. V. Buryak and Y. S. Kivshar, "*Solitons due to second harmonic generation*", Phys. Lett. A, Vol. **197**, pp.407–412 (1995).

[90] H. He, M. J. Werner, and P. D. Drummond, "*Simultaneous solitary-wave solutions in a nonlinear parametric waveguide*", Phys. Rev. E, Vol. **54**, p.896 (1996).

[91] W. J. Firth and D. V. Skryabin, "*Optical solitons carrying orbital angular momentum*", Phys. Rev. Lett., Vol. **79**, pp.2450–2453 (1997).

[92] J. P. Torres, J. M. SotoCrespo, L. Torner, and D. V. Petrov, "*Solitary-wave vortices in quadratic nonlinear media*", J. Opt. Soc. Am., Vol. **15**, pp.625–627 (1998).

[93] J. P. Torres, J. M. SotoCrespo, L. Torner, and D. V. Petrov, "*Solitary-wave vortices in type II second-harmonic generation*", Opt. Commun., Vol. **149**, pp.77–83 (1998).

[94] D. V. Skryabin and W. J. Firth, "*Instabilities of higher-order parametri solitons: Filamentation vs coalescence*", Phys. Rev. E, Vol. **58**, pp.R1252–R1255 (1998).

[95] D. V. Skryabin and W. J. Firth, "*Dynamics of self-trapped beams with phase dislocation in saturable Kerr and quadratic nonlinear media*", Phys. Rev. E, Vol. **58**, pp.3916–3930 (1998).

[96] M. Haelterman, S. Trillo, and P. Ferro, "*Multiple soliton bound states and symmetry breaking in quadratic media*", Opt. Lett., Vol. **22**, pp.84–86 (1997).

[97] H. A. Haus, "*Higher order trapped light beam solutions*", Appl. Phys. Lett., Vol. **8**, pp.128–129 (1966).

[98] J. M. Soto-Crespo, D. R. Heatley, E. M. Wright, and N. N. Akhmediev, "*Stability of the higher-bound states in a saturable self-focusing medium*", Phys. Rev. A, Vol. **44**, pp.636–644 (1991).

[99] H. T. Tran, J. D. Mitchell, N. N. Akhmediev, and A. Ankievich, "*Complex eigenvalues in stability analysis of nonlinear planar guided-waves*", Opt. Commun., Vol. **93**, p.227 (1992).

[100] V. V. Steblina, Y. S. Kivshar, and A. V. Buryak, "*Scattering and spiraling of solitons in a bulk quadratic medium*", Opt. Lett., Vol. **23**, p.156 (1998).

[101] A. A. Kanashov and A. M. Rubenchik, "*On diffraction and dispersion effect on 3 wave interaction*", Physica D, Vol. **4**, pp.122–134 (1981).

[102] A. D. Rossi, S. Trillo, A. V. Buryak, and Y. S. Kivshar, "*Snake instability of one-dimensional parametric spatial solitons*", Opt. Lett., Vol. **22**, pp.868–870 (1997).

[103] A. D. Rossi, S. Trillo, A. V. Buryak, and Y. S. Kivshar, "*Symmetry-breaking instabilities of spatial parametric solitons*", Phys. Rev. E, Vol. **56**, pp.R4959–R4962 (1997).

[104] R. A. Fuerst *et al.*, "*Spatial modulational instability and multisolitonlike generation in a quadratically nonlinear optical medium*", Phys. Rev. Lett., Vol. **78**, pp.2756–2759 (1997).

[105] D. V. Skryabin and W. J. Firth, "*Modulational instability of solitary waves in nondeghenerate three-wave mixing: The role of phase symmetries*", Phys. Rev. Lett., Vol. **81**, pp.3379–3383 (1998).

[106] D. M. Baboiu and G. I. Stegeman, "*Modulational instability of a strip beam in a bulk type I quadratic medium*", Opt. Lett., Vol. **23**, pp.31–33 (1998).

[107] N. Akhmediev and J. M. S. Crespo, "*Generation of a train of 3-dimensional optical solitons in a self-focusing medium*", Phys. Rev. A, Vol. **47**, pp.1358–1364 (1993).

[108] M. T. G. Canva *et al.*, "*Quadratic spatial soliton generation by seeded downconversion of a strong harmonic pump beam*", Opt. Lett., Vol. **22**, pp.1683–1685 (1997).

[109] S. Trillo and P. Ferro, "*Modulational instability in 2nd-harmonic generation*", Opt. Lett., Vol. **20**, pp.438–440 (1995).

[110] P. Ferro and S. Trillo, "*Periodical waves, domain-walls, and modulational instability in dispersive quadratic nonlinear media*", Phys. Rev. E, Vol. **51**, pp.4994–4998 (1995).

[111] H. He, P. D. Drummond, and B. A. Malomed, "*Modulational stability in dispersive optical systems with cascaded nonlinearity*", Opt. Commun., Vol. **123**, pp.394–402 (1996).

[112] L. Gagnon and C. Paré, "*Nonlinear radiation modes connected to parabolic graded-index profiles by the lens transformation*", J. Opt. Soc. Am. B, Vol. **8**, pp.601–607 (1991).

[113] A. Glass, "*Propagation modes in stationary self-focusing*", IEEE J. Quantum. Electron., Vol. **10**, pp.705–706 (1974).

[114] J. S. Hesthaven *et al.*, "*Dynamics of a nonlinear dipole vortex*", Phys. Fluids, Vol. **7**, p.2220 (1995).

[115] G. L. Alfimov *et al.*, "*New stationary field distributions in nonlinear optics and mechanics of continuous media*", Phys. Lett. A, Vol. **138**, p.443 (1989).

[116] G. L. Alfimov *et al.*, "*On existence of nontrivial solutions for the equation* $\Delta U - U + U^3 = 0$", Physica D, Vol. **44**, p.168 (1990).

[117] V. I. Kruglov, Y. A. Logvin, and V. M. Volkov, "*The theory of spiral laser-beams in nonlinear media*", J. Mod. Opt., Vol. **39**, p.2277 (1992).

[118] N. N. Rosanov, V. A. Smirnov, and N. V. Vysotina, "*Numerical simulation of interaction of bright spatial solutions in a medium with saturable nonlinearity*", Chaos, Solitons & Fractals, Vol. **4**, pp.1767–1782 (1994).

[119] M. Quiroga-Teixeiro and H. Michinel, "*Stable azimuthal stationary state in quintic nonlinear optical media*", J. Opt. Soc. Am. B, Vol. **14**, pp.2004–2009 (1997).

[120] N. V. Vysotina, L. A. Nesterov, N. N. Rosanov, and V. A. Smirnov, "*Interactions of spatial solitons in a medium with a saturable nonlinearity: II. Strong interaction of solitons for small angles of collision*", Opt. & Spectrosc., Vol. **85**, p.422 (1998).

[121] V. Tikhonenko, J. Christou, and B. Luther-Davies, "*Spiraling bright spatial solitons formed by the breakup of an optical vortex in a saturable self-focusing medium*", J. Opt. Soc. Am. B, Vol. **12**, p.2046 (1995).

[122] V. Tikhonenko, J. Christou, and B. L. Davies, "*Three dimensional bright spatial soliton collision and fusion in a saturable nonlinear medium*", Phys. Rev. Lett., Vol. **76**, p.2698 (1996).

[123] Z. Chen *et al.*, "*Steady-state vortex-screening solitons formed in biased photorefractive media*", Opt. Lett., Vol. **22**, pp.1751–1753 (1997).

[124] D. V. Petrov *et al.*, "*Observation of azimuthal modulational instability and formation of patterns of optical solitons in a quadratic nonlinear crystal*", Opt. Lett., Vol. **23**, pp.1444–1446 (1998).

[125] L. Torner and D. V. Petrov, "*Splitting of light beams with spiral phase dislocations into solitons in bulk quadratic nonlinear media*", J. Opt. Soc. Am. B, Vol. **14**, p.2017 (1997).

[126] D. I. Abakarov, A. A. Akopyan, and S. I. Pekar, "*Contribution to the theory of self-focusing of light in nonlinearly polarizing media*", Zh. Eksp. Teor. Fiz., Vol. **52**, pp.463–466 (1967) [Sov. Phys. JETP, **25**, 303-305 (1967)].

[127] V. M. Eleonskii, L. G. Oganesyants, and V. P. Silin, "*Cylindrical Nonlinear Waveguides*", Zh. Eksp. Teor. Fiz., Vol. **62**, pp.81–88 (1972) [Sov. Phys. JETP, **35**, 44-47 (1972)].

[128] J. Atai, Y. Chen, and J. M. SotoCrespo, "*Stability of 3-dimensional self-trapped beams with a dark spot surrounded by bright rings of varying intensity*", Phys. Rev. A, Vol. **49**, p.R3170 (1994).

[129] N. N. Akhmediev, V. I. Korneev, and R. F. Nabiev, "*Modulation instability of the ground-state of the nonlinear-wave equation - optical machine gun*", Opt. Lett., Vol. **17**, pp.393–395 (1992).

[130] S. Barnett and L. Allen, "*Orbital angular-momentum and nonparaxial light-beams*", Opt. Commun., Vol. **110**, p.670 (1994).

[131] L. Allen, M. W. Beijersbergen, R. J. C. Spreeuw, and J. Woerdman, "*Orbital angular-momentum of light and the transformation of laguerre- gaussian laser modes*", Phys. Rev. A, Vol. **45**, p.8185 (1992).

[132] K. Dholakia, N. B. Simpson, M. J. Padgett, and L. Allen, "*Second-harmonic generation and the orbital angular momentum of light*", Phys. Rev. A, Vol. **54**, p.R3742 (1996).

[133] A. W. Snyder, D. J. Mitchell, and Y. S. Kivshar, "*Unification of linear and nonlinear-wave optics*", Mod. Phys. Lett. B, Vol. **9**, p.1479 (1995).

[134] L. Poladian, A. W. Snyder, and D. J. Mytchell, "*Spiraling spatial solitons*", Opt. Commun., Vol. **85**, p.59 (1991).

[135] M. Shih, M. Segev, and G. Salamo, "*Three-dimensional spiraling of interacting spatial solitons*", Phys. Rev. Lett., Vol. **78**, pp.2551–2554 (1997).